**Faculty of Science and Technology**

# MASTER'S THESIS

| Study program/ Specialization:<br><br>MSc Petroleum Engineering/ Drilling | Spring semester, 2010<br><br><br>Open / Restricted access |
|---|---|
| Author: Ovwigho Ejiro Kenneth | …………………………………………<br>(Author's signature) |
| Faculty supervisor: Professor Bernt Aadnøy<br><br>External supervisor(s): | |
| Title of thesis: Fracture Propagation Modeling | |
| Credits (ECTS):   30 | |
| Key words: | Pages: …………………<br>+ enclosure: …………<br>Stavanger, ………………..<br>Date/year |

# Fracture Propagation Modeling

by

Ovwigho Ejiro Kenneth

Submitted to the Institute of Petroleum Technology,

On 15th June 2010, in partial fulfillment of the requirements for the degree of

Master of Science

# Abstract

In oil and gas production, hydraulic fracturing is often performed to increase the productivity of hydrocarbon reservoirs. During drilling operation, when the differential well pressure exceeds the strength of the formation, it causes undesired well fracturing. As a result, this cause loss of circulation and other associated problems.

This thesis seeks to understand the fracture propagation process through a review of previous works, and deriving new fracture models. A review of the basic concepts of rock mechanics required to understand this work is presented.

Based on various fracture geometry scenarios, new fracture propagation models are derived. These derived models are then compared with experimental data. A diffusivity equation for fluid flow in fractures is presented. A qualitative comparison analysis of fracture propagation velocity is also presented.

Experiments are conducted to understand the fracture propagation process and results are presented. Finally, recommendations are made and the appropriate conclusions are presented.

# Acknowledgements

# Contents

# List of Figures

# List of Tables

# Chapter 1 Overview

## 1.1    Introduction

The issue of wellbore stability has received a lot of attention over the last 20 years due to increased hydrocarbon exploration activities. Wellbore stability is a term that refers to a wide range of possible problems that can occur while drilling or producing an oil or gas well. The problem increases the drilling budget by 10-15% and that makes it an interesting issue for the industry. The aspect of wellbore stability addressed in this project is related to mechanical rock failure during drilling.

Rock failure is regarded as the origin of borehole stability problems. It is therefore important to be able to predict the conditions under which failure is likely to occur. Rock failure occurs when the rock is subjected to sufficiently large stresses. There are two main mechanisms responsible for rock failure namely: tensile failure and shear failure. This thesis focuses on one of the tensile failure mechanism called hydraulic fracturing.

Hydraulic fracturing is initiated by increasing the fluid pressure in the borehole to the point where the smallest principal stresses become tensile. Continued pumping at elevated pressures causes the formation to split and the fracture will grow (propagate) in the direction normal to the smallest in-situ stress.

Fracturing can occur during drilling or stimulation operations. When fracturing occurs during drilling, it results in lost circulation. Hydraulic fracturing is performed during well stimulation operation. The purpose is to increase the productivity of the well that has been damaged during drilling and production phases.

Understanding of the fracture mechanism is important to avoid costly wellbore stability problems, to avoid hole enlargement problems that can ultimately affect casing placement and log measurements. All these will of course translate into tremendous cost savings.

## 1.2 Scope and outline

The objective of this thesis is to study the fracture initiation and propagation mechanisms. The focus however, is on understanding the fracture propagation process and the mechanisms involved. Existing fracture initiation models will be reviewed and compared to experimental data with a view to analyzing to determine the most correct model. Furthermore, new fracture propagation models will be developed and also compared with experimental data. Efforts will also be made in understanding the fracture propagation process and experiments will be used to obtain a clearer picture of how fractures actually propagate.

Chapter 2 discusses the mechanical properties of rocks and the state of stress in the rocks before and after drilling. This chapter is therefore important for the understanding of chapter 3 Chapter 3 describes the stress situation around a borehole, the concept of stress transformation, and also the major failure mechanisms applicable to the failure of intact rocks. It reviews exixting fracture initiation models and compares their results with experimental data. The review helps us to have a more complete knowledge of the subject matter and also prepares us for chapter 4.Chapter 4 deals with fracture mechanics, and presents the supporting theories that will be used in the fracture propagation modeling work in chapter 5.

Chapter 5 is used to present some new concepts. It begins with a conceptual model of the fracture propagation process and then presents some new fracture propagation models. These models are then compared with experimental data to see how they perform. A diffusivity equation for fluid flow in fractures is presented and recommendations are made for future work on this new concept. A quantitative study of fracture propagation velocity is also presented. Once again, emphasis is made on future work on this area.

Chapter 6 shows an experiment conducted to understand the fracture propagation process and results are presented.

Chapter 7 discusses all the efforts made in this thesis, gives recommendations, and also presents the appropriate conclusions.

## 1.3    Description of the Problem

Hydraulic fracturing is a technique that has long been used in stimulating a well to improve its production and address wellbore damage issues. This work however, focuses on understanding the fracturing that occurs during drilling operation which is undesirable. The focus is on understanding the mechanisms responsible for fracture initiation and propagation during drilling. This is important to prevent costly lost circulation by designing appropriate mud system. It has been reported (Aadnøy and Belayneh, 2004) that the drilling mud contributes to the rock strength through a stress caging phenomenon. A better understanding of the fracturing process and proper mud engineering will therefore help to raise the stress limit that the formation can withstand before failure.

The primary focus of this work is on understanding the fracture propagation process and modeling. However, since fracturing occurs first by initiation, we will begin by reviewing some important fracture initiation models as a necessary starting point in order to have a more complete picture of the entire process.

A new experimental setup will be designed and presented for more robust fracture propagation analysis. This new setup should enable us to vary the horizontal stresses around a rectangular core. This will enable us to obtain a better understanding of the fracture propagation process and the fracture orientation.

Some new concepts will also be presented that can be pursued in the future to see the possible outcomes. Some of these concepts will not be fully exploited due to both time limitations and also due to the complexity involved. Others will just simply just be presented for quantitative analysis.

# Chapter 2 Theory

This chapter is dedicated to discussing the mechanical properties of rocks and the state of stress in the rocks before and after drilling. The chapter is therefore important for the understanding of chapter 3.

## 2.1 Rock mechanics

A rock is a naturally occurring solid aggregate of minerals. In general rocks are of three types, namely, igneous, sedimentary, and metamorphic rocks. Rock mechanics is the theoretical and applied science of the mechanical behaviour of rock and rock masses; it is that branch of mechanics concerned with the response of rock and rock masses to the force fields of their physical environment[4]. Solid mechanics is the branch of mechanics, physics, and mathematics that concerns the behavior of solid matter under external actions (e.g., external forces, temperature changes, applied displacements, etc.). It is part of a broader study known as continuum mechanics. The fundamental differences between rock mechanics and solid mechanics lie in the homogeneous and isotropic properties of the materials considered. Solid mechanics deals with materials that are homogeneous and isotropic. In other words, the properties of the material are the same at different locations inside the material (homogeneous) and the properties are the same in different directions (isotropic). Rock mechanics on the other hand, deals with materials that are heterogeneous and anisotropic. Often for simplicity, we assume that rocks are homogeneous and isotropic so as to make them easier for us to model. Consider the cylindrical body in Fig.1 under uniaxial compression loading. The deformation in $x$ direction is followed by an additional deformation in the $y$ direction. The Stress is defined as the force acting per unit area. Strain deals with deformation. Assuming a linear elastic material, the stress varies lineary with stain.

Mathematically,

$$Stress: \quad \sigma_{xx} = \frac{F}{A}$$

$$Strains: \quad \varepsilon_{xx} = \frac{\Delta L}{L} \quad \varepsilon_{yy} = \frac{\Delta D}{D}$$

$$Young's\ modulus: E = \frac{\sigma_{xx}}{\varepsilon_{xx}}$$

$$Poisson's\ ratio: \quad v = -\frac{\varepsilon_{yy}}{\varepsilon_{xx}}$$
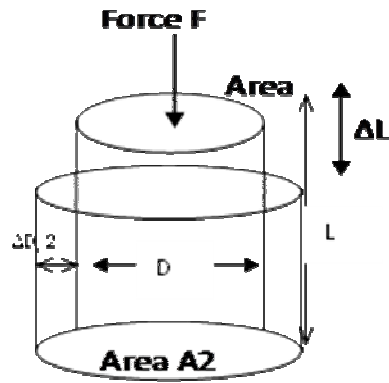
**Figure 1:** Uniaxial compression: Determination of Young's modulus and Poisson's ratio

## 2.2   Material properties of rock

The mechanical behaviors of rocks into three group. These are 1) High strength, brittle rocks that fail by micro fissuring; 2) Low strength, ductile materials that fail predominantly by frictional process and relative slip of grains and; 3) Viscous materials that flow without significant weakening. All of these materials may be anisotropic and may have stress dependent on their strength and stiffness properties.

For a linear elastic brittle material, the elastic response is terminated and stress suddenly drops to zero when it reaches its strength limit (Fig. 2a). For elastic-plastic material, shown in Fig. 2b, stress approaches a constant after a certain level of stress. However, stress in a quasi-brittle material gradually decreases peak strength. A softening type stress-strain curve as shown in Fig. 2c is usually observed with quasibrittle material such as concrete and ceramics.
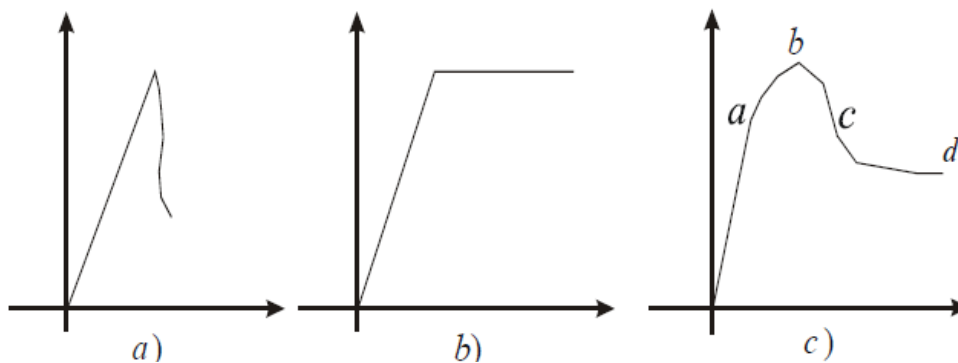


**Figure 1:** Stress –strain rock behavior

The energy principle can be used to describe crack propagation in a non-linear material, which can be non-linear elastic, elastic-plastic or quasi-brittle. In a linear elastic material, any propagation of a crack means catastrophic failure of the material. However, in a nonlinear material, a crack may steadily propagate until it reaches a critical length. The behavior of Fig. 2c in many cases is observed in laboratory and field reservoir rock. Rock commonly exhibits elastic brittle behavior at a low confining stress. Upon unloading, the deformation is completely recovered and follows the original stressstrain path if a rock has not broken. At higher confining stress, a brittle-ductile transition material behavior occurs. Once the elastic deformation reaches yield, the material begins to deform plastically. Upon unloading, the plastic deformation is not recovered.

## 2.3   In-situ stress

*Before drilling*, the state of stresses at any point in the subsurface are called in-situ stresses, which are perpendicular to each other. These are vertical stress is the overburden, ($\sigma_v$) and the maximum and minimum horizontal stresses are $\sigma_H$ and $\sigma_h$, respectively. Figure 3 illustrates this.
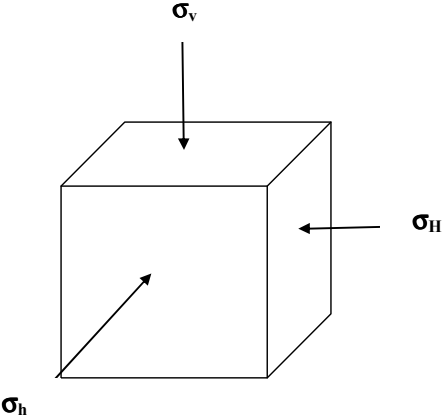


**Figure 2:** In-situ state of stress before drilling

*During drilling*, the earlier mentioned in-situ stresses are redistributed and concentrated around the wellbore. These are called stress concentrations. Figure 4 illustrates the components of the stresses.
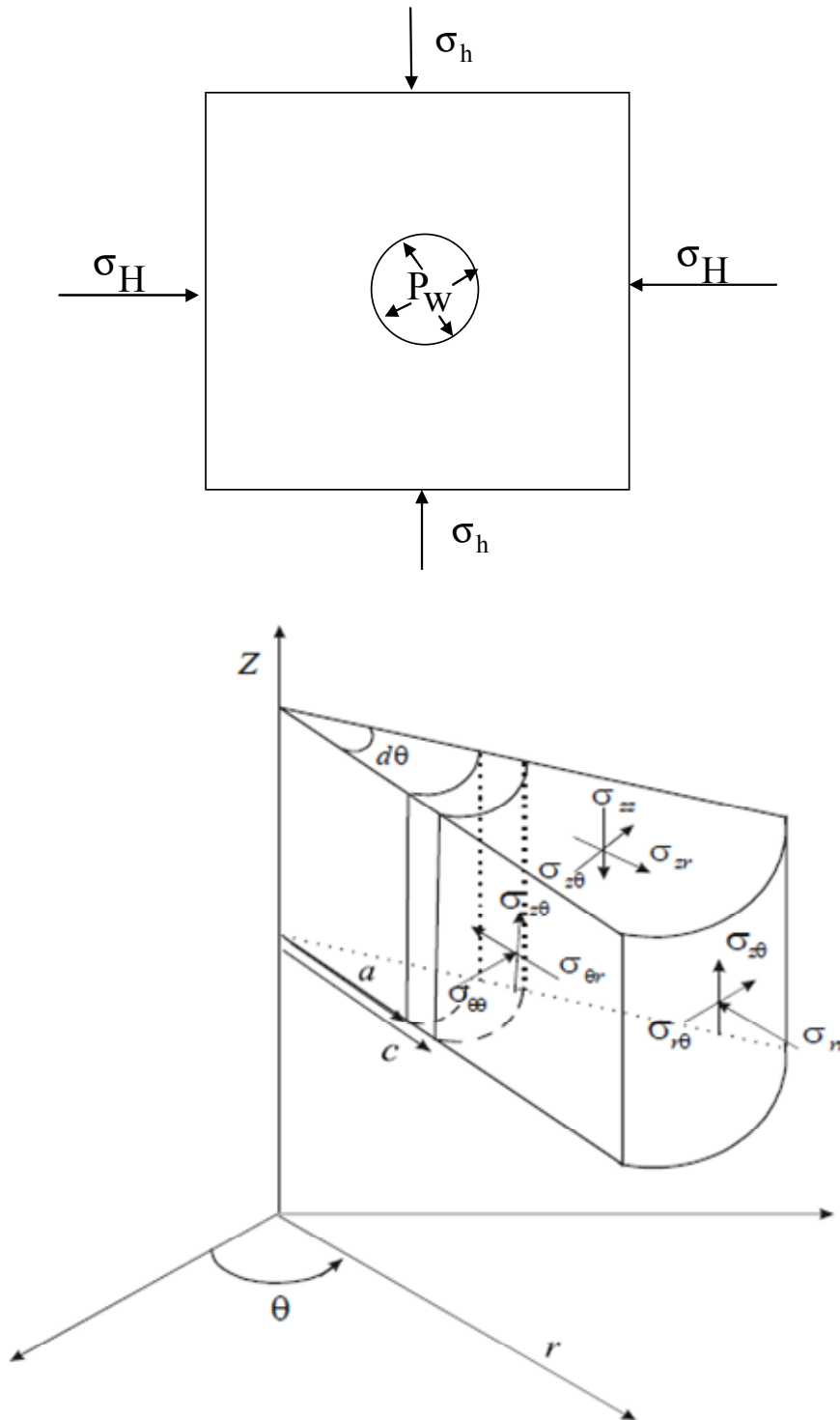
**Figure 3:** Stress concentration around a wellbore after drilling

Kirsch solved the stress concentrations around a wellbore loaded with anisotropic maximum and minimum horizontal stresses, and vertically with an overburden given in the following section.

# Chapter 3 Stresses around borehole and failure mechanism

This chapter describes the stress around a borehole, the mathematics of stress transformation, and also the major failure mechanisms applicable for the modeling of the failure of intact rocks. It reviews existing fracture initiation models. The review helps us to have a more complete knowledge of the subject matter and also prepares us for chapter 4.

## 3.1    Stresses around boreholes

The stress distribution around a circular hole in an infinite plate in one-dimensional tension was first published by Kirsch and was hence called the Kirsch equations. The Kirsch equations apply to a vertical borehole with unequal far-field stress.

**Stress transformation**

Assuming that the principal stresses are the vertical stress $\sigma_v$, and the major and minor horizontal stresses are $\sigma_H$ and $\sigma_h$ respectively, we can futher assume that $\sigma_v$ is parallel to the z'-axis while $\sigma_H$ and $\sigma_h$ are parallel to the x'- and y'-axis respectively. When a well is drilled, these principal stresses are re-distributed around the wellbore. If a well is drilled in a direction x-y-z, we can transform the in-situ principal stresses to this hole direction.

This is illustrated in the figure 5 below:
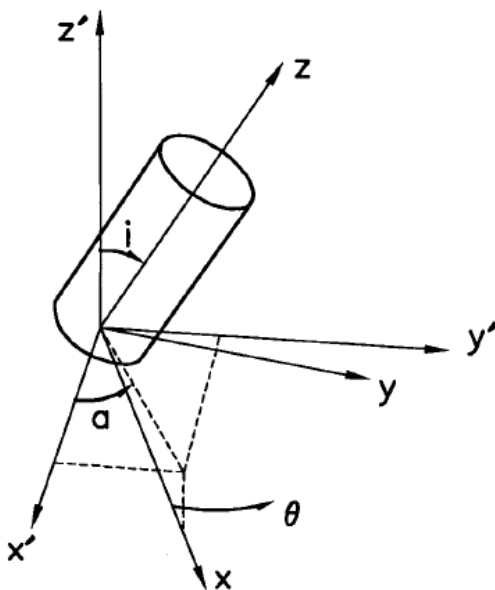


**Figure 4:**  Stress transformation (Fjaer et al[3])

A transformation from (x',y',z') to (x,y,z) can be obtained by a rotation 'a' around the z'-axis, and a rotation 'i' around the y'-axis. Where 'a' = i= 0 for a vertical well, a= 90, i=90 for a horizontal well drilled in the direction of $\sigma_h$, and a= 0, i=90 for a horizontal well drilled in the direction of $\sigma_H$.

Using this knowledge, we can compute the direction cosines using

$$l_{xx'} = \cos a \cos i, \quad l_{xy'} = \sin a \cos i, \quad l_{xz'} = -\sin i, \quad l_{yx'} = -\sin a, \quad l_{yy'} = \cos a, \quad l_{yz'} = 0,$$

$$l_{zx'} = \cos a \sin i, \quad l_{zy'} = \sin a \sin i, \quad l_{zx'} = \cos i \tag{3.1}$$

The formation stresses $\sigma_H, \sigma_h \, and \, \sigma_v$ expressed in the (x,y,z) coordinate system becomes:

$$\sigma_{xx} = l_{xx'}^2 \sigma_H + l_{xy'}^2 \sigma_h + l_{xz'}^2 \sigma_v, \tag{3.2}$$

$$\sigma_{yy} = l_{yx'}^2 \sigma_H + l_{yy'}^2 \sigma_h + l_{yz'}^2 \sigma_v \tag{3.3}$$

$$\sigma_{zz} = l_{zx'}^2 \sigma_H + l_{zy'}^2 \sigma_h + l_{zz'}^2 \sigma_v \tag{3.4}$$

$$\tau_{xy} = l_{xx'} l_{yx'} \sigma_H + l_{xy'} l_{yy'} \sigma_h + l_{xz'} l_{yz'} \sigma_v \tag{3.5}$$

$$\tau_{yz} = l_{yx'} l_{zx'} \sigma_H + l_{yy'} l_{zy'} \sigma_h + l_{yz'} l_{zz'} \sigma_v \tag{3.6}$$

$$\tau_{xz} = l_{zx'} l_{xx'} \sigma_H + l_{zy'} l_{xy'} \sigma_h + l_{zz'} l_{xz'} \sigma_v \tag{3.7}$$

## 3.2    The Kirsch Equations

Referring to Figure 4, Kirsch[3] has derived the stresses concentrations around a well bore and given as:

$$\sigma_r = \frac{\sigma_{xx}+\sigma_{yy}}{2}\left(1-\frac{R_w^2}{r^2}\right)+\frac{\sigma_{xx}-\sigma_{yy}}{2}\left(1+3\frac{R_w^4}{r^4}-4\frac{R_w^2}{r^2}\right)cos2\theta + \tau_{xy}\left(1+3\frac{R_w^4}{r^4}-\right.$$
$$\left. 4\frac{R_w^2}{r^2}\right)sin2\theta + P_w\frac{R_w^2}{r^2}$$

(3.8)

$$\sigma_\theta = \frac{\sigma_x^o+\sigma_y^o}{2}\left(1+\frac{R_w^2}{r^2}\right)-\frac{\sigma_x^o-\sigma_y^o}{2}\left(1+3\frac{R_w^4}{r^4}\right)cos2\theta - \tau_{xy}^o\left(1+3\frac{R_w^4}{r^4}\right)sin2\theta - $$
$$P_w\frac{R_w^2}{r^2}$$

(3.9)

$$\sigma_z = \sigma_z^o - v_{fr}\left[2(\sigma_x^o-\sigma_y^o)\frac{R_w^2}{r^2}cos2\theta + 4\tau_{xy}^o\frac{R_w^2}{r^2}sin2\theta\right] \qquad (3.10)$$

$$\tau_{r\theta} = \frac{\sigma_x^o-\sigma_y^o}{2}\left(1-3\frac{R_w^4}{r^4}+2\frac{R_w^2}{r^2}\right)sin2\theta + \tau_{xy}^o\left(1-3\frac{R_w^4}{r^4}+2\frac{R_w^2}{r^2}\right)cos2\theta$$

(3.11)

$$\tau_{\theta z} = \left(-\tau_{xz}^o sin\theta + \tau_{yz}^o cos\theta\right)\left(1+\frac{R_w^2}{r^2}\right) \qquad (3.12)$$

$$\tau_{rz} = \left(\tau_{xz}^o cos\theta + \tau_{yz}^o sin\theta\right)\left(1-\frac{R_w^2}{r^2}\right) \qquad (3.13)$$

At the borehole, $r = R_w$ and these equations reduce to

$$\sigma_r = P_w \qquad (3.14)$$

$$\sigma_\theta = (\sigma_x^o + \sigma_y^o - P_w) - 2(\sigma_x^o - \sigma_y^o)cos2\theta - 4\tau_{xy}^o\ sin2\theta \qquad (3.15)$$

$$\sigma_z = \sigma_z^o - 2v_{fr}(\sigma_x^o - \sigma_y^o)cos2\theta - 4v_{fr}\tau_{xy}^o sin2\theta \quad \text{(Plain strain)} \qquad (3.16a)$$

$$\sigma_z = \sigma_z^o \qquad \qquad \text{(Plain stress)} \qquad (3.16b)$$

$$\tau_{r\theta} = 0 \qquad (3.17)$$

$$\tau_{\theta z} = -\tau_{xz}^o sin\theta + \tau_{yz}^o(\sigma_x^o - \sigma_y^o)cos\theta \qquad (3.18)$$

$$\tau_{rz} = 0 \qquad (3.19)$$

## 3.3    Principal Stresses

19

Knowing the stresses at the borehole, we can compute the principal stresses using:

$$\sigma_1 = \sigma_r = P_w \qquad (3.20)$$

$$\sigma_{2,3} = \frac{1}{2}(\sigma_z + \sigma_\theta) \pm \frac{1}{2}\sqrt{[(\sigma_\theta - \sigma_z)^2 + 4\tau_{\theta z}^2]} \qquad (3.21)$$

After computing, we re-arrange such that $\sigma_1 > \sigma_2 > \sigma_3$.

## 3.4 Failure Mechanisms

Rocks can fail by two main mechanisms: tensile failure and shear failure.

### 3.4.1 Tensile failure and criterion

Tensile failure occurs when the effective stress across some plane in a rock exceeds a critical limit[3]. For rocks, this limit is the tensile strength To. The tensile strength is a characteristic property of a rock. The tensile strength is very sensitive to the presence of cracks. The presence of cracks reduces the tensile strength of the rock.

When a rock fails due to tensile failure, it normally splits along one or very few fracture plane. This fracture plane often originate from existing cracks. The highest probability for further damage of the rock is at the perimeter of the large cracks. As a result, the largest crack will grow increasingly faster than the other cracks and rapidly split the sample[3].

A fracture initiates in a rock when the applied tensile stress exceeds a critical value which is an intrinsic property of the rock. Fracture initiation modelling requires a continuum mechanics approach while fracture propagation requires a rock mechanics approach. Several models have been proposed for fracture initiation. From a macroscopic point of view, it is observed that fracturing is related to tensile failure. It is believed that the condition for tensile failure for a porous and permeable material is that: 'The effective stresses must exceed the tensile strength of the material[3].

$$\sigma - P_f < -T_o. \tag{3.22}$$

Where $P_f$ is the pore pressure and $T_o$ is the tensile strength of the porous material, and $\sigma$ is the tensile stress acting on the rock. When a fracture has been formed, either naturally or man-made, it assumed that the tensile strength is zero such that the criteria for re-opening of existing fractures become:

$$\sigma - P_f < 0. \tag{3.23}$$

For isotropic rocks, this condition will first be fulfilled for the least principal stress, such that the criterion becomes

$$\sigma'_3 = -T_o \tag{3.24}$$

### 3.4.2   Shear failure and criterion

Shear failure occurs when the shear in some plane in the sample is sufficiently high. Eventually, a fault zone will develop along the failure plane and the two sides of the plane will move relative to each other in a frictionless process[3]. Since the frictional force that acts against the relative motion of the two sides depends on the force pressing the two sides together, the critical shear stress for which shear failure occurs depends on the normal stress acting over the failure plane[3].

$$\tau = f(\sigma)$$

This assumption is called Mohr's hypothesis.

## 3.5 Fracture Initiation Models

This section simply reviews the fracture initiation models proposed by other authors in literature and the governing mechanism behind the models. No model development will be attempted here.

### 3.5.1 Linear Elastic models

The Kirsch equation is mostly used to model fracture initiation in the oil industry. The kirsch equation is a linear elastic models which assumes that the borehole is penetrating or non-penetrating. The penetrating model assumes that fluid flows into the formation such that at the well bore the formation pressure equals the well bore pressure, while the non-penetrating model assumes that a mud cake is formed which prevents filtrate losses. The penetrating model applies to stimulation jobs while the non-penetrating model applies to drilling operations.

### *3.5.1.1 Penetrating fracture model*

Recall that when the vertical borehole is along a principal stress direction, all the shear stresses will varnish such that $\sigma_r, \sigma_\theta$ and $\sigma_z$ becomes the principal stresses.

This model states that the borehole will fracture when the minimum in-situ stress is exceeded[7]. Recall the criterion for fracture initiation as:

$$\sigma'_\theta = -T_o \tag{3.25}$$

where $\sigma'_{\theta,min} = 3\sigma_h - \sigma_H - P_w - P_o$. Thus the failure criteria becomes

$$3\sigma_h - \sigma_H - P_w - P_o = -T_o. \tag{3.26}$$

For a penetrating case, $P_o = P_w$.

If we assume hydrostatic stress state, $\sigma_h = \sigma_H$, and ignoring the tensile strength, $T_o = 0$, the failure criterion simplifies to

$$P_W{}^{frac} = \sigma_h. \tag{3.27}$$

It states that fracturing will occur when the well bore pressure exceeds the minimum in-situ stress. It is applicable for well operations such as hydraulic fracturing and stimulation. It requires the use of pure fluids such as water, acids or diesel. This model works well for predicting fracture initiation when pure fluids are used[7].

If we assume hydrostatic stress state , $\sigma_h = \sigma_H$, and if the borehole is assumed to be fully permeable, $P_o = P_w$, and the pressurisation rate slow enough to ensure steady state condition during pumping, the tangential stress becomes[3]

$$\sigma_\theta = 2\sigma_h - P_w + 2\eta(P_w - P_{fo}). \tag{3.28}$$

where $\eta$ is the poroelastic stress coefficient, $\eta = \frac{(1-2v_{fr})}{2(1-v_{fr})}\alpha$ and $\alpha$ =biot constant

Using this expression and the condition for failure

$$\sigma_\theta - P_o = -T_o, \tag{3.29}$$

We obtain the following model for fracture initiation

$$P_W{}^{frac} = \frac{2\sigma_h - 2\eta P_{fo} + T_o}{2 - 2\eta}. \tag{3.30}$$

Fjaer et al[3] refers to this as the **lower pressurisation limit** for fracture initiation.

### 3.5.1.2 Non Penetrating model

During drilling operations, the fluids build up a filter cake barriers such that the well bore pressure is different from the formation pressure at the bore hole wall. The Kirsch equation in this case assumes linear elasticity and perfect mud cake (zero filtrate loss). This result of these assumptions is an underestimation of the fracture pressure[5].

Recall the criterion for fracture initiation as:

$\sigma'_\theta = -T_c$ where $\sigma'_{\theta,min} = 3\sigma_h - \sigma_H - P_w - P_o$. Thus the failure criteria becomes

$$3\sigma_h - \sigma_H - P_w - P_o = -T_c. \tag{3.31}$$

For a non-penetrating case, $P_o \neq P_w$.

If we assume hydrostatic stress state, $\sigma_h = \sigma_H$, and ignoring the tensile strength , $T_o = 0$, the failure criterion described by the kirsch equation simplifies to

$$P_w{}^{frac} = 2\sigma - P_o \tag{3.32}$$

If however we choose not to neglect the tensile strength, the condition for the initiation of hydraulic fracture is reached when

$$P_w{}^{frac} = 2\sigma - P_o + T_o. \tag{3.33}$$

Fjaer et al[3] refers to this as the **upper pressurisation limit**.

For a vertical well (principal stresses are $\sigma_r, \sigma_\theta, \sigma_z$) in an anisotropic reservoir, $(\sigma_h \neq \sigma_H)$
The tangential stress is

$$\sigma_\theta = 3\sigma_h - \sigma_H - P_w. \tag{3.34}$$

Thus, using the condition for failure

$\sigma_\theta - P_o = -T_o$, we get:

$$P_w{}^{frac} = 3\sigma_h - \sigma_H - P_o + T_o. \tag{3.35}$$

24

Observe that the largest horizontal stress reduces the upper stability limit for the well pressure. Therefore, anisotropy in the formation around the wellbore reduces the region where the borehole is stable.

Daneshy[1] presented the criterion for fracture initiation when one principal stress is in the direction of the borehole axis. Under this condition, only vertical or horizontal fractures can initiate at the borehole. He presented the criteria for vertical fracture initiation as

$$P_w = P_o + \frac{\sigma_t - 3\sigma_{22} + \sigma_{11}}{2 - 2\eta} \tag{3.36}$$

When $3\sigma_{22} = 3\sigma_h$ and $\sigma_{11} = \sigma_H$, this is the same as the **lower pressurisation limit** described by Fjær at al.

For horizontal fracture initiation, the model applicable is

$$P_w = P_o + \frac{\sigma_t - 3\sigma_{33}}{1 - \eta} \tag{3.37}$$

where $\eta$ is the poro-elasticity stress coefficient defined earlier as $\eta = \frac{(1 - 2v_{fr})}{2(1 - v_{fr})} \alpha$

Ong and Roegiers[8] presented a model for fracture initiation which includes the effect of anisotropy. The model assumes linear elastic theory but it neglects chemical, plastic, potential (temperature and fluid flow), and other time-dependent effects. The model they presented for fracture initiation is also based on the tensile failure criterion and it is presented as:

$$P_w{}^{frac} = \sigma_{xx} + \sigma_{yy} - 2(\sigma_{xx} - \sigma_{yy})\cos2\theta - 4\tau_{xy}\sin2\theta - \frac{(\sigma'_z)^2 - (\tau_{xy})^2 - \sigma'_s\sigma'_{zz}}{\sigma'_s - \sigma'_{zz}} - P_f.$$

$$\tag{3.38}$$

The expression indicates that each angle $\theta$ will have a corresponding value of $P_w{}^{frac}$ that satisfies the tensile failure criterion. The location of the fracture initiation on the borehole wall would then be determined by minimising $P_w$ with respect to angle $\theta$, or by setting $\frac{\partial P_w}{\partial \theta} = 0$ and

finding the roots of the resulting equation. The root that minimises $P_w$ $(\theta_m)$ is the borehole wall location where failure will initiate. The critical wellbore pressure required to initiate tensile fracture at the borehole wall is then found by substituting $\theta_m$ into the above equation. The critical wellbore pressure is constrained by the relation $P_w \geq -T_o + P_f$ because at $P_w = -T_o + P_f$, the effective stress $\sigma'_r$ becomes equal to the tensile strength of the formation and failure along the radial direction dominates. Thus, we cannot have a wellbore pressure less than that specified by $P_w = -T_o + P_f$.

The fracture inclination is determined by: $\gamma = \frac{1}{2}\tan^{-1}\frac{2\tau_{\theta z}}{\sigma_{\theta z}-\sigma_{zz}}$ (3.39)

Kårstad and Aadnoy[9] presented a 3-dimensional fracture model for well path optimisation. They reported that the maximum hole stability could be obtained at intermediate orientations, and that they are controlled by the magnitude and direction of the in-situ stresses. The fracture pressure may have its maximum value at a non-zero inclination. For unequal horizontal in-situ stresses and a well drilled in a direction different from the major horizontal in-situ stresses, the behaviour of the borehole principal stresses and shear stresses will result in a maximum fracture pressure at a non-zero inclination. They therefore presented the general fracture equation:

$$P_w = \sigma_{xx} + \sigma_{yy} - 2(\sigma_{xx} - \sigma_{yy})cos2\theta - 4\tau_{xy}sin2\theta - \frac{(\tau_{xy})^2}{\sigma_{zz}-P_f} - P_f$$ (3.40)

The inclination of maximum fracture is computed numerically. The absolute maximum fracture pressure for a well can be determined analytically by the singularity of the equation $\frac{\partial P_w}{\partial \theta} = 0$. The inclination can be determined by using

$$\gamma = \sin^{-1}\left(\sqrt{\frac{(\sigma_H-\sigma_h)(\sigma_v-P_f)}{(\sigma_v-\sigma_h)(\sigma_H-P_f)}}\right)$$ (3.41)

Zhang et al[10], presented two fracture initiation pressure models with 3-dimensional stress state that are based on tensile failure mechanism and shear failure mechanism respectively.

The fracture pressure based on tensile failure mechanism is based on the assumption that fracturing occurs when the minor principal effective stress becomes negative with a magnitude exceeding the tensile strength of the rock. They presented the minor principal effective stress as $\sigma_\theta = 3\sigma_h - \sigma_H - P_w$, which obviously ignores the pore pressure.

He therefore presented the fracture pressure obtained using $\sigma_\theta = -T_o$ as

$$P_w = 3\sigma_3 - \sigma_2 + T_o. \tag{3.42}$$

They pointed out that if the original minor principal effective stress becomes negative with a magnitude exceeding the tensile strength of the rock, the rock around the borehole may reach undrained shear failure before the minor principal effective stress become negative or reach the tensile strength of the rock. On shear failure, the difference between the radial and the circumferential stresses remain equal to $2S_u$. i.e, $\sigma_r - \sigma_\theta = 2S_u$ (*where* $2S_u$ *is the undrained shear strength*). They therefore proposed a maximum fracture pressure based on tensile failure mechanism as:

$$P_{w,max} = \frac{1}{2}(3\sigma_3 - \sigma_2) + S_u. \tag{3.43}$$

Therefore, if the calculated fracture pressure based on tensile failure mechanism exceeds $P_{w,max}$, then the fracturing is controlled by shear failure mechanism. The shear failure mechanism assumes that fracture occurs when the stress in a rock intercepts the mohr-coulomb strength envelop which is described as $(\sigma_r - \sigma_\theta) = (\sigma_r + \sigma_\theta)sin\varphi + 2C cos\varphi$.

Substituting the polar expressions for $\sigma_r$ *and* $\sigma_\theta$ gives the expression for the fracture based on the shear failure mechanism[10] as:

$$P_{w,max} = \frac{1}{2}(3\sigma_3 - \sigma_2)(1 + sin\varphi) + C cos\varphi + \frac{\sigma_t}{2}(1 + sin\varphi). \tag{3.44}$$

Mitchell et al 2006 gave a possible explanation for fracturing due to yielding. They explained that the increase of the plastic shear failure zone created shear bands or an unstable state

around the cavity. This leads to localised micro-scale cracks and the injected fluids or gas can penetrate into the crack to produce local tensile stresses at the crack tips.

## 3.5.2 Elasto-plastic model

Aadnoy et al[7], identified the variation in fracture pressure depending on the quality of the mud and also found that the mudcake behaves plastically. They therefore proposed an elasto-plastic model of fracture initiation which assumes a thin plastic layer of mud cake, followed by a linearly elastic rock. This model assumes that when a fracture opens, the mud cake does not split up but deforms plastically thus maintaining the barrier. This thus accounts for the higher fracture pressure that is normally observed. Recall that the Kirsch non-penetrating model underestimates the fracture pressure. This model which is also a non-penetrating model, gives a more accurate description of the fracture initiation pressure.

The conventional continuum mechanics model (based on Kirsch equations) is based on only the stress concentration around a borehole and does not include the effect of well size and of the drilling fluid. The so-called Kirsch equation is based on linear elasticity and assumes either penetrating or fully non-penetrating conditions. In reality, a fluid barrier is not perfectly non-penetrating. It is interesting to observe that the laboratory measurements using different fluids gave considerably higher fracturing pressures than predicted by the Kirsch equation. The Kirsch equations therefore underestimate fracture pressures.

This fact was confirmed by experiments performed by Addis and Barton[11] who concluded that the application of linear elasticity and Mohr–Coulomb failure criterion under-predicts the fracturing pressure, and also claimed that the measured fracture pressure is four to eight times the theoretically obtained value. Guenot and Santarelli[12] and Papanastasiou[13] came up with similar conclusions as well.

The elasto-plastic model assumes two distinct regions: a plastic region at the inner wall of the borehole and the rock outside behaves linearly elastic. This elasto-plastic model is based on the assumption that the fluid barrier, and possibly a part of the borehole wall, behaves plastically. In the linear elastic model, the tensile tangential stresses change linearly with changing borehole pressure. In the plastic model, the tensile stresses are not fully developed because the barrier and the wall have essentially a compressive state.

For the plastic region, failure occurs when the yield strength is reached, or when sufficient deformation has taken place to reduce the thickness of the barrier.

The elastoplastic model is shown pictorially below:
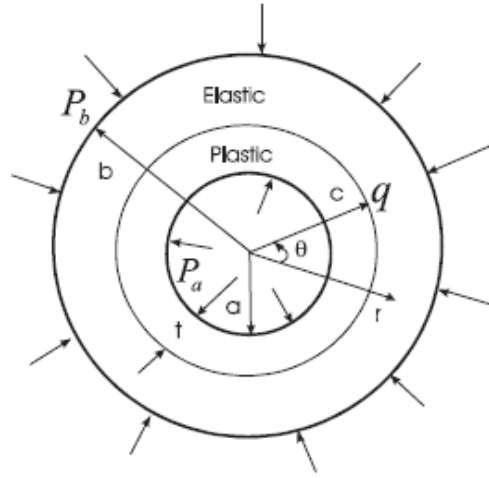


**Figure 5:** The elasto-plastic modell (Aadnoy and Belayneh, 2004)

A plastic zone exists at the inner wall of the borehole. The rock outside behaves linearly elastic. The model is derived assuming borehole pressure $P_a$ as the inner boundary condition for the plastic zone, and a pressure match q at the plastic/elastic interface, whereas the in situ stresses $P_b$ act as the external boundary condition at infinity. The model derived is a continuum mechanics model only valid for an intact borehole up to the point of initial failure. The elasto-plastic model reads:

$$P_{wf} = 3\sigma_h - \sigma_H - P_o + \sigma_t + \frac{2Y}{\sqrt{3}} In\left(\frac{c}{a}\right)$$ (3.45)

If we introduce the thickness of the plastic zone as t, c = t+a, we get:

$$P_{wf} = 3\sigma_h - \sigma_H - P_o + \sigma_t + \frac{2Y}{\sqrt{3}} In\left(1 + \frac{t}{a}\right)$$ (3.46)

This gives the elasto-plastic fracture initiation pressure for a vertical well with an anisotropic stress state.

For an isotropic stress state, the model reduces to

$$P_w = 2\sigma - P_o + \frac{2\sigma_y}{\sqrt{3}} In\left(1 + \frac{t}{a}\right)$$ (3.47)

Aadnoy and Belayneh[13], pointed out that the fracture equation used in the oil industry and derived from the kirsch equation is not useful for the analysis of load history. In addition, they do not include temperature effects neither do they consider the change in stresses that occur during fracturing. Since changes in stresses at the borehole occur during fracturing, the local stress field is also affected in 3-dimensions which imply a coupling between the stresses. This coupling is taken into account with Poisson's ratio. Their new model for fracture initiation thus includes load history, temperature, and Poisson's ratio. The general fracturing model for arbitrary wellbore inclination allows for the in-situ stresses to be transformed in space in an x-, y- coordinate system. The model is:

$$P_{wf} = \sigma_y + \frac{2(1+v)(1-v^2)}{3v(1-2v)+(1+v)^2}\left\{\frac{3}{2}\sigma_x - \sigma_y - P_o\right\} + P_o + \frac{(1+v^2)}{3v(1-2v)+(1+v)^2} E\kappa(T - T_{init}) +$$
$$\frac{2Y}{\sqrt{3}}In\left(1 + \frac{t}{a}\right)$$

$$(3.48)$$

where Y is the yield strength of filter cake particles, $N/m^2$.

For isotropic stress loading, there are equal normal stresses around the wellbore wall. The initial stress condition is simply equal to the in-situ stresses before the hole was drilled, σ. The model for isotropic stress loading which includes the elasto-plastic mudcake barrier effect and temperature effect is

$$P_{wf} = \sigma + P_o + \frac{(1+v)(1-v^2)}{3v(1-2v)+(1+v)^2}\left\{\sigma - 2P_o\right\} + \frac{(1+v^2)}{3v(1-2v)+(1+v)^2} E\kappa(T - T_{init}) +$$
$$\frac{2Y}{\sqrt{3}}In\left(1 + \frac{t}{a}\right)$$

$$(3.49)$$

For anisotropic loading, the two normal stresses acting on the borehole wall have different magnitudes $\sigma_H$ and $\sigma_h$, which are the maximum and minimum horizontal stresses respectively. Both of these cannot be the initial condition simultaneously because the borehole is filled with fluid. At the position of fracture initiation, the initial stress state is $\sigma_H$ and it will thus be chosen as the initial condition. The fracturing equation thus becomes:

$$P_{wf} = \sigma_H + P_o + \frac{2(1+v)(1-v^2)}{3v(1-2v)+(1+v)^2} \left\{ \frac{3}{2}\sigma_h - \sigma_H - P_o \right\} + \frac{(1+v^2)}{3v(1-2v)+(1+v)^2} E\kappa(T -$$

$$T_{init}) + \frac{2Y}{\sqrt{3}} ln\left(1+\frac{t}{a}\right)$$

<div align="right">(3.50)</div>

# Chapter 4 Fracture Mechanics

This chapter deals with fracture mechanics, and presents the supporting theories that will be used in the fracture propagation modeling work in the next chapter.

Fracture initiation and propagation mechanisms are basically tensile failure mechanisms. As a result, the failure criteria mentioned here will be focussed on the tensile failure criteria and other criteria that are relevant to this work.

There are three ways of applying a force to enable a fracture to propagate as illustrated in Figure 7:

- **Mode I** – Opening mode (a tensile stress normal to the plane of the fracture)
- **Mode II** – Sliding mode (a shear stress acting parallel to the plane of the fracture and perpendicular to the fracture front)
- **Mode III** – Tearing mode (a shear stress acting parallel to the plane of the fracture and parallel to the fracture front)



MODE I          MODE II          MODE III
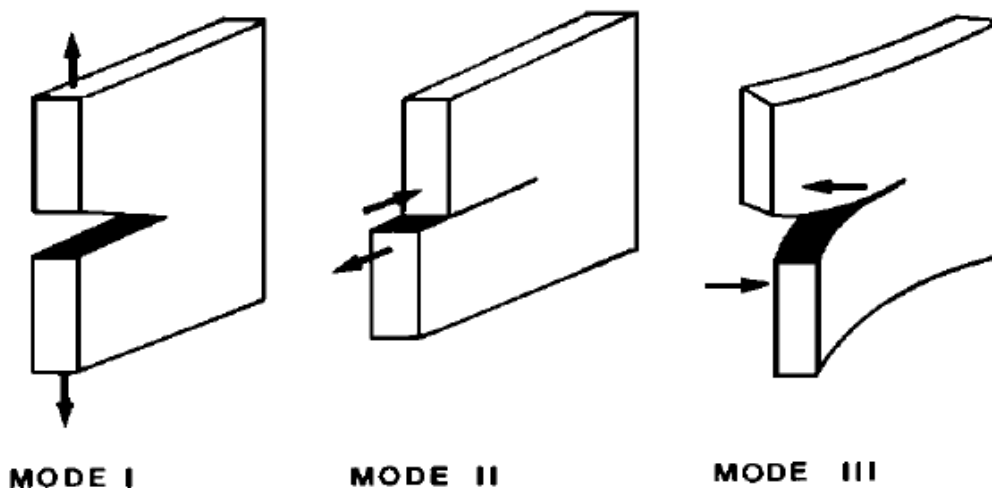
**Figure 6:** The three fracture modes (Wikipedia)

## 4.1 Stress intensity factor

Irwin and his colleagues developed a method of calculating the amount of energy available for fracture in terms of the asymptotic stress and displacement fields around a fracture front in a linear elastic solid. For a fracture experiencing tensile stress, this asymptotic expression for the stress field around a fracture tip is[3]

$$\sigma_{ij} \approx \left(\frac{K}{\sqrt{2\pi r}}\right) f_{ij}(\theta) \tag{4.1}$$
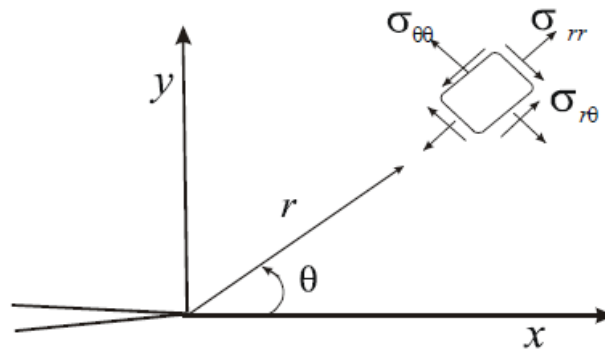


**Figure 7:** A plane elastic body with a crack

The functions $f_{ij}^{(I)}(\theta)$ define the angular dependence of the stress at the fracture tip.

$$f_{11}^{(I)}(\theta) = \cos\frac{\theta}{2}\left[1 - \sin\frac{\theta}{2}\sin\frac{3\theta}{2}\right] \tag{4.2}$$

$$f_{22}^{(I)}(\theta) = \cos\frac{\theta}{2}\left[1 + \sin\frac{\theta}{2}\sin\frac{3\theta}{2}\right] \tag{4.3}$$

$$f_{12}^{(I)}(\theta) = \cos\frac{\theta}{2}\sin\frac{\theta}{2}\cos\frac{3\theta}{2} \tag{4.4}$$

For plane strain conditions, $f_{33}^{(I)}(\theta) = v\left(f_{11}^{(I)}(\theta) + f_{22}^{(I)}(\theta)\right)$ \hfill (4.5)

while for plane stress, $f_{33}^{(I)}(\theta) = 0$. \hfill (4.6)

32

Note that $\upsilon = poisson\ ratio.$

$K_I$ is called the stress intensity factor for mode I loading. It is a measure of the stress singularity at the fracture tip. It is a function of the far field stress and the fracture length and is represented by: $\quad K_I = -y\sigma\sqrt{\pi a}$ \hfill (4.7)

y  is a dimensionless constant dependent on the geometry. For a slit in a plane described earlier, y= 1 while for a penny shaped fracture with radius 'a' in an infinite medium, y = 2/π.

where $\sigma_{ij}$ are the Cauchy stresses, $r$ is the distance from the fracture tip, $\theta$ is the angle with respect to the plane of the fracture, and $f_{ij}$ are functions that are independent of the fracture geometry and loading conditions. Irwin called the quantity $K$ the *stress intensity factor*. Since the quantity $f_{ij}$ is dimensionless, the stress intensity factor can be expressed in units of   MPa–m^0.5.

## 4.2    Fracture propagation Criteria

After a fracture has been initiated, changes in the stress state of the rock can cause the fracture to grow or even close, depending on the orientation and sign of the principal stresses relative to the orientation of the fracture. Once the borehole is fractured, the fracture initiation models and criteria are no longer valid.

In the near borehole region, the fracture propagation is a complex issue due to stress concentration effects[5]. The tangential stress is now controlled by the in-situ stresses at the tip of the fracture.

Once the fracture is outside the stress propagation region (about 10 borehole radii), fracture propagation is controlled by the least in situ stress.

### 4.2.1   The Griffith criterion

The Griffith criterion is widely accepted in the industry for modelling fracture propagation.

**Historical review:** A. A. Griffith invented Fracture mechanics during World War I to explain the failure of brittle materials[6]. Griffith's work was motivated by two contradictory facts:

- The stress needed to fracture bulk glass is around 15,000 psi.
- The theoretical stress needed for breaking atomic bonds is approximately 1,500,000 psi.

Griffith introduced an artificial flaw in his experimental specimens as shown in fig. 9.
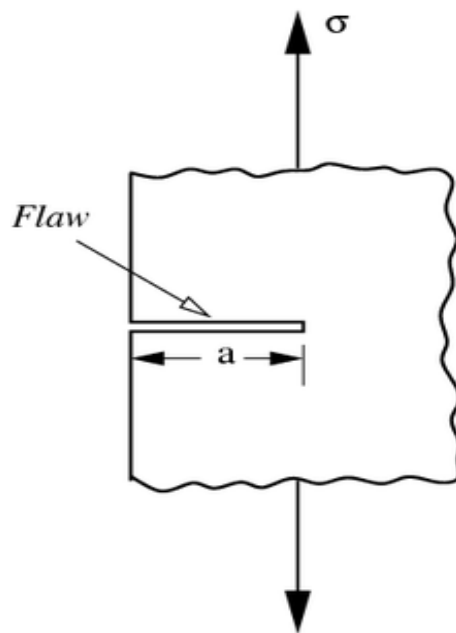


**Figure 8:** Griffith specimen

The experiments showed that the product of the square root of the flaw length ($a$) and the stress at fracture ($\sigma_f$) was nearly constant, which is expressed by the equation:

$$\sigma_f \sqrt{a} \approx C \qquad (4.5)$$

Linear elasticity theory predicts that stress (and hence the strain) at the tip of a sharp flaw in a linear elastic material is infinite. To avoid that problem, Griffith developed a thermodynamic approach to explain the relation that he observed.

The growth of a fracture requires the creation of two new surfaces and hence an increase in the surface energy. Griffith found an expression for the constant $C$ in terms of the surface energy of the fracture by solving the elasticity problem of a finite fracture in an elastic plate.

34

Griffith found that

$$C = \sqrt{\frac{2E\gamma}{\pi}}$$  (4.6)

where $E$ is the Young's modulus of the material and $\gamma$ is the surface energy density of the material

For the simple case of a thin rectangular plate with a fracture perpendicular to the load Griffith's theory becomes:

$$G = \frac{\pi \sigma^2 a}{E}$$  (4.7)

where $G$ is the strain energy release rate, $\sigma$ is the applied stress, $a$ is half the crack length, and $E$ is the Young's modulus. The strain energy release rate can otherwise be understood as the rate at which energy is absorbed by growth of the crack.

However, we also have that:

$$G = \frac{\pi \sigma_f^2 a}{E}$$  (4.8)

***Fracture propagation criterion:*** If $G \geq Gc$, this is the criterion for which the fracture will

begin to propagate.

This simplifies to $\sigma \geq \sigma_t$ where $\sigma_t$ is the tensile strength of the rock.

In most rock mechanics application, the Griffith criteria can be stated as follows:
*''When the tensile stress at the tip of a* fracture *exceeds a value, which is characteristic of the rock, the* fracture *will grow and the failure process would be initiated''.*

Mathematically, it can be written as[3]

$$(\sigma'_1 - \sigma'_3)^2 = 8T_0(\sigma'_1 + \sigma'_3) \text{ if } (\sigma'_1 + 3\sigma'_3) > 0,$$  (4.9)

where $8T_o = C_o = $ Uniaxial compressive strength

$$\text{And } \sigma'_3 = -T_o \text{ if } (\sigma'_1 + 3\sigma'_3) < 0 \tag{4.10}$$

In terms of only one equation, the Griffith's criterion is $\tau^2 = 4T_o(\sigma' + T_o)$ (4.11)

### 4.2.2 Strain energy release rate

Irwin[6] was the first to observe that if the size of the plastic zone around a fracture is small compared to the size of the fracture, the energy required to grow the fracture will not be critically dependent on the state of stress at the fracture tip. In other words, a purely elastic solution may be used to calculate the amount of energy available for fracture.

The energy release rate for fracture growth or *strain energy release rate* may then be calculated the change in elastic strain energy per unit area of fracture growth, i.e.,

$$G = -\left[\frac{\partial U}{\partial a}\right]_P = -\left[\frac{\partial U}{\partial a}\right]_u \tag{4.12}$$

where $U$ is the elastic energy of the system and $a$ is the fracture length. Either the load $P$ or the displacement $u$ can be kept fixed while evaluating the above expressions.

Irwin showed that for a mode I fracture (opening mode) the strain energy release rate and the stress intensity factor are related by:

$$G = G_I = \begin{cases} \dfrac{K_I^2}{E} & \textit{Plane stress} \\ \dfrac{(1-v^2)K_I^2}{E} & \textit{Plane strain} \end{cases} \tag{4.13}$$

where $E$ is the Young's modulus, $v$ is Poisson's ratio, and $K_I$ is the stress intensity factor in mode I.

In this modification of Griffith's solids theory, a term called stress intensity replaced strain energy release rate and a term called fracture toughness replaced surface weakness energy. Both of these terms are simply related to the energy terms that Griffith used:

$$K_I = \sigma\sqrt{\pi a} \tag{4.14}$$

and

$$K_c = \sqrt{EG_c} \qquad \text{(for plane stress)} \tag{4.15}$$

$$K_c = \sqrt{\frac{EG_c}{(1-v^2)}} \qquad \text{(for plane strain)} \tag{4.16}$$

where $K_I$ is the stress intensity, $K_c$ the fracture toughness, and $v$ is Poisson's ratio. It is important to recognize the fact that fracture parameter $K_c$ has different values when measured under plane stress and plane strain

***Fracture propagation criterion:*** 'If the stress intensity factor $K_I$ exceeds a critical limit $K_c$ called the fracture toughness, the fracture will start to grow'. In other words, if $K_I \geq K_c$ the fracture will propagate.


### 4.2.3   Hillerborg's Failure Criteria:

Hillerborg's theory: The effective loading at the tip of the fracture should overcome the tensile strength of the rock at the tip. This is illustrated in the figure 10.
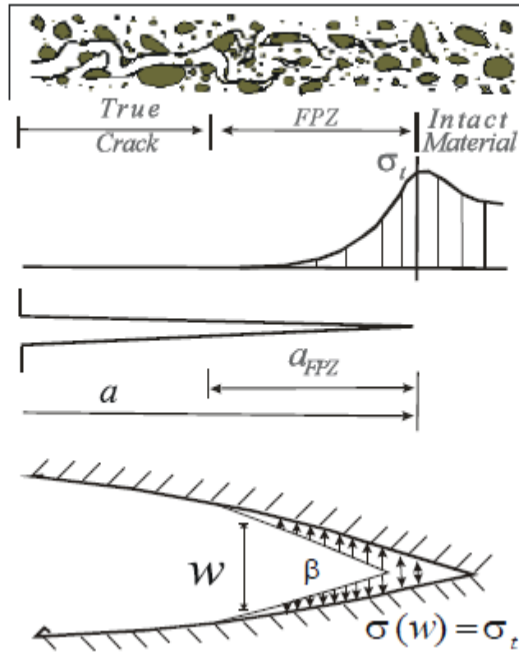
**Figure 9:** Fracture Process Zone in concrete, and Hillerborg's fictitious model

## 4.3 Fracture Pressure with Continuous Pumping

It has been reported both experimentally and from field observation that when fracturing occurs during continuous pumping, the fracture pressure builds up and drops continuously. This is illustrated by the figure 11[18].
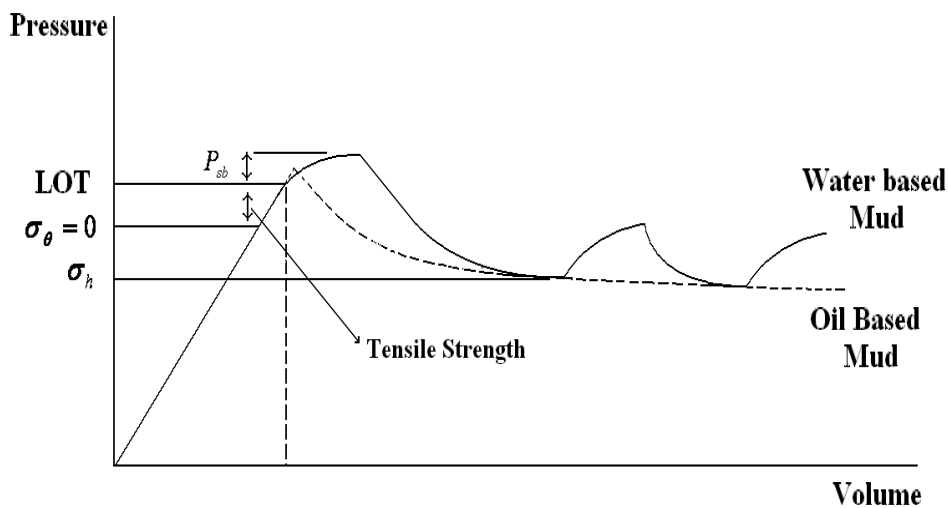


**Figure 10:** Fracture pressure behavior using oil based mud and water based mud

Aadnoy et al[18] presented a model for leak-off interpretation that includes evaluation after the borehole is fractured. The Kirsch equation based on continuum mechanics is valid for fracture

initiation. After a fracture has been initiated, the Kirsch equation becomes invalid and a fracture mechanics approach has to be used.

The fracture propagation pressure based on the Kirsch equation is $LOT = 3\sigma_h - \sigma_H - P_o + \sigma_{tensile}$

The above expression is valid up to the conventional leak-off point, but beyond leak-off the hole is fractured, and an elasto-plastic bridge model applies to ultimate failure[18]. Leak off points are defined as the point where the pressure vs volume/time plot deviates from a straight line. This is the point where the borehole actually fractures. This point is indicated as LOT in the figure above. Aadnoy et al[18] identified a *post-failure phase* which is observed after the borehole is fractured. They presented an argument for the *post-failure phase* fracture behaviour. They explained that solid particles in the mud form a bridge across the fracture which allows the pressure to increase further. At the maximum pressure $P_{sb}$, this bridge fails and the pressure drops as mud invades the fractures. This behaviour is observed for water based muds. Oil based drilling fluids behave differently. Often a more abrupt breakdown is seen, and the propagation pressure is constant with continuous pumping. This constant fracture propagation pressure is equal to the minimum horizontal in-situ stress. This effect is well known from drilling operations where it is known that with oil-based mud, it is often difficult to cure circulation losses. One mechanism attributed to this effect is wettability contrast between the rock and the drilling fluid, leading to low filtrate losses. We have, however, an additional plausible mechanism. To form a stable bridge of mud particles, a certain friction is required to make the bridge stable. In other words, too much lubricity between the particles let them slide instead of locking up as a bridge. It may be pointless to decrease lubricity to oil base muds. Instead we may use more angular particles which may lock up easier.

### 4.3.1 Previous laboratory fracturing experimental results

Belayneh[18] reported that the fracture build-up and drop-down pattern is not uniform even for a given core plug when different drilling fluids are used. The results of the experiment clearly show that the fluid properties also affect the pressure at which a fracture will be initiated and propagated.

The figures below show the result of fracture propagation experiments using three different drilling fluids: Glydril, Warp and Aphrons. Observe the different behaviour even when similar cores are used.

Figures 12, 13 and 14 show the pressure response of the fracturing and re-fracturing experiment with Glydril drilling fluid.
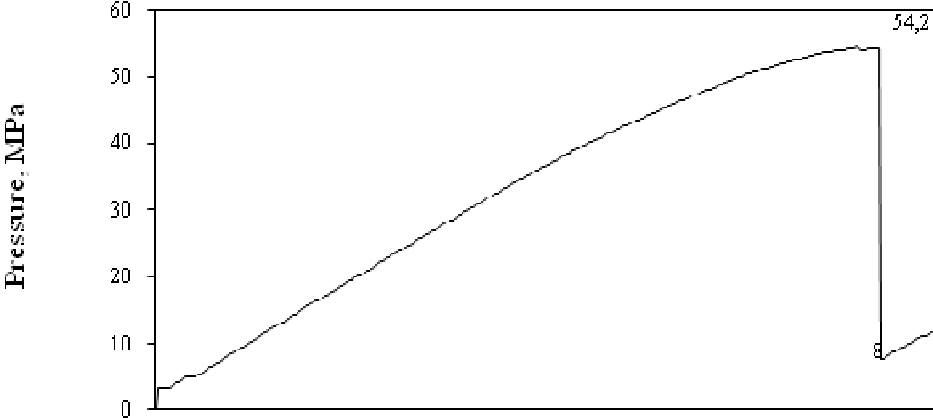


**Figure 11:** Glydril mud used for fracturing
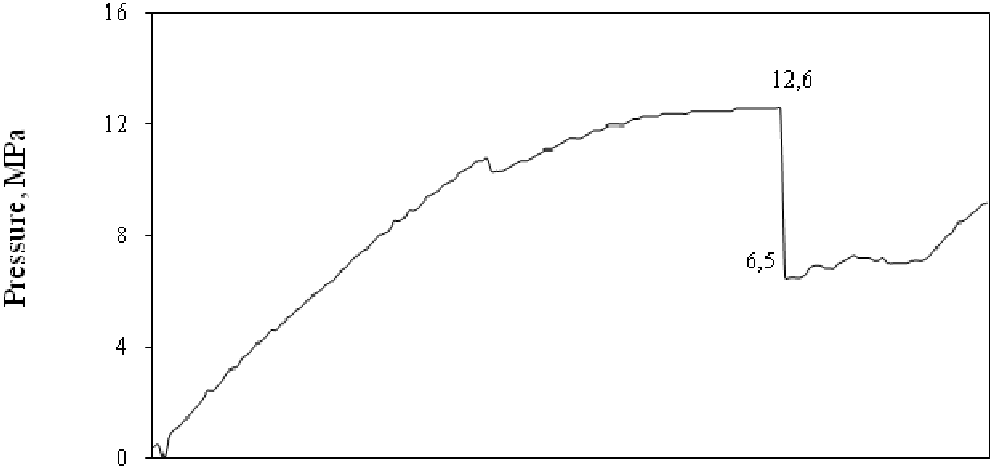


**Figure 12:** Glydril mud used for fracture reopening after 10 minutes
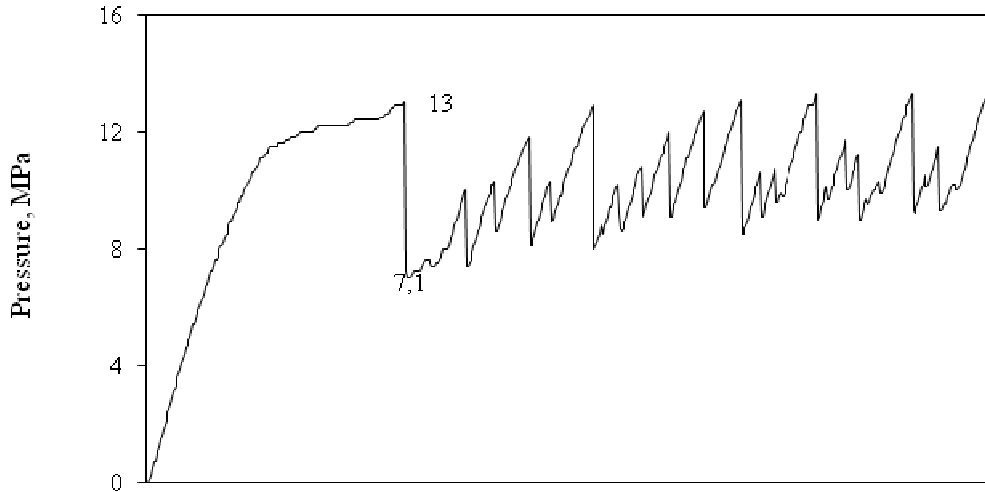
**Figure 13:** Glydril mud used for fracture reopening after 60 minutes

When the specimen was inspected after the experiment, multiple fractures was observed.

The experiment was repeated using a similar core but now using another mud called Warp drilling fluid. The result of the experiment is shown in figures 15, 16 and 17.



**Figure 14:** Warp mud used for fracturing

**Figure 15:** Warp mud used for fracture reopening after 10 minutes
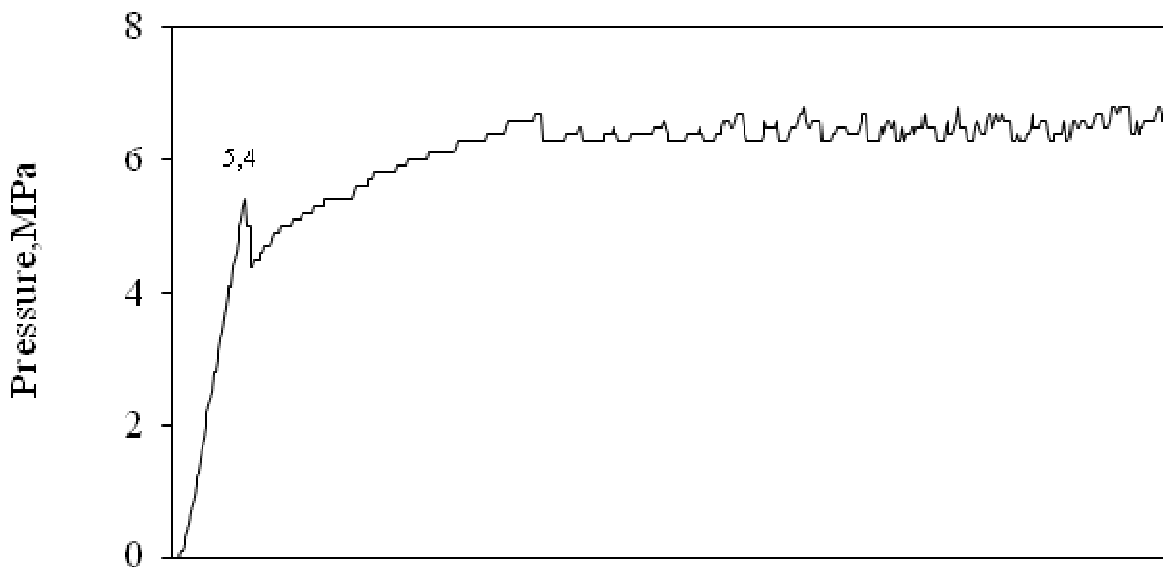


**Figure 16:** Warp mud used for fracture reopening after 60 minutes

The test result shows two fractures forming at 170-180$^0$ and in many cases, two wings diametrically propagating fractures are observed. The important thing to note in these fracture pressure plots is the nature of the pressure response due to the effect of the fluid used.

Similar fracturing experiment was conducted, this time using Aphrons drilling fluid. The test result shows two fractures forming at 170-180$^0$ as observed in Warp testing as shown in the picture of the top view of the core above.
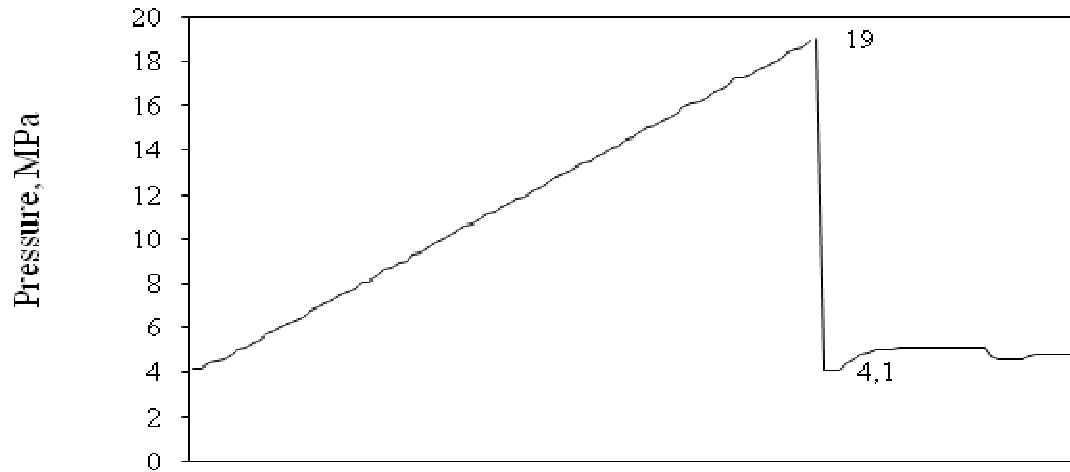
**Figure 17:** Aphrons mud used for fracturing
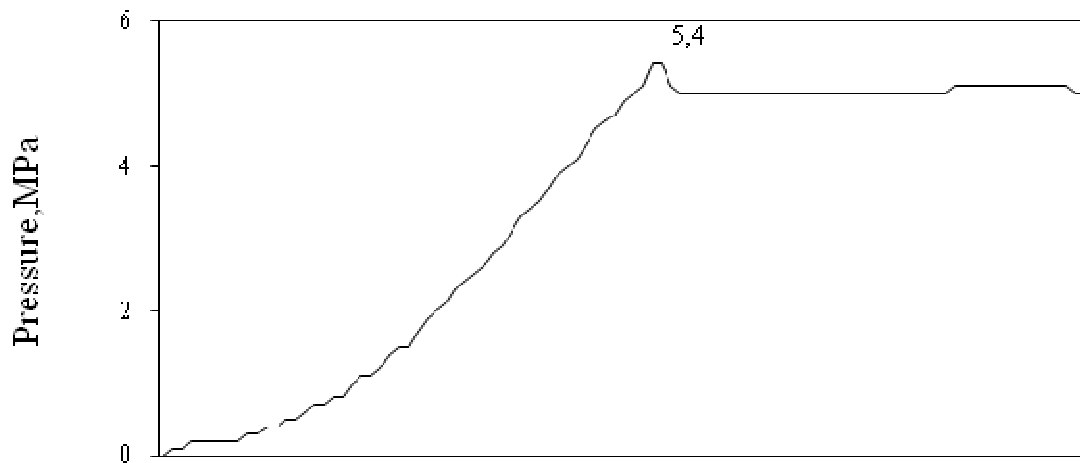


**Figure 18:** Aphrons mud used for fracture reopening after 10 minutes



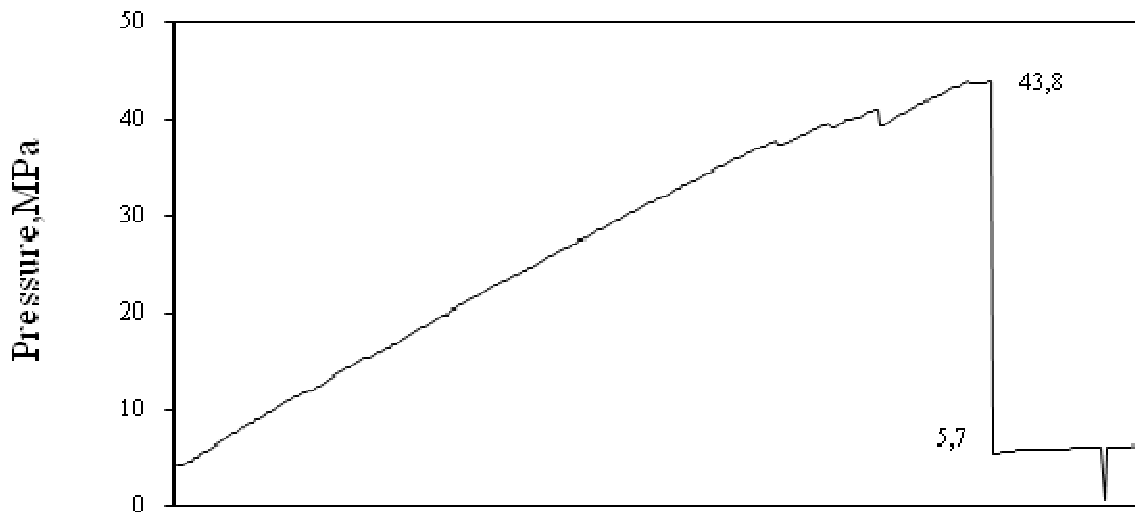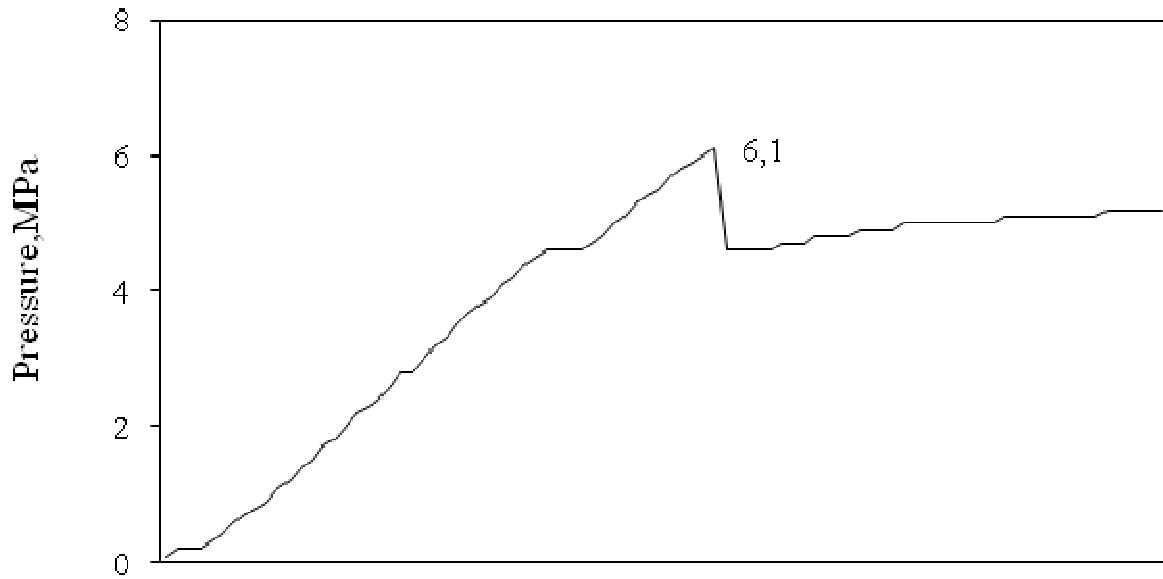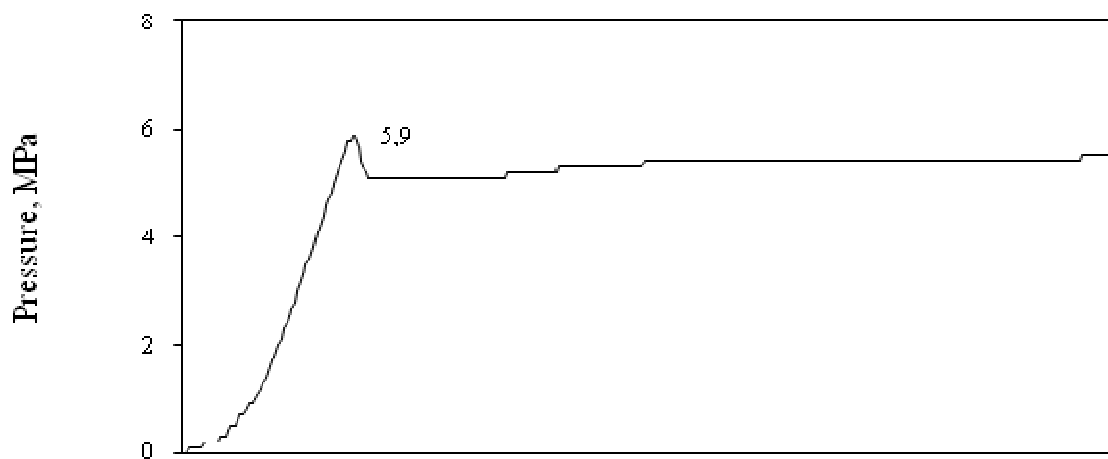**Figure 19:** Aphrons mud used for fracture reopening after 60 minutes

43

The different pressure response obtained when the three different fluids are used is attributed to a lot of controlling parameters such as the in-homogeneity of the rock material at the tip of the fracture, the fluid properties, the solid content of the fluid and the compressibility of the solids used, and even the state of stress.

## 4.3.2 Previous Work on Filtration behaviour

In addition to the bridge formed by solid particles in the mud, the filtrate loss capacity of the mud cake formed may hold the key to explaining the water based mud fracture propagation pressure behavior and the different behavior observed when different fluids are used.

Outmans[19] presented a theoretical basis for laboratory and field observation of filtration behavior. He presented a theoretical-empirical non-linear diffusion equation which may be linearised and solved explicitly to describe filtration through filter cakes. He also derived the well known $\sqrt{t}$ laws that says that the thickness of mud cakes is directly proportional to the

$\sqrt{t}$. The problem with this law is that is predicts the formation of a continuously increasing mud cake. This is not what obtains in reality. The mud cake thickness normally increases towards a terminal value.

Dewan and Chenevert[20] presented a single phase flow mathematical model to reproduce laboratory experiments. They presented a methodology to predict the time evolution of mud cake build up and the effective properties of the mud cake based on six mud filtrate parameters that can be determined form a standard on-site mud filtrate test. They presented the effective mud cake permeability as

$K_{mc}(t) = \frac{K_{mc0}}{P_{mc}^{v}(t)}$   where $K_{mc0}$ is a reference permeability defined at 1 psi differential

pressure and v is a compressibility exponent which typically ranges from 0.4 -0.9, and a value of zero would represent a completely incompressible mud cake and a value of unity would

apply to a mud cake so compressible that its permeability would be inversely proportional to the differential pressure across it. Appropriate expressions for $K_{mc0}$ and v are available on the paper by Dewan and Chenevert[20]. Wu et al[21] models the complete invasion process quantitatively with a finite difference invasion simulator. They concluded that for high permeability zones, both mud cake growth rate and mud filtrate invasion rate are controlled primarily by mud properties such as mud cake permeability, mud cake porosity and mud solids fraction, while for low permeability zones, both mud cake growth rate and mud filtrate invasion rate will be influence by both mud properties formation properties such as formation permeability and oil relative permeability end point. They also presented an expression for mud cake thickness as a function of $\sqrt{t}$ as

$$x_{mc}(t) = \sqrt{\frac{2t\Delta P_s f_s}{(1-f_s)(1-\emptyset_{mc})\mu_f} K_{mc}}$$ 
(4.24)

This shows that the mud cake thickness in a linear flow grows in time proportional to $\sqrt{t}$. It is therefore only valid when $K_{mc}$, $\Delta P_s$ and $\emptyset_{mc}$ are constant. If they are functions of time, then the mud cake thickness are obtained from the numerical integration of

$$\frac{\partial x_{mc}}{\partial t} = \frac{f_s}{(1-f_s)(1-\emptyset_{mc})\mu_f x_{mc}} K_{mc}\Delta P_s$$ 
(4.25)

## 4.4 Effect of Lithology on Fracture length and aperture

Makov et al[2] found that the fracture aperture is inversely proportional to the formation elastic modulus which implied that a constant injection rate, a higher elastic modulus results in a decreased aperture which in turn leads to a higher inlet pressure. This clearly show the effect of lithology on the fracture geometry as a fracture will have a much larger width in sand compared to shale as shown in figure 21.
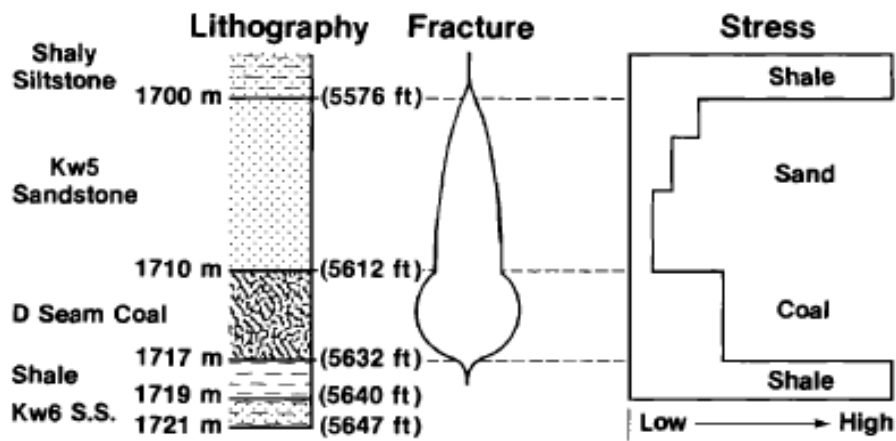
**Figure 20:** Lithology and relative minimum horizontal stress of the fracture environment[2]

## 4.5 Formation and linkage of Micro-fractures

Fossen and Gabrielsen[21] reports that veins and fissures formed in a stress field are aligned to the direction of the maximum horizontal stress as shown in Figure 22.
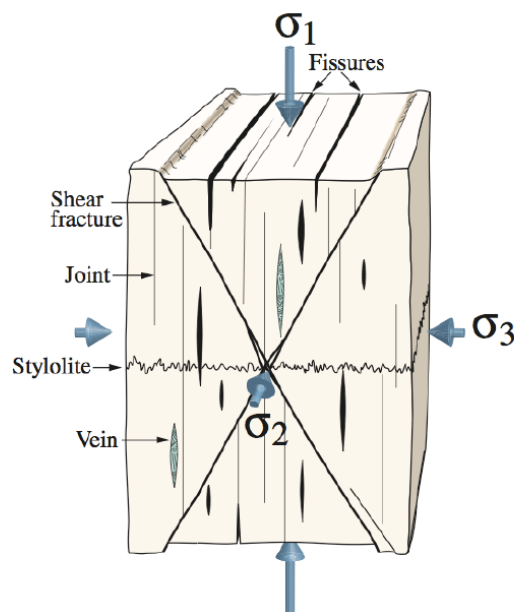


**Figure 21:** Fissures and veins orientation with respect to the maximum horizontal stress

If subjected to sufficient stresses, tensile or shear fractures may form. These tensile or shear fractures formed may then grow by the linkage of favorably aligned micro-fracture which forms a plane of weakness as shown in Figure 23.
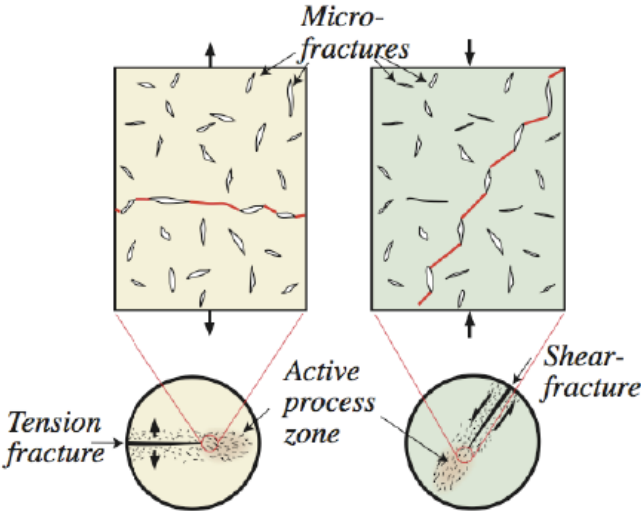


**Figure 22:** Linkage of favourably oriented micro-fractures

# Chapter 5      Modeling of fracture propagation

This section starts with a description of the fracture propagation process, and thereafter some fracture propagation models would be developed and proposed. These models would be compared with experimental results in order to analyze their prediction power.

## 5.1 Fracture Propagation Process

Reference is made to sections 4.3, 4.4 and 4.5. That section shows previous works that will be used in supporting a possible conceptual model of the fracture propagation process. One of the objectives of this work is to understand the fracture propagation process. Once the fracture initiation pressure is exceeded, the rock fractures instantaneously and contuinuously. The length of the fracture will depend on both rock properties (particularly the tensile strength), the fluid pressure applied in the well bore, and the magnitude of the minimum horizontal stresses. It is expected that when the tensile strength is low, the horizontal stresses are low, and the well is pressurized at a high pump rate, then the extent (length) of the initial fracture will be high as indicated in section 4.4. The reverse is expected for a rock with high tensile strength. This is illustrated also in figure 24.
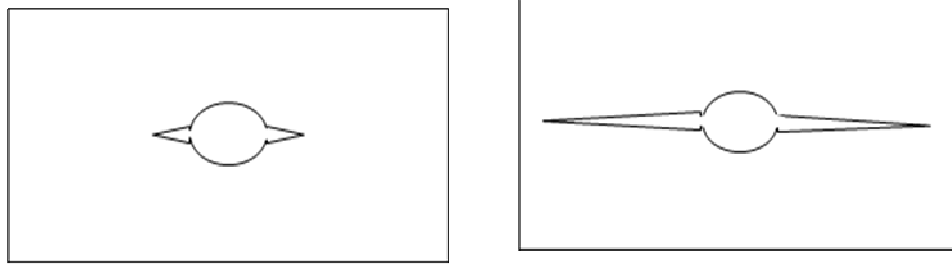
**Figure 23a:** High tensile strength, reduced fracture length b): Low tensile strength, higher length

After the fracture initiation, the pressure builds up in the fracture until it exceeds the fracture propagation pressure and then the fracture propagates. This propagation is accompanied by pressure drop which is due to the formation of a large fracture surface over a relatively short period of time, and also due to other processes such as fluid leak-off and frictional losses. We can thus imagine the fracture propagation process to be a series of pressure build-up, fracture propagation, and pressure decline cycles. Experiments have shown that this is true when water based muds are used. For oil based muds, we observe just a single cycle : pressure build-up to the fracture initiation pressure and then a fracture is initiated. This fracture propagates as the fracture pressure declines with time towards the minimum in-situ stress as shown in fig. 11.

Different fluids form different mud cakes having different properties. These mud cakes form at different rates, depending on different factors such as filtration rate, porosity, permeability, pressure differential, solid content, and other factors. For a newly opened fracture, at the time when the mud is exposed to the fracture face, fluid loss due to filtration occurs to the of formation peameability Kf, and porosity $\varnothing_f$. As mud cake is being formed, the permeability decreases exponentially from the initial value $K_f$ to a value K (t). K (t) depends on time, fluid property (viscosity), solids property (such as compressibility), rate of filter cake formation, among others. This fluid loss will contribute to the observed pressure drop during fracture propagation. The longer the time the fracture face is exposed to the mud, the more will be the filter cake deposition. It therefore implies that the pressure drop due to filtrate loss will decrease with time due to the reducing fracture face permeability.

The higher the permeability, the more the filtrate loss and this of course translates to a higher pressure drop. Thus, there will be a higher pressure drop at the tip of the fracture compared to at other parts of the fracture.

If we assume that the walls of the fracture initially (at time t=0) have a permeability that is equal to the formation permeability $K_f$. If the permeability is assumed to decrease instantaneously or continuously with cake formation, then the plot of permeability against time will appear like Figure 25
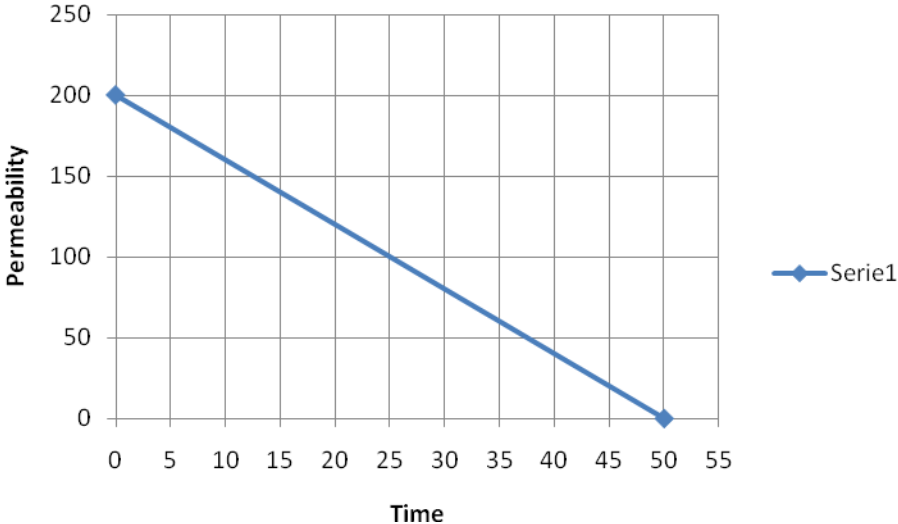


**Figure 24:** Fracture wall permeability as a function of time

The slope of the curve is

$$D = \frac{-dK/dt}{K}$$ where the minus sign is introduced because $dK$ and $dt$ have opposite signs.

If we choose to call the permeability at time t as K (t), then if we integrate the expression above, we get

$$\int_{K_f}^{K} \frac{dK}{K} = -D \int_0^t dt \tag{6.50}$$

This gives,

$$K = K_f e^{-Dt} \tag{6.51}$$

Dewan and Chenevert[20] pointed out that the log-log plot of mud cake permeability against pressure across mud cake is a linear plot such as
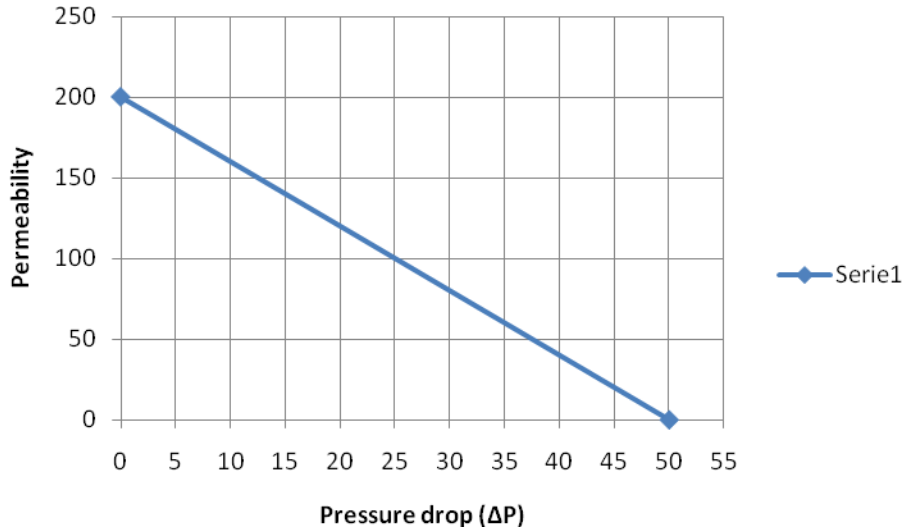
**Figure 25:** Log-log plot of mud cake permeability against pressure across mud cake

$$\text{Slope, } D \ = \ \frac{d(\log K)}{d(\log t)} = \frac{\log K_f - \log K}{\log \Delta P} \tag{6.52}$$

Thus we can write

$$K = \ K_f e^{-\left[\frac{\log K_f - \log K}{\log \Delta P}\right]t} \tag{6.53}$$

This presents the permeability mud cake permeability as a function of both the pressure across the filter cake and time. This can be solved numerically by iteration.

This presents a challenge since the pressure drop across the cake is unknown. If we assume a formation of permeability of 0.1 mD and also assume a constant pressure drop of 0.4 psi after four iterations, the plot of the permeability against time obtained is



50
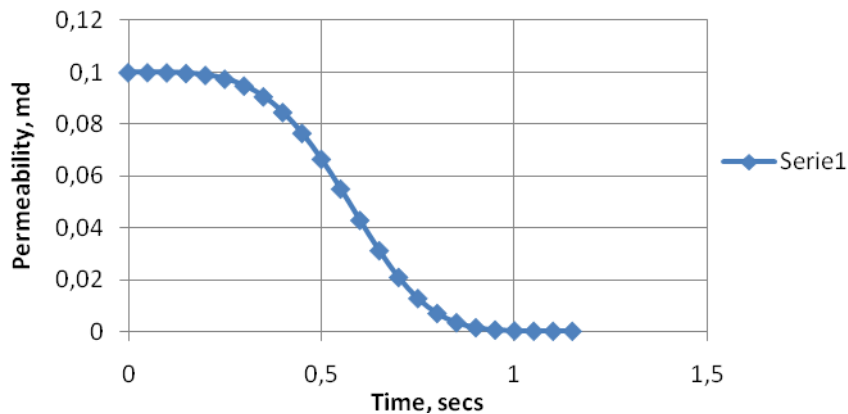
The assumption of constant pressure drop across mud cake results in varying values of the slope D, which is supposed to be constant. If however we assume a constant slope D = 3, we get the permeability profile as a function of time as shown in Figure 28.
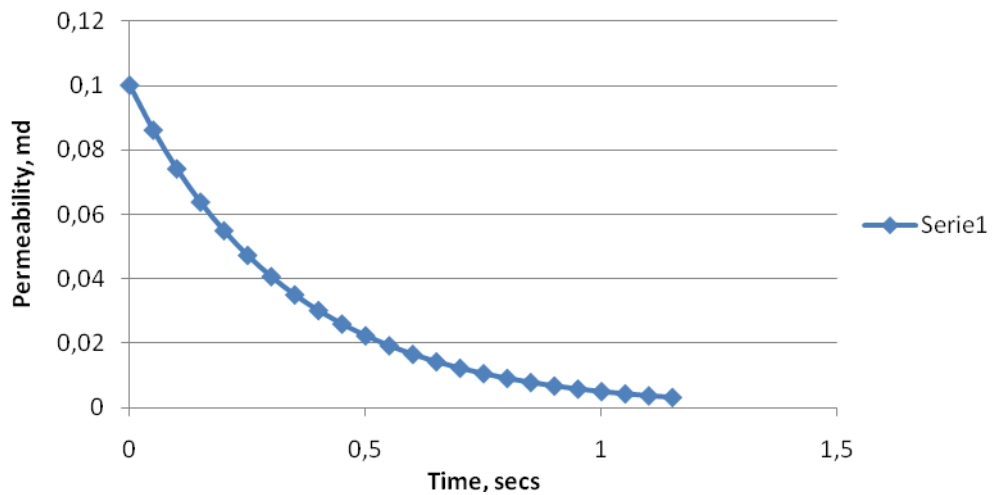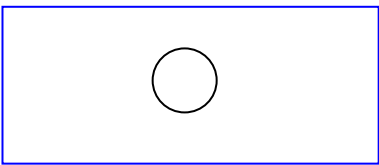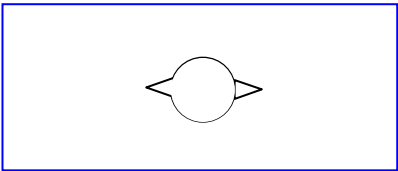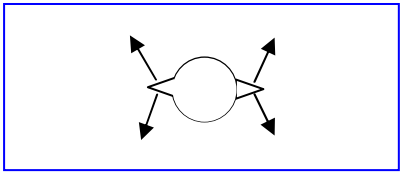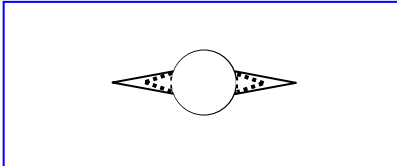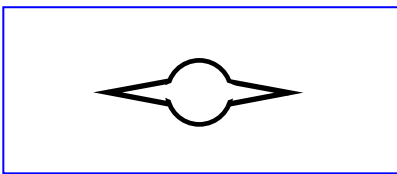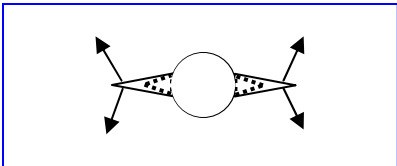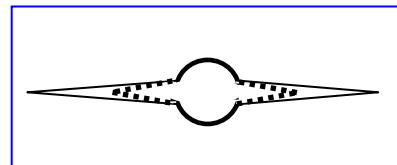


**Figure 27:** Mud cake permeability as a function of time when D = 3

**Table 1:** Summary of the fracturing process

| Steps | Diagram | Description |
|---|---|---|
| Step 1:<br>The Differential pressure is less than the tensile strength of the rock. | | Intact hole. |
| Step 2:<br>Fracture initiation | | The length and width of the fracture depends on rock tensile strength and fluid properties. |
| Step 3:<br>Pressure build-up | | Pressure builds-up in the fracture as pumping continues but the fracture does not propagate because the pressure is less than the propagation pressure. |

51

| Step 4:<br>Fracture propagation |  | Propagation pressure is exceeded and fracture propagates. Pressure drops due to fluid loss and formation of new fracture surface over a short time interval. |
|---|---|---|
| Step 5:<br>Formation of mud cake on fracture surface and sand bridges at fracture tip. |  | Mud cake reduces the permeability of borehole wall. Together with sand bridge formed at the fracture tip, the reduced rate of formation of new fracture surface, and the reduced permeability results in decreased pressure drop and eventual buildup of pressure in the fracture. |
| Step 6:<br>Pressure buildup |  | The pressure in the fracture builds-up due to the processes described in step 5 and this buildup continues until the fracture starts to propagate again. |
| Step 7:<br>Fracture propagates again. |  | Fracture propagation pressure is exceeded and the fracture propagates again. There is also a simultaneous pressure decline due to factors described in step 4 |
| Step 8:<br>Repeated process, observed only in water based mud. | Oil based muds have limited fluid loss due to filtration and the nature of the fluid does not allow for sand bridging either. Thus the cyclic phenomenon is not observed as shown in fig. 11. | Steps 5,6 and 7 are repeated like a cycle as the fracture continues to propagate. This happen in very short time periods that it may not be visible to the naked eye. |

At time zero, the permeability is largest and the pressure drop due to filtration effect is largest compared to that at other times. If fluid is pumped into the fracture at a constant rate, the resultant effect of fluid flow into the fracture from the well bore, fracture area increase, and fluid loss to the formation will result in a pronounced decrease in pressure. This pressure decrease will continue to reduce in magnitude as the healing properties of the mud improves due to cake formation. When the pressure drops below the fracture propagation pressure, new fracture area will not be formed. Thus, the resultant effect of the fluid flow into the fracture from the well bore, solid bridge at the fracture tip (section 4.3), and fluid loss due to filtration will result in a pressure build up process. This pressure continues to build up until the pressure in the fracture exceeds the fracture propagation pressure. At this point, the fracture will start to propagate again and pressure decline will be observed. This cyclic process in addition to the solid bridge described in section 4.3 is what is responsible for the observed pressure behavior during continuous pumping.

Section 4.5 highlights the concept of fracture linkage reported by Fossen and Gabrielssen. The fracture propagation process may also be viewed as a process in which micro fractures are formed at the tip of a fracture. Theses micro-fractures are formed due to stress concentration at the tip of the fractures fluid is pumped into the fracture. They may then link up and form a fracture plane through which a new fracture will propagate. The orientation of these micro-fractures is therefore important for the fracture propagation direction. The magnitude and orientation of the in-situ stresses will play a major role in the orientation of these micro-fractures. It is expected that these fractures will align with the maximum in-situ stress.
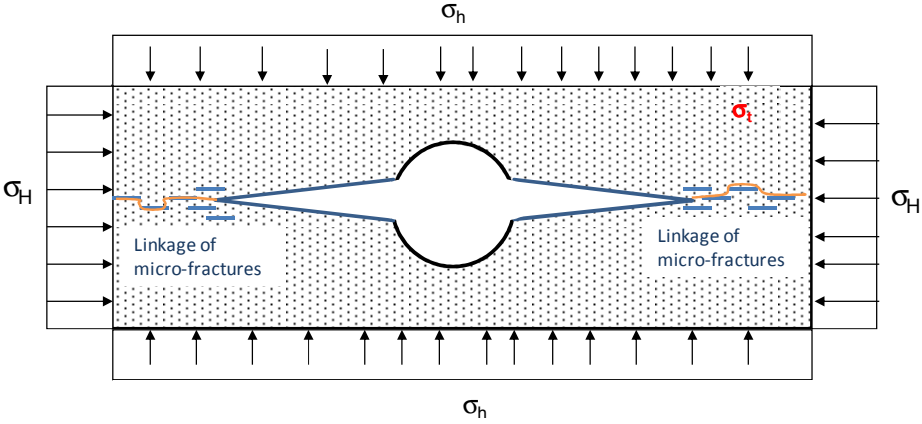


**Figure 28:** Linkage of micro-fractures at the tip of a fracture to form a failure plane.

Note: The above argument presented above consists of the author's opinion combined with results obtained from previous work by other authors in literature.

## 5.2 Fracture models

This section presents developed fracture propagation models based on fracture geometry and failure criteria. Emphasis was laid on developing models having triangular and the elliptical fracture geometries. Some of these models are derived while considering the contributions from the maximum horizontal stress, while others are derived ignoring the maximum horizontal stress. The stress concentration at the tip of the fracture is also considered in some models. My consultations with Belayneh have resulted in his development of rectangular models[21]. This will be presented and also compared with my models and also with experimental data.

### 5.2.1 Model 1- Triangular fracture

Loading:

- Externally     In-situ stresses
- Internally     Well pressure/Fracture pressure

Assumption:

- Non-Darcy flow
- Constant injection pressure
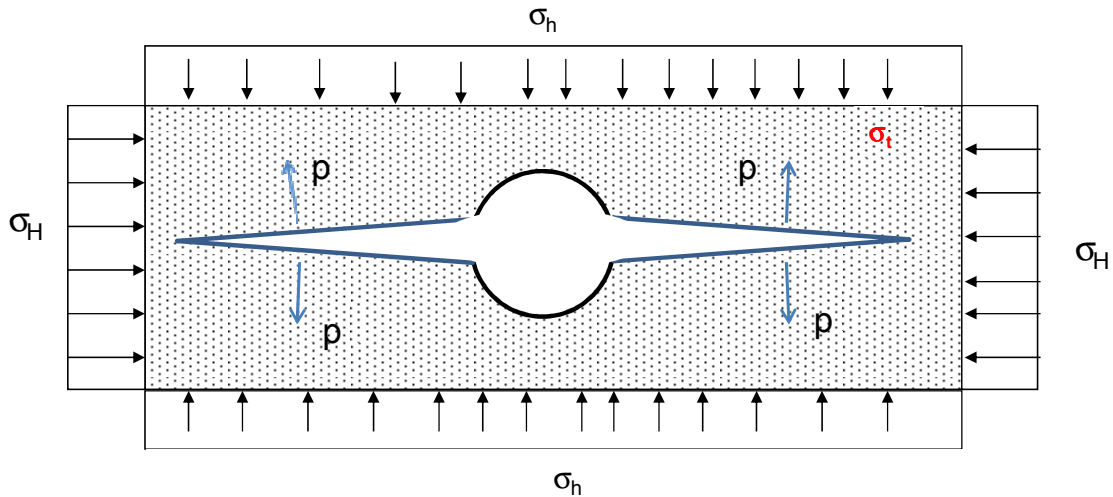


**Figure 29:** Stresses acting on a triangular fracture

Let the angle at the fracture tip be $\beta$. Thus, half of the angle at the tip is $\beta/2$. Let the normal stress on the fracture face be $\sigma$ and the shear stress on the fracture face be denoted by $\tau$ as shown below.
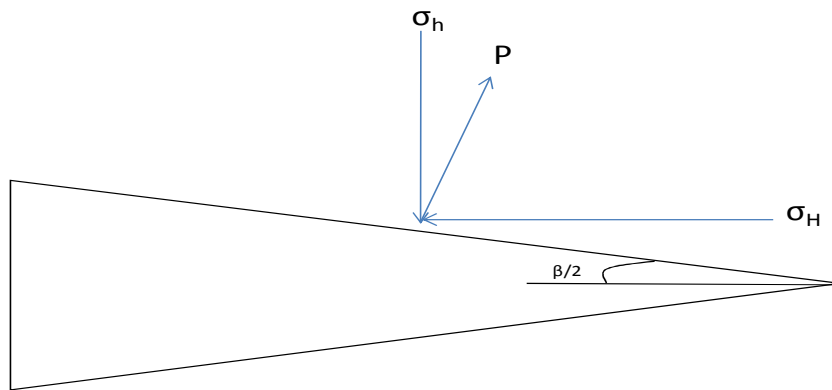


**Figure 30:** Forces acting on a fracture half-width

If we choose not to neglect the maximum horizontal stress, and resolve the two horizontal stresses first we get:
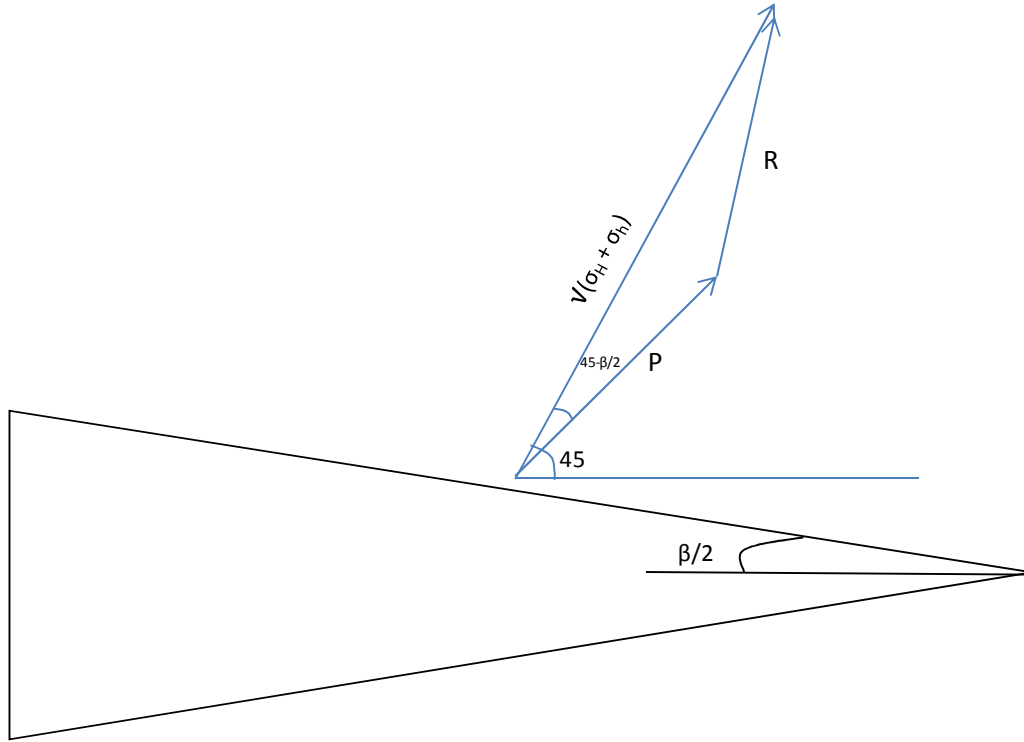
**Figure 31:** Final force resolution

From trigonometry, we get that the resultant is

$$R^2 = P^2 + (\sigma_h{}^2 + \sigma_H{}^2) - 2P\sqrt{(\sigma_h{}^2 + \sigma_H{}^2)}Cos(45 - \frac{\beta}{2}) \tag{5.1}$$

Using Griffith's criteria for fracture propagation, $R = \sigma_t$,

$$P^2 - 2P\sqrt{(\sigma_h{}^2 + \sigma_H{}^2)}Cos\left(45 - \frac{\beta}{2}\right) + (\sigma_h{}^2 + \sigma_H{}^2 - \sigma_t{}^2) = 0$$

When solved, the fracture propagation model is obtained:

$$P_f = $$

$$\sqrt{(\sigma'_h{}^2 + \sigma'_H{}^2)}Cos\left(45 - \frac{\beta}{2}\right) \pm$$

$$\sqrt{\left((\sigma'_h{}^2 + \sigma'_H{}^2)Cos\left(45 - \frac{\beta}{2}\right)^2 - (\sigma'_h{}^2 + \sigma'_H{}^2 - \sigma_t{}^2)\right)}$$

$$\tag{5.2}$$

**Numerical Example**

An analysis of the fracture propagation pressure based on the assumed data below is presented. The well inclination is from vetrical to horizontal directions. Figure 33 shows the pressures propagation at various wellbore inclnations.

55

**Table 2:** Data used for analysis

| $\sigma_h$ | $\sigma_H$ | $\sigma_v$ | $\sigma_t$ | Po |
|------|------|------|---|------|
| 1,6 | 1,7 | 1,8 | 1 | 1,25 |

**Model 1: Fracture propagation pressure, azimuth= 45 deg.**
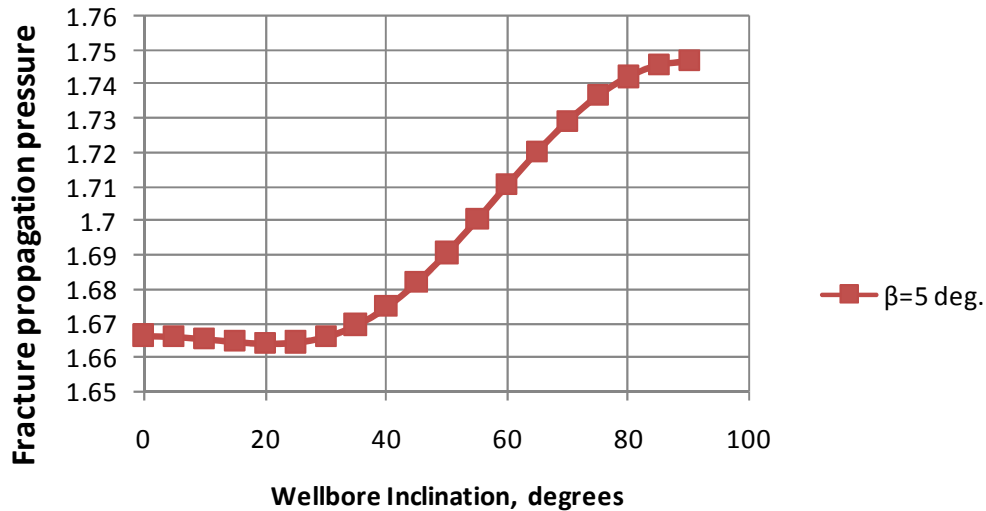


**Figure 32**: Fracture propagation pressure for model 1 as a function of inclination

This shows an increase in the fracture propagation pressure with increasing wellbore inclination. Note also that the predicted pressures are also reasonably high and they support the common belief that the propagation pressure is a sum of the minimum horizontal stress and added term which is difficult to model exactly. The good thing here is that this model does not ignore the contribution of the maximum horizontal stress yet it gives reasonable fracture propagation pressure prediction.

Since this model makes use of fracture geometry, particularly the angle at the fracture tip, an analysis will be conducted to observe the effect of varying tip angle. It is assumed that when a fracture has been initiated and assuming that the fracture has stopped propagating, continuous pumping will result in pressure buildup in the fracture. However, the fracture will only propagate when the propagating pressure has been exceeded. It will thus be reasonable to assume that as the pressure increases in the fracture, the angle at the fracture tip will continue to increase until a critical value at which the fracture propagates. This critical value will depend on the in-situ stresses and the tensile strength of the rock. It is to be expected that if

the tensile strength of the rock is high, the critical tip angle will also be higher. Here, it is assumed that as the fracture begins to propagate, the angle at the tip decreases.

The same data set in table 2 is used in the experiment however, we now choose to vary the tip angle, β. The result is shown in figure 34.

**Model 1: Fracture propagation pressure, azimuth= 45 deg.**
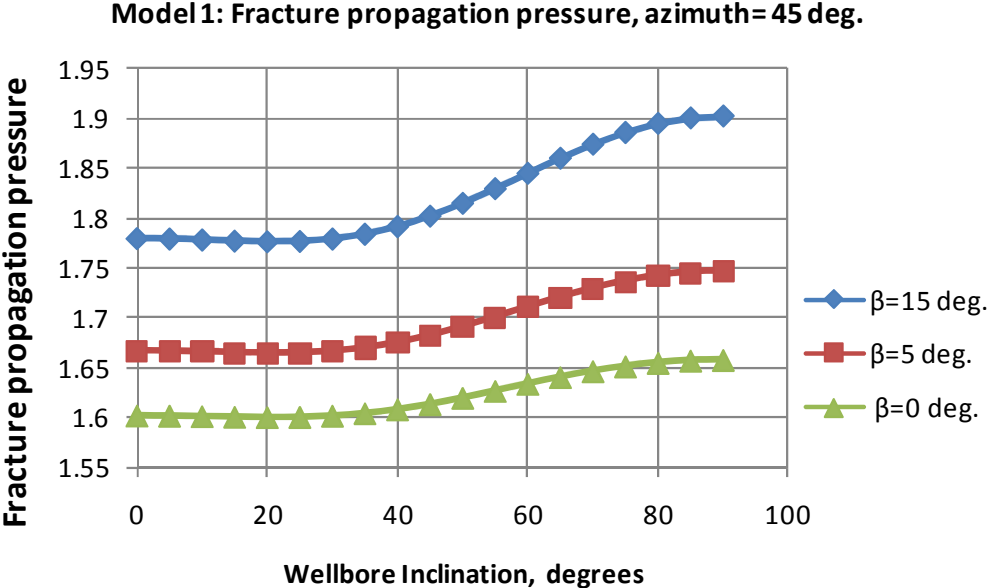


**Figure 33:** Effect of varying tip angle for model 1 as a function of inclination

The result shows a decreasing fracture propagation pressure with decreasing tip angle. This can be interpreted to mean that the fracture propagation pressure decreases as the fracture propagates since it is expected that the angle at the tip will reduce during propagation.

## 5.2.2 Model 2- Triangular fracture

Loading:

- Externally     In-situ stresses
- Internally     Well pressure/Fracture pressure

**Assumption:**

- Non-Darcy flow
- Constant injection pressure

Plane strain

Fracture propagation criteria: Hillerborg et al criterion – fracture occurs when the stress at the tip reaches the tensile strength of the rock.
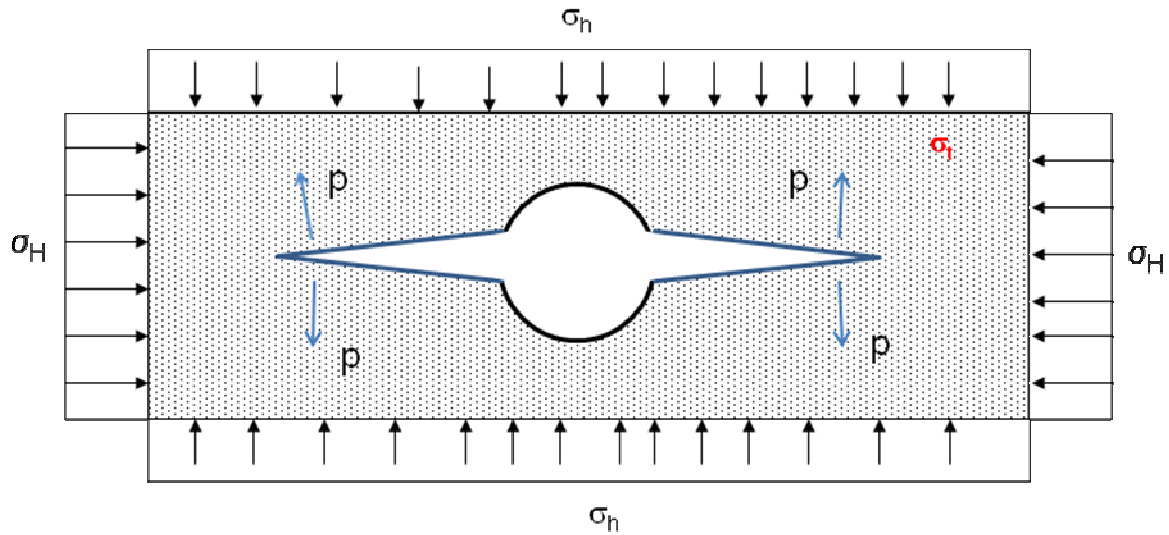
If we consider one fracture face and assume that the contribution of the maximum horizontal stress is negligible, the forces acting are:
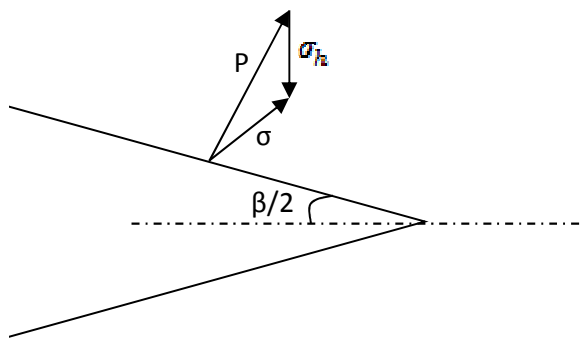


Using trigonometric law for force resolution, the normal force on the fracture face is determined to be

$$\sigma = \sqrt{\sigma_h{}^2 + P^2 - 2P\sigma_h \cos\beta/2} \tag{5.3}$$

Using Hillerborg's theory, fracture occurs when $\sigma = \sigma_t$ or

Thus,

$$P^2 - 2P\sigma_h \cos\frac{\beta}{2} + (\sigma_h{}^2 - \sigma_t{}^2) = 0 \tag{5.4}$$

This is a quadratic equation in P that when solved, results in the fracture propagation model:

$$P_f = \sigma'_h Cos\left(\frac{\beta}{2}\right) \pm \sqrt{\left(\left(\sigma'_h Cos\left(\frac{\beta}{2}\right)\right)^2 + \sigma_t{}^2 - \sigma'_h{}^2\right)} \qquad (5.5)$$

For this model to be valid,

$$((\sigma_h Cos\beta/2)^2 + \sigma_t{}^2 - \sigma_h{}^2) \geq 0. \qquad (5.6)$$

This provides the limiting value of $\beta = 2\sin^{-1}\frac{\sigma_t}{\sigma_h}$ $\qquad (5.7)$

If the width of the fracture is taken as w, the angle in half-section as $\beta/2$ and the fracture length as L, then from the fracture geometry we can obtain:
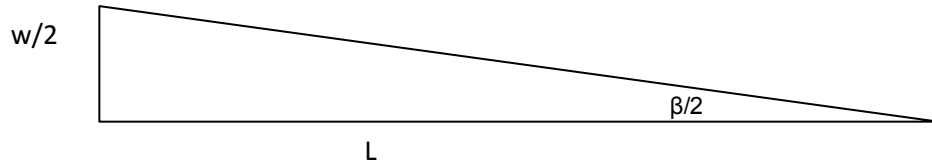


**Figure 34:** Calculation from fracture geometry

We can obtain from trigonometry that

$$tan\beta/2 = \frac{w}{2L}, \qquad (5.8)$$

$$Sin\beta/2 = \frac{1}{2\sqrt{\frac{1}{4} + \frac{L^2}{w^2}}} \text{ and} \qquad (5.9)$$

$$Cos\beta/2 = \frac{1}{\sqrt{1 + \frac{w^2}{4L^2}}} \qquad (5.10)$$

We can therefore write the fracture propagation model as

$$P_f = \frac{\sigma'_h}{\sqrt{1 + \frac{w^2}{4L^2}}} \pm \sqrt{\left(\frac{\sigma'_h{}^2}{1 + \frac{w^2}{4L^2}} + \sigma_t{}^2 - \sigma'_h{}^2\right)} \qquad (5.11)$$

We can make use of the fact that $Sin \frac{\beta}{2} = \frac{1}{2\sqrt{\frac{1}{4}+\frac{L^2}{w^2}}} = \frac{\sigma_t}{\sigma_h}$ to obtain a critical fracture

propagation pressure in terms of in-situ properties only by writing

$$\frac{w^2}{L^2} = \frac{4\sigma_t}{2\sigma_h - \sigma_t} \tag{5.12}$$

This yields,

$$P_{f,crit} = \frac{\sigma'_h}{\sqrt{1+\frac{\sigma_t}{2\sigma'_h - \sigma_t}}} \pm \sqrt{\left(\frac{\sigma'^2_h}{1+\frac{\sigma_t}{2\sigma'_h - \sigma_t}} + \sigma_t^2 - \sigma'^2_h\right)} \tag{5.13}$$

**Numerical Example**

An analysis of the fracture propagation models based on the assumed data below is presented. The well inclination is from vetrical to horizontal directions. The data set in table 3 will be used in the analysis to be presented below.

**Table 3:** Data used for analysis

| $\sigma_h$ | $\sigma_H$ | $\sigma_v$ | $\sigma_t$ | Po |
|------------|------------|------------|------------|------|
| 1,6        | 1,7        | 1,8        | 1          | 1,25 |
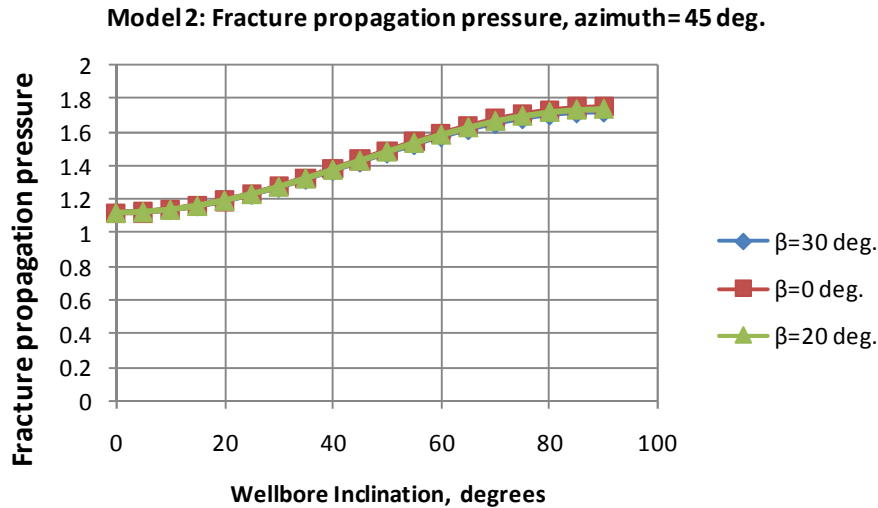
**Figure 35**: Fracture propagation plot for model 2 as a function of inclination

This model shows a similar trend to the previous fracture propagation models. However, it predicts a lower fracture propagation pressure. The results, some of which are shown in table 4, show that the fracture propagation pressure decreases as the angle decreases.

**Table 4:** Predicted fracture propagation pressures for varying tip angles

| Wellbore inclination | Pf, β=0 deg. | Pf, β=20 deg | Pf, β=30 deg |
|---|---|---|---|
| 0 | 1.118533 | 1.119688 | 1.121124 |
| 5 | 1.12333 | 1.124421 | 1.125779 |
| 10 | 1.137575 | 1.138474 | 1.139593 |
| 15 | 1.160834 | 1.161409 | 1.162125 |
| 20 | 1.192401 | 1.192516 | 1.192658 |

This trend is expected if we assume that the angle at the tip increases as the fracture is pressurized until the fracture pressure is reached at which point the fracture propagates and the tip angle decreases accordingly. Observe also that the value of the angle at the fracture tip does not make a significant difference to the value of the fracture propagation pressure. Thus, for convenience we can assume that the angle at the tip tends to zero.

An analysis was also done to determine the effect of the rock tensile strength on the fracture propagation pressure. The result is shown in figure 36.
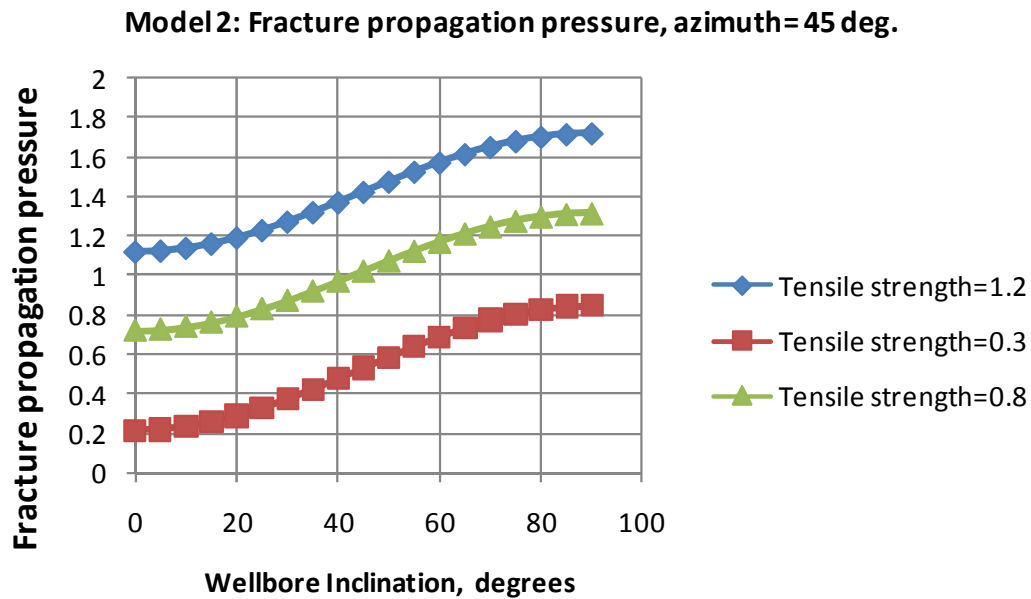
**Figure 36:** Effect of rock tensile strength on fracture propagation pressure

The result in figure 36 show that the fracture propagation pressure decreases as the tensile strength decreases. Once again this is to be expected.

A critical fracture propagation model was developed (equation 5.13). This represents a lower limit for fracture propagation pressure. Unfortunately, some instability is observed when applying the model which makes it unreliable.

A simple illustration of this problem is given below:

The example below computes the fracture pressure in a formation having the following state of stress: a maximum horizontal stress of 1.7, a minimum horizontal stress of 1.6, an overburden stress of 1.8 and a low tensile strength of 0.3. The fracture propagation pressures are computed using the triangular model 2 (equation 5.5), and the critical fracture propagation pressure equation (equation 5.13).

The result is shown in figure 37.
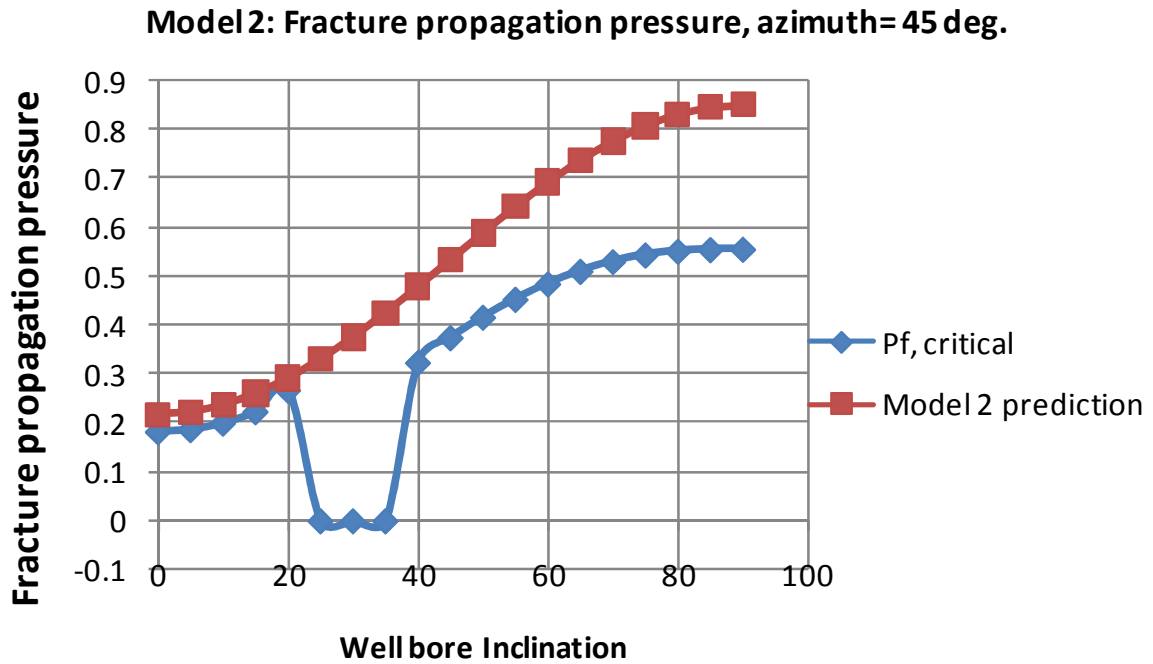
**Figure 37:** Fracture propagation plot for model 2 including the critical fracture pressure

Figure 37 compares the fracture propagation model and the the lower limit of fracture pressure. Some unexplainable anomalies are observed at intermediate wellbore inclination. Nonetheless, figure 37 indicates the possibility of there being a lower limit for fracture propagation pressure. Some more work is therefore required to be done on improving the model. However, as the plot above shows, if this concept can be explored it would provide us with a lower limit of fracture propagation pressure that must be exceeded for any given inclination.

### 5.2.3 Model 3 - Elliptical fracture

Elliptical fracture propagating in direction of maximum horizontal in-situ stress
Loading:

- Externally      In-situ stresses
- Internally      Well pressure/Fracture pressure

Assumption:

- Non-Darcy flow
- Constant injection pressure

Assuming a fracture propagating in the direction of the maximum horizontal stress as shown below:
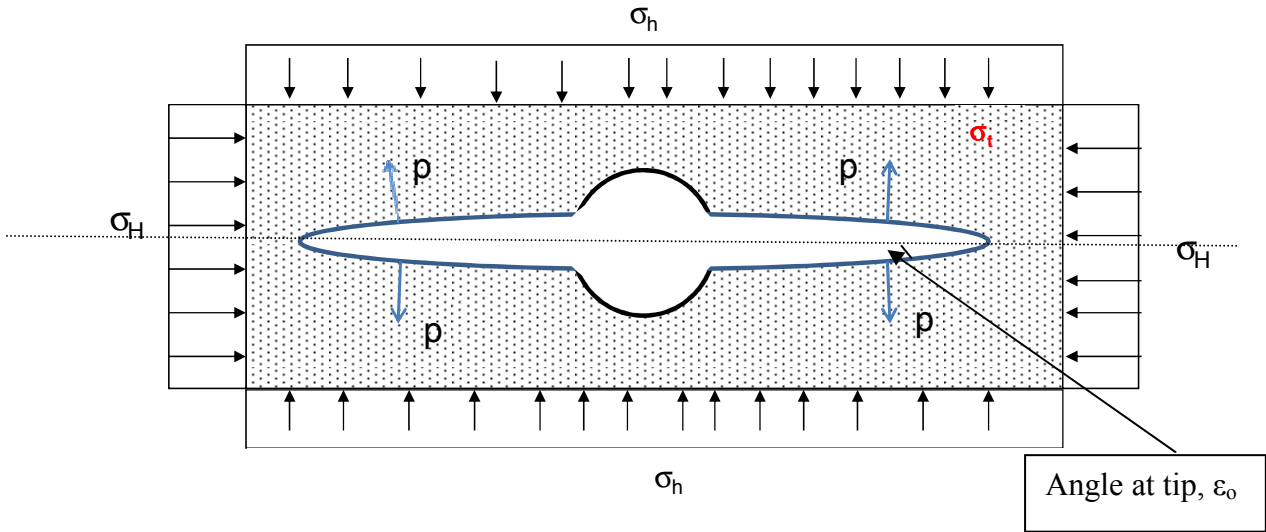


**Figure 38:** Elliptical fracture model

We can resolve the stresses acting on the fracture face into two components. If we assume that fluid pressure acts normal to the fracture surface, the normal stress on the fracture face simplifies to:

$$\sigma_{xx} = \sigma_h - P \tag{5.14}$$

Griffith derived an expression for the tangential stress acting on an elliptical surface[23]. Using series expansion, the tangential stress[23] - Griffith becomes:

$$\sigma_{n,max} = \frac{\sigma_{xx}\left(4\varepsilon_0 + 2\varepsilon_0{}^2 - \eta^2\left(2 + 4\varepsilon_0 + 4\varepsilon_0{}^2\right)\right)}{\varepsilon_0{}^2 + \eta^2} \tag{5.15}$$

This becomes:

$$\sigma_{n,max} = \frac{(\sigma_h - P)\left(4\varepsilon_0 + 2\varepsilon_0{}^2 - \eta^2\left(2 + 4\varepsilon_0 + 4\varepsilon_0{}^2\right)\right)}{2(\varepsilon_0{}^2 + \eta^2)} \tag{5.16}$$

If fracture propagation occurs when the maximum tangential stress exceeds the tensile strength of the rock, and using the necessary sign convention, $\sigma_{n,max} = -\sigma_t$.

This gives the fracture propagation model:

$$P_f = \sigma_h + \frac{\sigma_t\left(\varepsilon_0{}^2 + \eta^2\right)}{\left(2\varepsilon_0 + \varepsilon_0{}^2 - \eta^2\left(1 + 2\varepsilon_0 + \varepsilon_0{}^2\right)\right)} \tag{5.17}$$

$\eta$ is the angle any position makes with respect to the fracture axis. At the tip of the fracture, $\eta = 0$. The fracture propagation model thus simplifies to:

$$P_f = \sigma_h + \frac{\sigma_t\left(\varepsilon_0{}^2\right)}{\left(2\varepsilon_0 + \varepsilon_0{}^2\right)} \tag{5.18}$$

Numerical Example

The same data set is used to analyse the fracture propagation model. The well inclination is from vetrical to horizontal directions. The figure shows the pressures propagation at various azimuth direction.

**Table 5:** Data used for the analysis

| $\sigma_h$ | $\sigma_H$ | $\sigma_v$ | $\sigma_t$ | Po |
|------------|------------|------------|------------|------|
| 1,6 | 1,7 | 1,8 | 1 | 1,25 |

The result obtained using this model is plotted in figure 39. The result show that this model predicts lower fracture propagation pressure than the previous models.
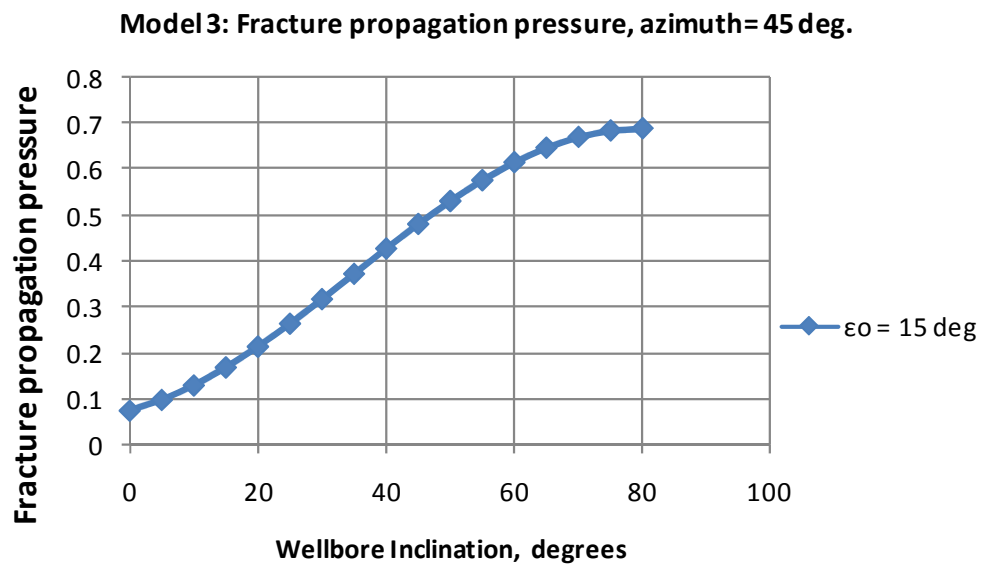


**Figure 39:** Fracture propagation results for model 3 as a function of inclination

Note however that the result is widely affected by the pore pressure. If a pore pressure of 0.2 is used, the model will predict much higher fracture pressures as shown below:
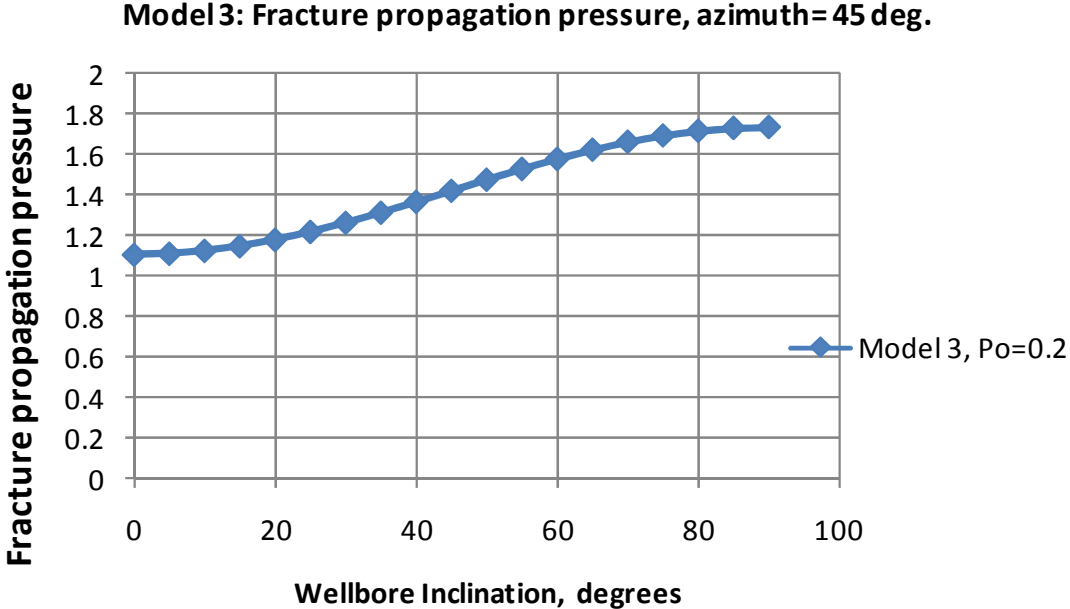


**Figure 40:** Fracture propagation results for model 3 using a pore pressure of 0.2.

## 5.2.4 Model 4 - Elliptical fracture

Elliptical fracture propagating in direction of maximum horizontal in-situ stress

Loading:

- Externally        In-situ stresses
- Internally        Well pressure/Fracture pressure

**Assumption:**

- Non-Darcy flow
- Constant injection pressure

This model is similar to the above model, with the exception that here we introduce the stress concentration concept.
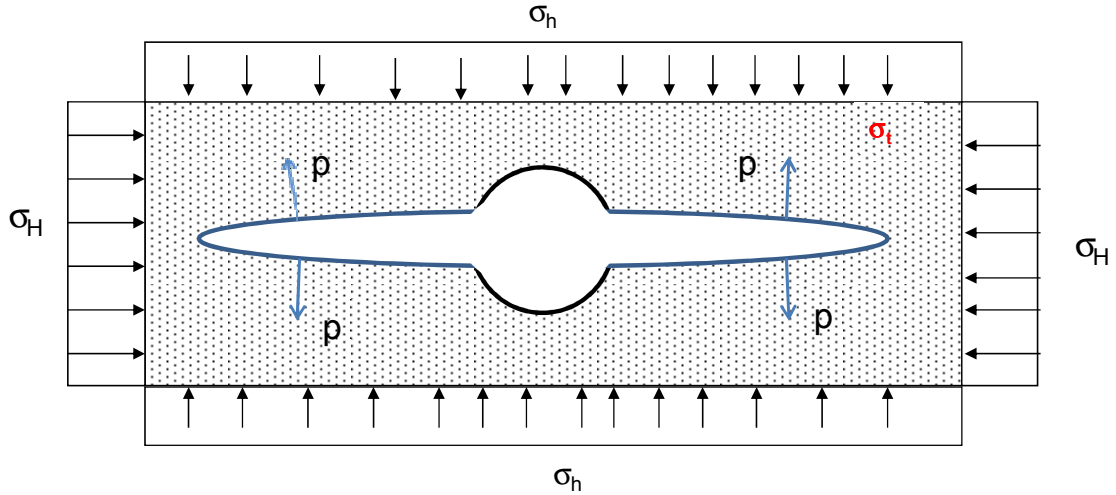
Consider an elliptical fracture propagating in direction of maximum horizontal in-situ stress. Thus the normal stress on the fracture face simplifies to:

$$\sigma_{xx} = \sigma_h - P \qquad (5.19)$$

If we view the fracture as an ellipse of major axis length 2b and minor axis length 2a such that the fracture width w= 2a and the fracture half-length L = b, we can express the maximum stress in the fracture in terms of the gracture geometry.
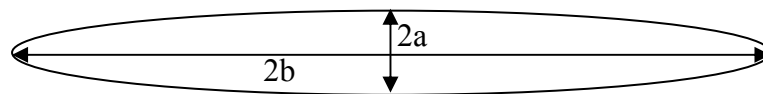


Due to stress concentration effects, the maximum stress in an elliptical crack can be expresses as

$$\sigma_{max} = \sigma\left(1 + \frac{2a}{b}\right). \qquad (5.20)$$

Thus we can re-write it as:

$$\sigma_{max} = \sigma_{xx}\left(1 + \frac{2L}{w}\right) \qquad (5.21)$$

Using Hillerborg's theory, the fracture will propagate when the maximum stress exceeds the tensile strength of the rock.

Thus using $\sigma_{max} = -\sigma_t$ where the negative sign is due to the chosen notation used in the force balance. we can thus write:

$$\left(\sigma_h - P\right)\left(1 + \frac{2L}{w}\right) = -\sigma_t \tag{5.22}$$

This yields a simple fracture propagation model given as:

$$P_f = \sigma_h + \frac{\sigma_t}{\left(1 + \frac{2L}{w}\right)} \tag{5.23}$$

Numerical Example

The same data set is used to analyse the fracture propagation model. In addition, we will make use of the fracture length to width ratio in this analysis. The well inclination is from vetrical to horizontal directions. The figure shows the pressures propagation at various azimuth direction.

**Table 6:** Data used for the analysis

| $\sigma_h$ | $\sigma_H$ | $\sigma_v$ | $\sigma_t$ | Po |
|---|---|---|---|---|
| 1,6 | 1,7 | 1,8 | 1 | 1,25 |
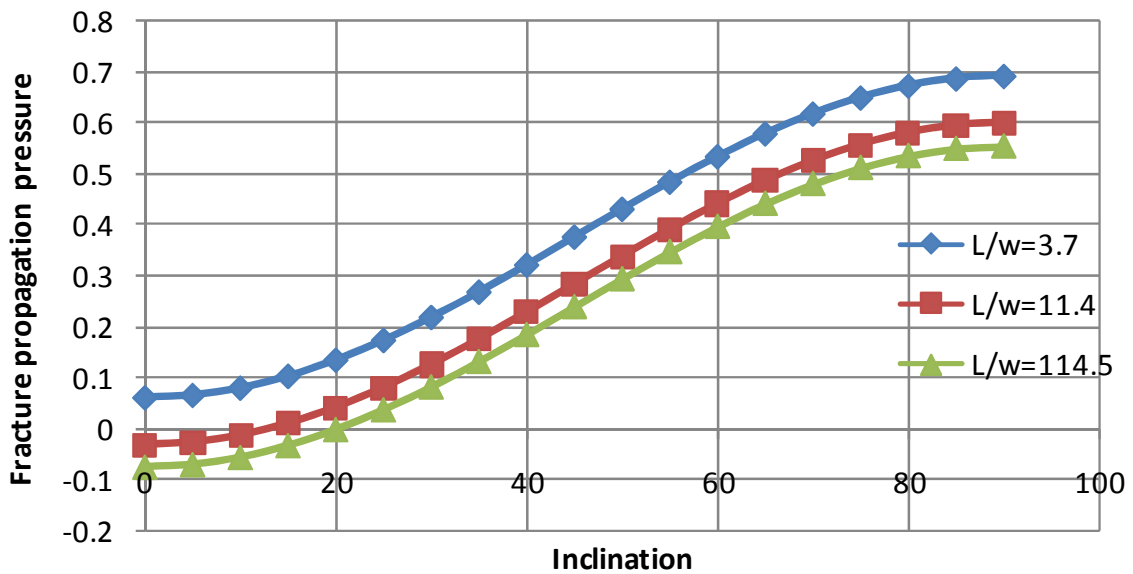


**Figure 41:** Fracture propagation results for model 4 as a function of inclination

Like the previous model, this model predicts low fracture pressures for the given data set. In addition to the expected prediction of the behavior of the fracture pressure with inclination, this model also clearly show that the fracture propagation pressure decreases as the length of the fracture increases.

If however, we assume a low pore pressure of 0.2, the predicted propagation pressures become considerably larger as shown below.

Model 4: Fracture propagation pressure, azimuth= 45 deg.
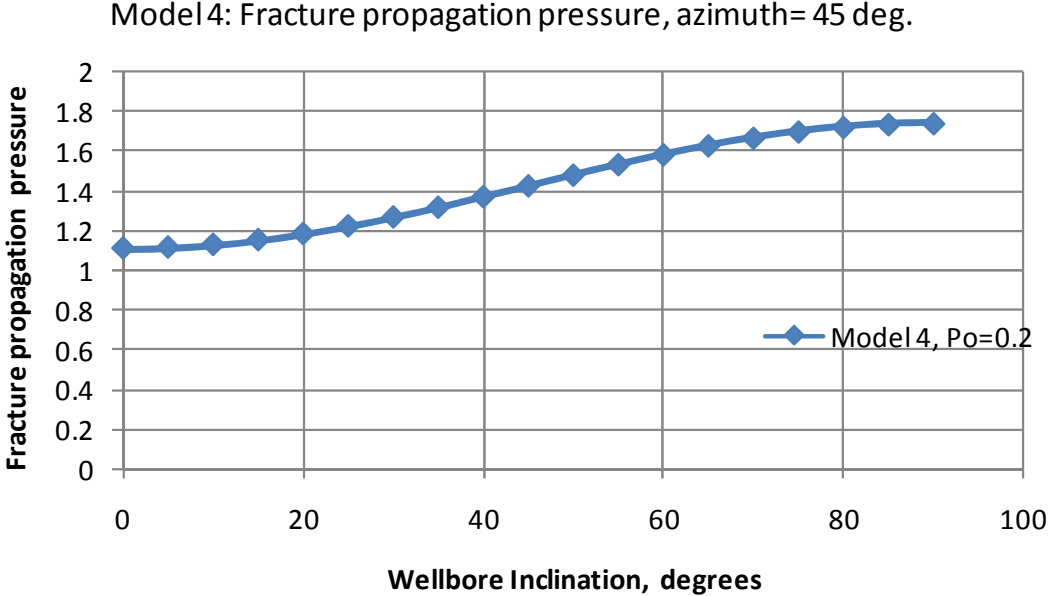


### 5.2.5  Model 5 - Elliptical fracture

Elliptical fracture propagating in direction of maximum horizontal in-situ stress

Loading:

      Externally     In-situ stresses

      Internally     Well pressure/Fracture pressure

Assumption:

      Non-Darcy flow

      Constant injection pressure

Plane strain conditions
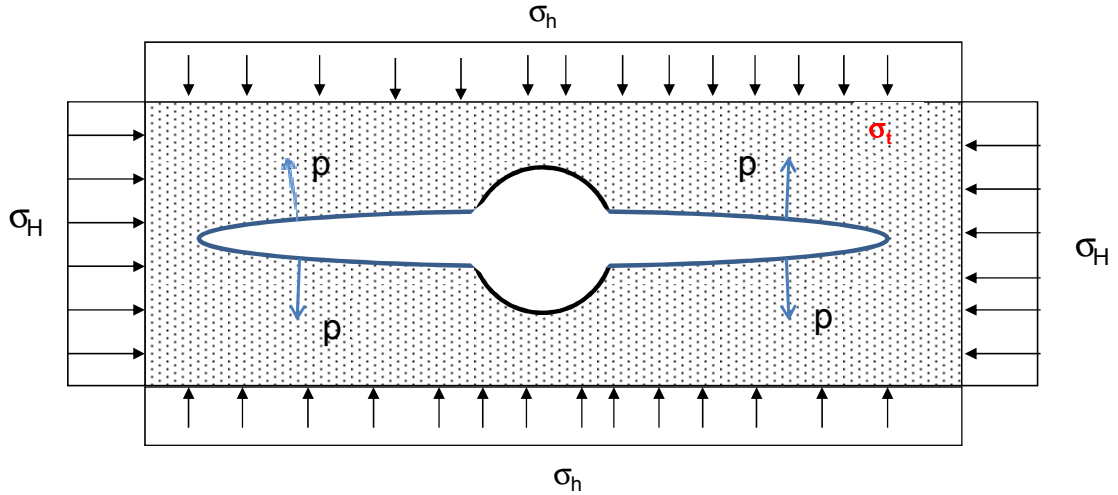
This model is very similar to the above model, with the exception that here we make use of the Irwin's expression for the stress field around a crack tip to account for stress concentration effects.

The normal stress on the fracture face simplifies to:

$$\sigma_{xx} = \sigma_h - P \qquad (5.24)$$

According to Irwin et al., the stress at the crack tip is $\sigma_{ij} \approx \frac{\sigma\sqrt{\pi r}}{\sqrt{2\pi r}} f_{ij}(\theta) \approx \frac{\sigma}{\sqrt{2}} f_{ij}{}^I(\theta)$

$$\sigma_{ij} \approx \frac{\sigma_h - P}{\sqrt{2}} f_{ij}(\theta) \qquad (5.25)$$

The stresses at the tip can thus be expressed in cylindrical coordinates as:

$$\sigma_r = \frac{\sigma_h - P}{\sqrt{2}} f_{11}(\theta) \qquad (5.26)$$

$$\sigma_\theta = \frac{\sigma_h - P}{\sqrt{2}} f_{22}(\theta) \qquad (5.27)$$

$$\sigma_z = \frac{\sigma_h - P}{\sqrt{2}} f_{33}(\theta) \qquad (5.28)$$

$$\tau_{\theta z} = \frac{\sigma_h - P}{\sqrt{2}} f_{12}(\theta) \qquad (5.29)$$

$$\tau_{r\theta} = \tau_{rz} = 0 \qquad (5.30)$$

The functions $f_{ij}^{(l)}(\theta)$ define the angular dependence of the stress at the crack tip are given in section 4.1.

70

Therefore, we can compute the principal stresses as:

$$\sigma^1_1 = \sigma_r - P_o \qquad (5.31)$$

$$\sigma^1_{2,3} = \tfrac{1}{2}(\sigma^1_z + \sigma^1_\theta) \pm \tfrac{1}{2}\sqrt{[(\sigma^1_\theta - \sigma^1_z)^2 + 4\tau^1_{\theta z}{}^2]} \qquad (5.32)$$

Where $\sigma_1 > \sigma_2 > \sigma_3$

Griffith's fracture propagation criteria may be presented as:

$$\text{if } (\sigma'_1 + 3\sigma'_3) > 0, \qquad (5.33)$$

$$(\sigma'_1 - \sigma'_3)^2 = 8T_o(\sigma'_1 + \sigma'_3) \quad \text{where } 8T_o = C_o = \text{Uniaxial compressive strength} \qquad (5.34)$$

$$\text{And} \quad \text{if } (\sigma'_1 + 3\sigma'_3) < 0 \qquad (5.35)$$

$$\sigma'_3 = -T_o \qquad (5.36)$$

The solution method is briefly described below:

The value of $(\sigma'_1 + 3\sigma'_3)$ is computed and the appropriate criteria is chosen. The fracture propagation pressure is then solved numerically by iteration. The usual starting point is to assume a fracture pressure P and compute the principal stresses. Then the appropriate criteria is chosen to solve for a new P. The process continues till the differences between subsequent results are acceptably small. This iteration process is thus used to obtain the fracture propagation pressures.

A numerical example of this model application is shown below. The data used in the analysis are:

**Table 7:** Data used for analysis

| $\sigma_h$ | $\sigma_H$ | $\sigma_v$ | $\sigma_t$ | Po |
|------|------|------|------|------|
| 1,6 | 1,7 | 1,8 | 1 | 1,25 |

The result showing the angular dependence of the fracture pressure is presented below:
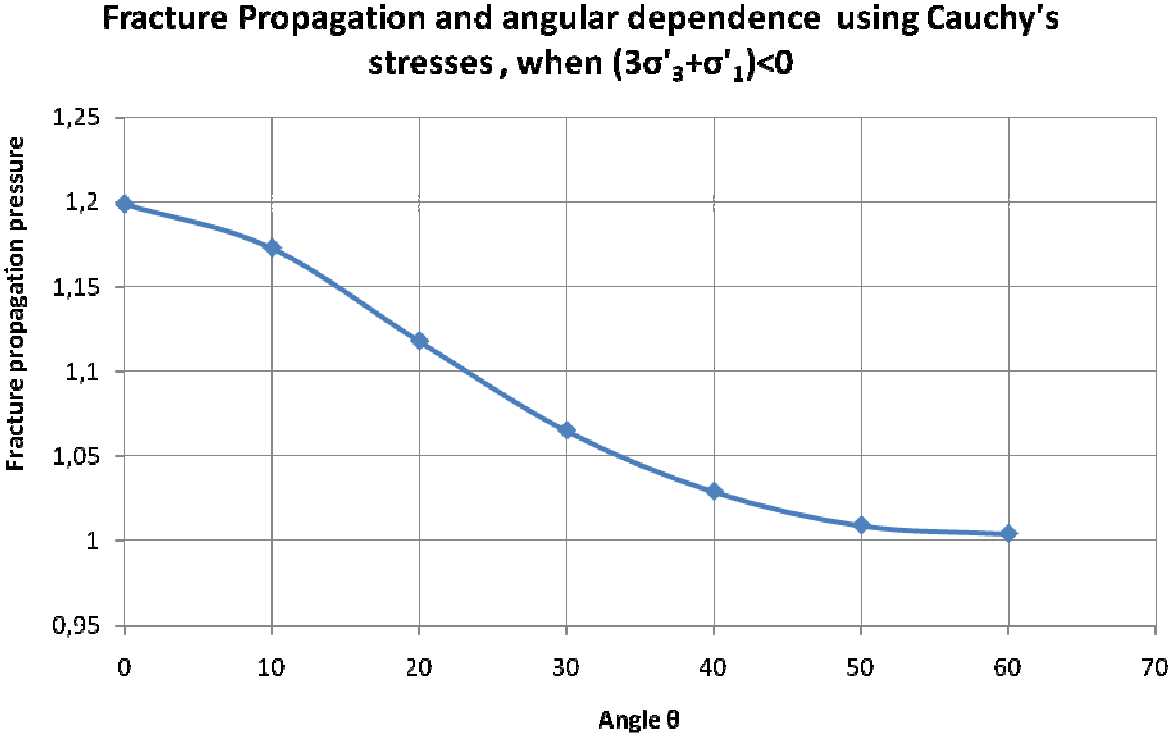


**Figure 42:** Fracture propagation results showing angular dependence.

Since this model which includes pressure requires us to determine stresses that are pressure dependent, the solution method I used was to assume a pressure and then compute the principal stresses. When $3\sigma_3+\sigma_1 < 0$, then I simply varied the pressure until $\sigma_3^1$ equalled the tensile strength. This corresponding pressure needed to meet this fracture propagation criteria is then the fracture propagation pressure.

The plot shows a decrease in fracture propagation pressure with increasing angle $\theta$.

When plotted against hole inclination, the result obtained for $\theta = 0$ ( at the tip) is presented below
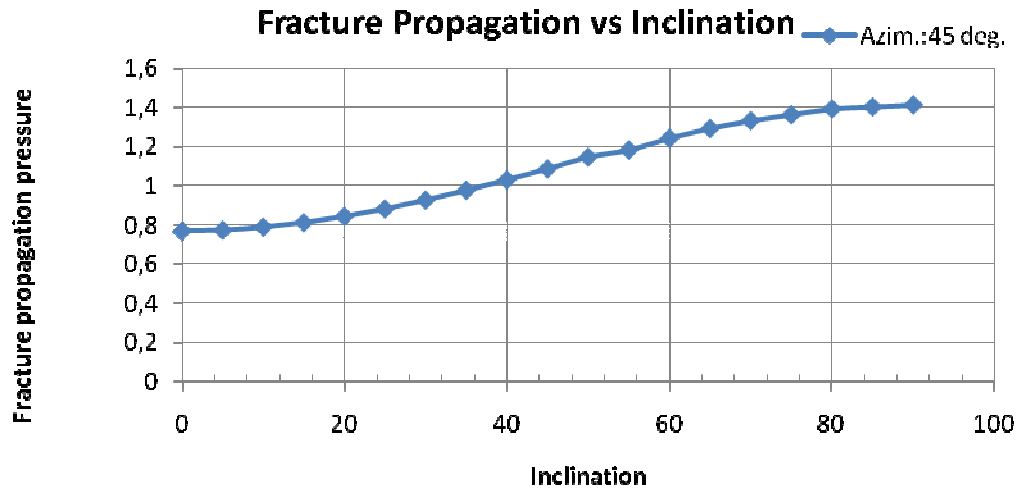
**Figure 43:** Fracture propagation pressures for model 5 as a function of inclination

This model clearly predicts higher fracture propagation pressure than the other models.

## 5.3 Rectangular Fracture Models:

Belayneh[22] introduces the concept of rectangular fracture propagation models. They are presented below:

Loading:

- Externally     In-situ stresses
- Internally     Well pressure/Fracture pressure

Assumption:

- Non-Darcy flow
- Constant injection pressure
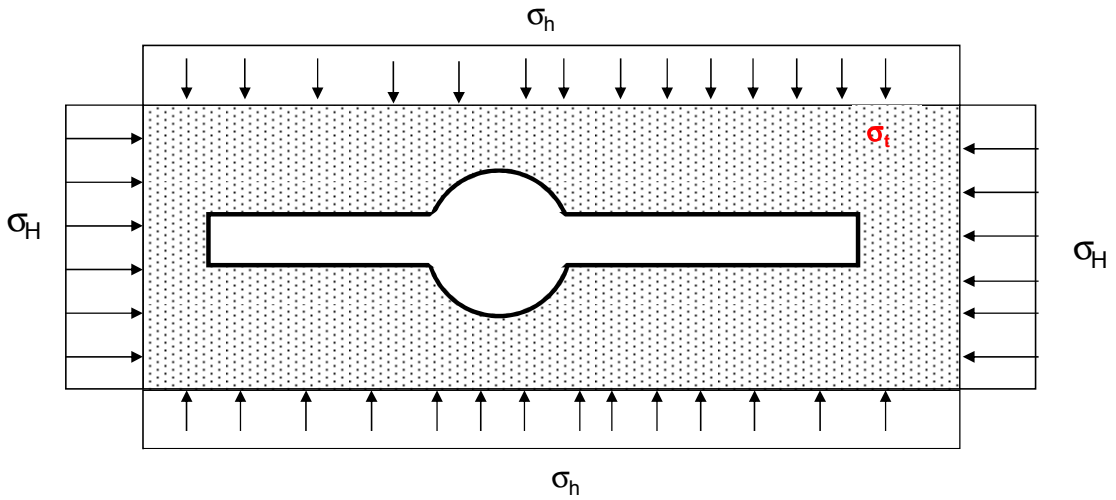
**Figure 44:** Rectangular model

**Failure criterion**

Hillerberg theory: The effective loading at the tip of the fracture should overcome the tensile strength of the rock at the tip

Effective loading: Body diagram at the tip of the fracture



$$P_{effective} = \sqrt{\left(P_{fp} - \sigma'_h\right)^2 + \left(P_{fp} - \sigma'_H\right)^2}$$
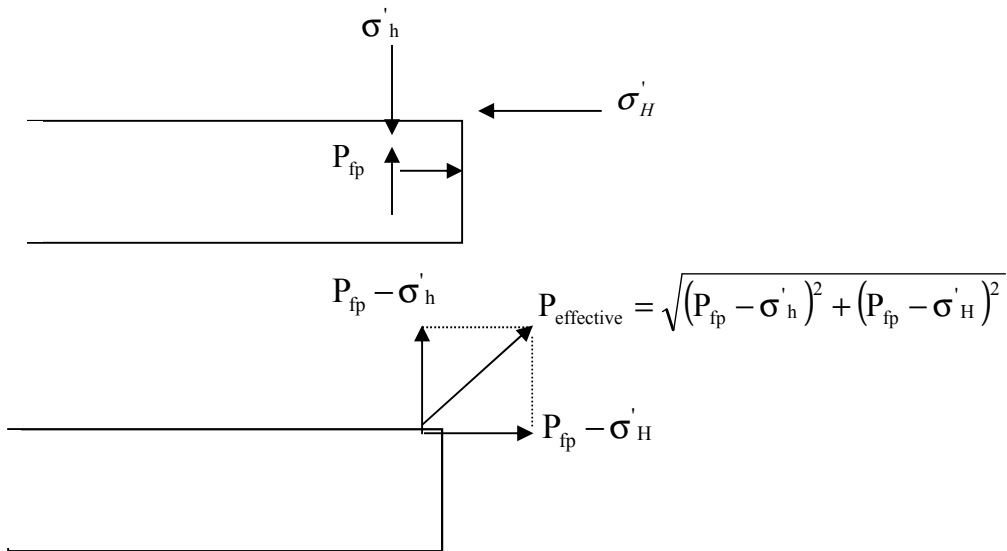
### 5.3.1  Model 1: Maximum Horizontal in-situ stress has effect

Applying Hillerborgs criterion, one obtains:

$$P_{effective} = \sqrt{\left(P_{fp} - \sigma'_h\right)^2 + \left(P_{fp} - \sigma'_H\right)^2} = \sigma_{tensile}$$

(5.37)

Solving for fracturing pressure

$$P_{fpe} = 0.5\left\{\sigma'_h + \sigma'_H \pm \sqrt{2\sigma'_h * \sigma'_H + 2\sigma_t - \sigma'^2_h - \sigma'^2_H}\right\}$$

(5.38)

### 5.3.2  Model 2: Maximum Horizontal in-situ stress has no effect

The above failure criteria simplifies to the following when $\sigma'_H$ is set equal to zero:

$$P_{effective} = P_{fp} - \sigma'_h = \sigma_{tensile}$$

(5.39)

Solving for fracture pressure, we get

$$P_{fp} = \sigma'_h + \sigma_{tensile}$$

(5.40)

### 5.33  Model 3: Maximum Horizontal in-situ stress has effect, but no the internal pressure effect in the direction of the horizontal stress
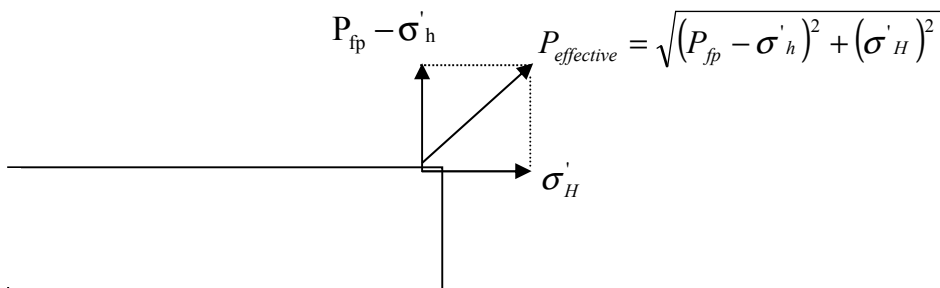


$$P_{effective} = \sqrt{\left(P_{fp} - \sigma'_h\right)^2 + \left(\sigma'_H\right)^2} = \sigma_{tensile}$$

(5.41)

$$P_{fpe} = \sigma'_h + \sqrt{\sigma_t^2 - \sigma'^2_H}$$

(5.42)

Where: the effectives stresses: $\sigma'_{H/h} = \sigma_{H/h} - P_o$

### 5.3.4 Model 4: Maximum Horizontal in-situ stress has no effect, but there is internal pressure effect in the direction of the maximum horizontal stress
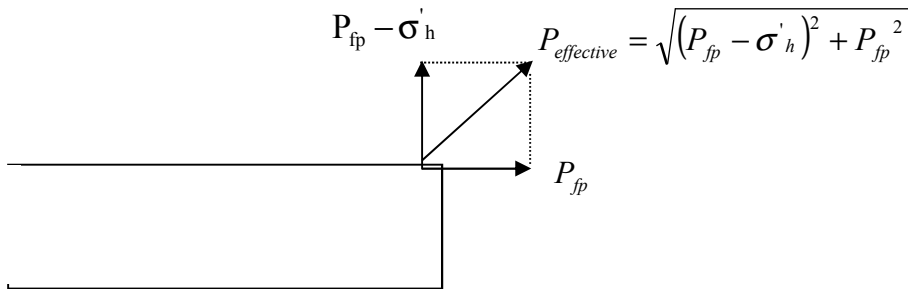


Using failure criteria,

$$P_{effective} = \sqrt{\left(P_{fp} - \sigma'_h\right)^2 + P_{fp}^{\ 2}} = \sigma_{tensile}$$

(5.43)

$$P_{fpe} = 0.5\left\{\sigma'_h + \sqrt{2\sigma_t^2 - \sigma'^{\ 2}_h}\right\}$$

(5.44)

Where: the effectives stresses: $\sigma'_{H/h} = \sigma_{H/h} - P_o$

**Numerical example:**

In this example both the fracture initiation and the fracture propagations are presented. The well inclination is from vetrical to horizontal directions. The figure shows at various azimuth direction. The three models fracture initiation pressures and the fracture pressures propagation pressure are plotted in Fig 45 and 46 respectivley.

**Table 8:** Data used for the analysis

| $\sigma_h$ | $\sigma_H$ | $\sigma_v$ | $\sigma_t$ | Po |
|---|---|---|---|---|
| 1,6 | 1,7 | 1,8 | 1 | 1,0 |
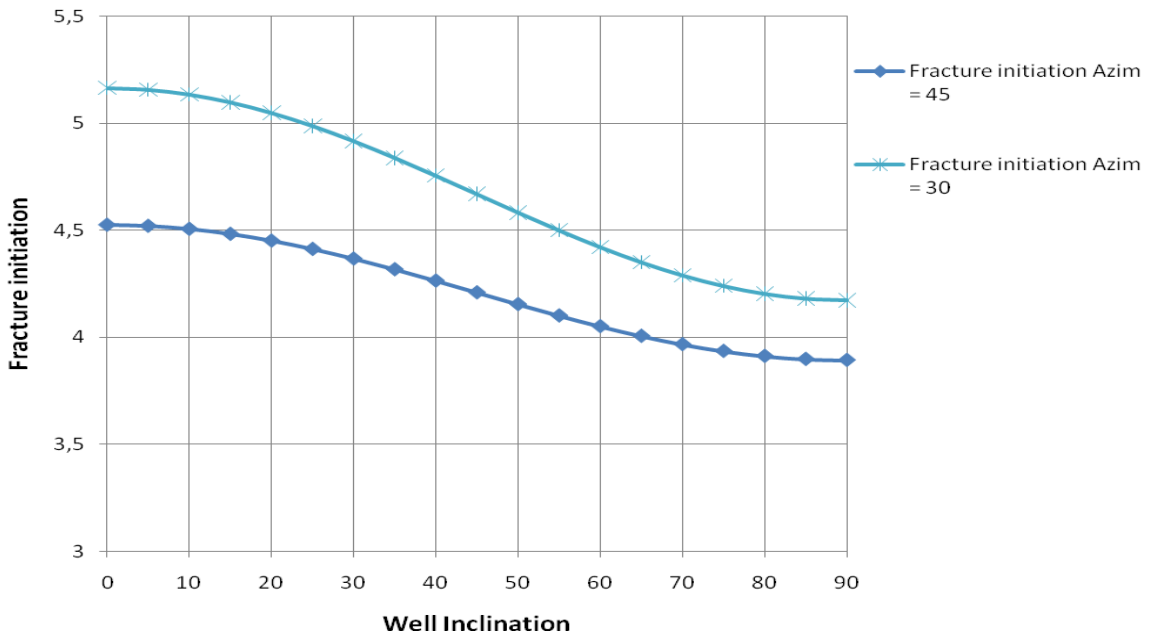
**Figure 45:** Fracture initaition result against well inclination

Figure 45 shows that the fracture initiation pressures decreases with increasing wellbore inclination.
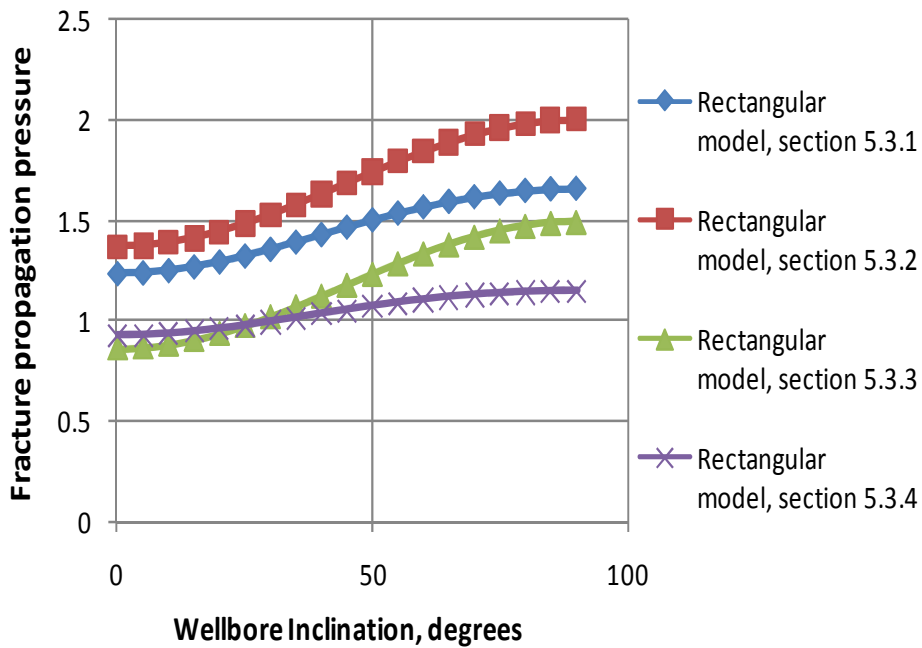
**Figure 46:** Rectangular models Fracture propagation results against well inclination for various azimuths

## Comparison of the triangular and elliptical models

The models will be compared using the following data in table 9:

**Table 9:** data set for model comparison

| $\sigma_h$ | $\sigma_H$ | $\sigma_v$ | $\sigma_t$ | Po |
|------|------|------|------|------|
| 1,6 | 1,7 | 1,8 | 1 | 1,0 |

Due to the rigorous approach to solving model 5, we will limit this comparison to models 1 to 4. The result of the calculations are shown in the figure 47.
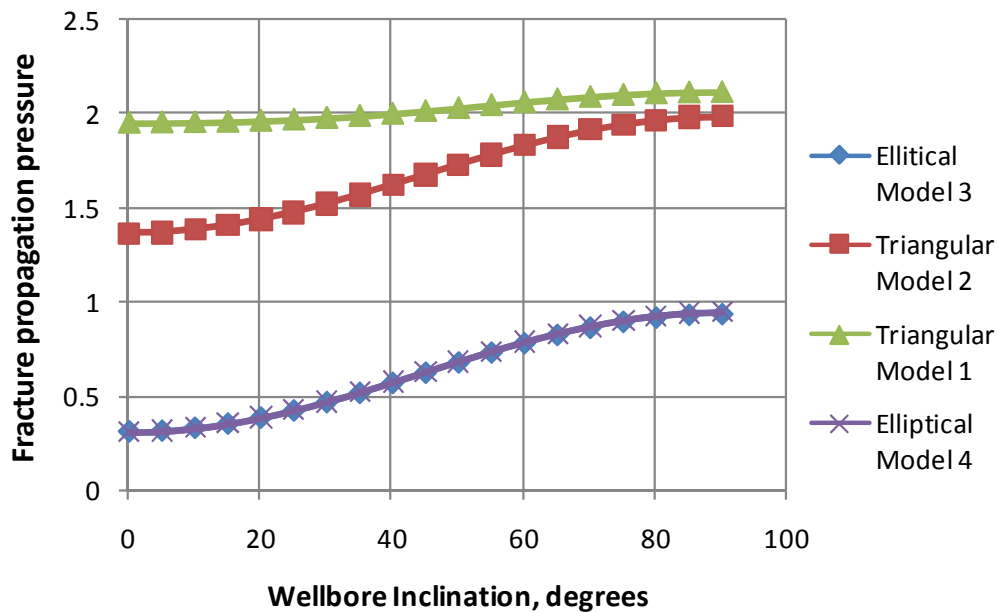


**Figure 47:** Comparison of elliptical and triangular models

The figure 47 shows that the triangular models give the highest prediction of the fracture propagation pressures. The elliptical models surprisingly give approximately the same pressure predictions.

## Comparison of the triangular, elliptical and rectangular models

All the fracture propagation models presented in this work will briefly be compared using the data in table 10.

**Table 10**: Data set for model comparison

| $\sigma_h$ | $\sigma_H$ | $\sigma_v$ | $\sigma_t$ | Po |
|---|---|---|---|---|
| 1,6 | 1,7 | 1,8 | 1 | 1,0 |
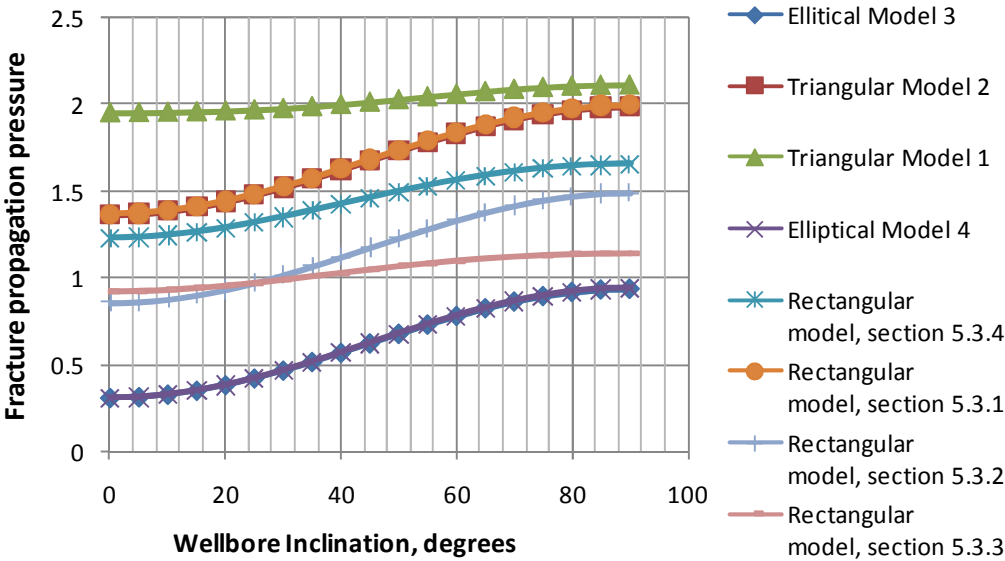


**Figure 48:** Comparison of all the models

The result presented in the figure below show that the triangular model 1 predicts the highest fracture propagation pressures. The Triangular model 2 and the rectangular model presented in section 5.3.2 predict the next highest pressures and they both predict approximately the same pressures. the elliptical models give the lowest predictions while the other rectangular models gives values that are in-between.

## 5.4 Comparisons of models with experimental data

The difference between the Rectangular models and the triangular and elliptica models is that the rectangular model considers only the stresses while the other models takes into account the fracture parameters such as tip angle, width, and length. Assume the fracture length = 5cm and width =0.3mm, the triangular and elliptical models give the following prediction:

Rectangular fracture model: comparison of one of the rectangular fracture models (equation 5.40) and experimental data is shown in figure 49.
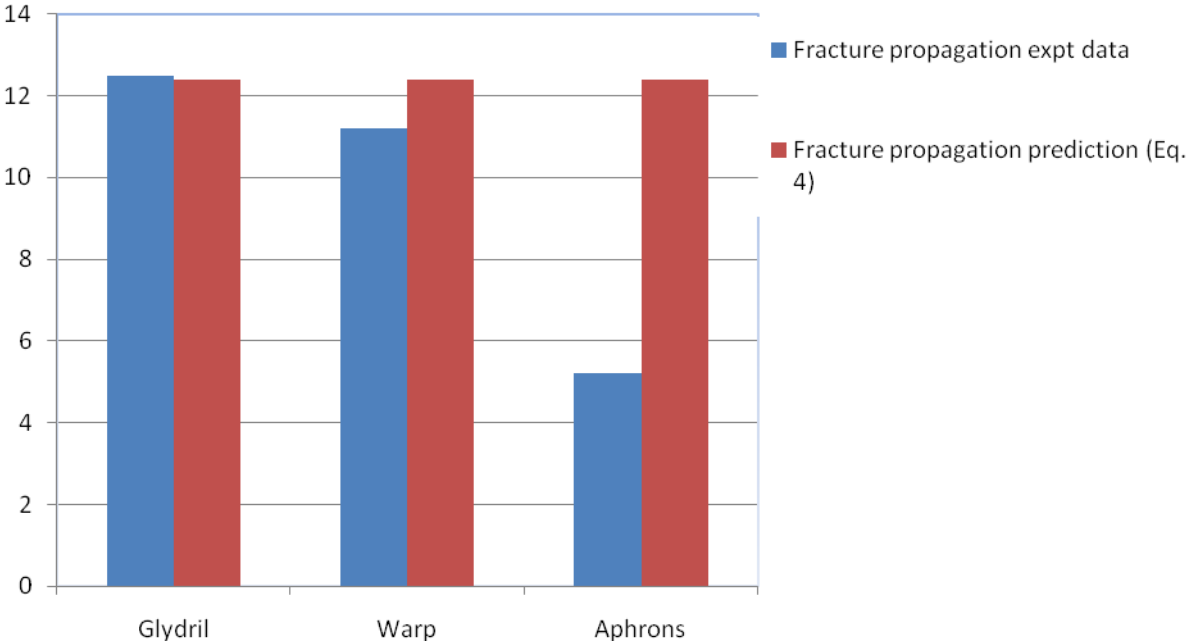


**Figure 49:** Comparison between Rectangular models and experimental results

The figure shows that the model compares well with the result obtained when Glydril mud was used. It also gives a prediction that is close to the result obtained using Warp drilling fluid, It however over-estimates the result obtained using Aphrons drilling fuid.
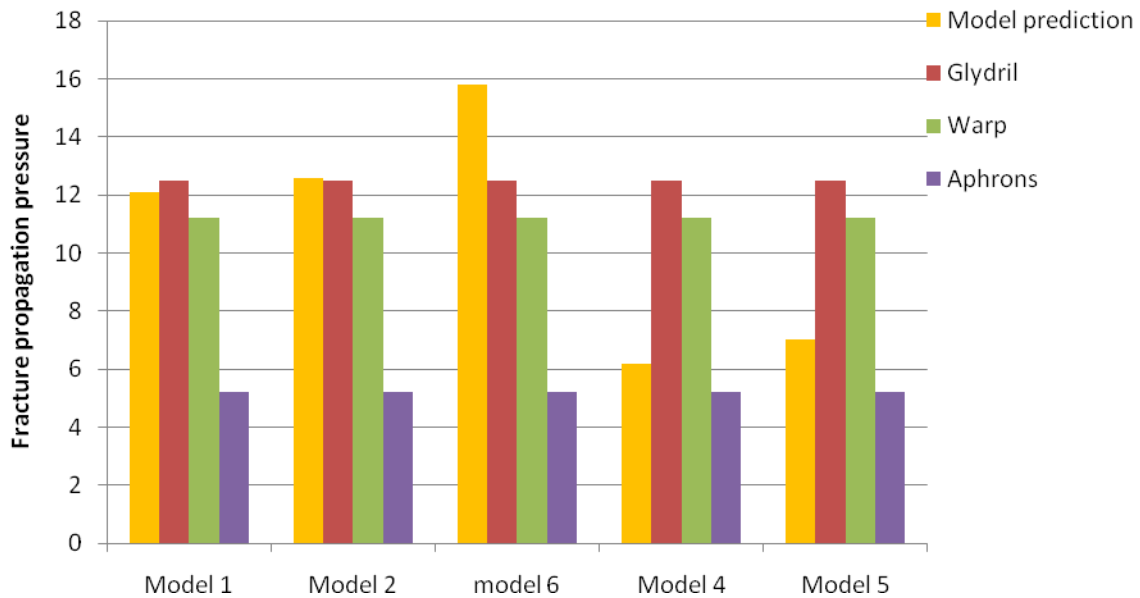
Figure 50 - Comparison between the other models and experimental results

Figure 50 shows that models 1 and 2 gives acceptable prediction of the fracture propagation pressure when Glydril and Warp drilling muds are used in the experiment but they over predict the fracture pressure when Aphrons drilling mud is used. Models 4 and 5 underpredict the fracture pressure when Glydril and Warp drilling muds are used. They however give low fracture pressure predictions which are closest to the observed fracture pressure using Aphrons mud. However, their predictions are dependent on angle εo and L/w respectively. Thus, they predict the accurate fracture pressure when the correct value of angle εo and L/w same value are used as shown in the plots below. The only problem is that both angle εo and L/w are unknowns which need to be determined.

**Model 4: varying angle εo.**

This model under predicts the fracture propagation pressure when Glydril and Warp Drilling muds were used in the experiment, but it which agrees with the measure values when Aphron drilling mud is used in the experiment as shown below.

**Figure 51:** Comparison between model 4 and experimental results

Notice that as the angle εo decreases the fracture propagation pressure decreases accordingly such that some specific angle, the measured and predicted values of fracture pressure are equal. Observe that at an angle of about 0.3 radians, both the predicted and the measured fracture propagation pressures are equal. This seeming high angle is due to the high tensile strength of the material compared to the magnitude of the in-situ stresses. This shows that this model may be sufficient to predict fracture pressure using this mud. The major uncertainty in this model is the value of the angle εo, which is unknown. However, the fracture pressure do not change so much with slight increase in the angle.

This model predicts a critical angle of 0.618 radians, at which fracture propagation occurs. This angle is independent of the formation properties as shown in the derivation. It is however worth noting that the predicted fracture pressure at the critical fracture angle is not so far from the actual measured value using Aphron drilling mud.

## Model 5: varying L/w

As mentioned earlier, this model under predicts the fracture propagation pressure when Glydril and Warp Drilling muds were used in the experiment, but it which agrees with the measure values when Aphron drilling mud is used in the experiment as shown below.



**Figure 52:** Comparison between model 5 and experimental results

Notice that as the length of the fracture increases, the fracture propagation pressure decreases towards a value that is equal to the tensile strength of the rock. Observe also that at some value of L/w, the predicted and measured value of fracture pressure become equal. This model however predicts an L/w ratio of 4, as the experimental and measured data agree closely at this value.

The value of L/w ratio after fracture initiation and before fracture propagation is unknown. The model above clearly shows the length of the fracture play some role in the magnitude of the fracture propagation pressure.

In summary, the experiments show that the fluid properties play a significant role in the fracture pressure. The subsequent section will be dedicated to understanding the effect of fluid properties on fracture propagation.

## 5.5 Fracture propagation modeling including fluid flow

To explain the different pressure behavior when different fluids are used, we have to consider the properties of the mud cake formed by the different fluids and the fluid properties themselves. A less viscous fluid with a poorer mud cake formation capability will clearly yield a higher pressure drop due to filtration than a more viscous one. The compressibility of the solids fraction that forms the filter cake and their sizes compared to the pore throats should also play an important role.

With these concepts at the back of our minds, we can now derive a continuity equation for fluid flow in fractures.

## 5.5.1 Continuity Equation for Flow in Fractures

The fracture propagation models developed at the beginning of this chapter were derived based on the assumption of non-Darcy flow. Typical borehole fracture modeling assumes either a perfectly sealing mudcake for drilling operations, or a non-sealing mudcake for stimulation operations. It has been observed experimentally[5] that the fracture initiation and propagation pressures vary when different drilling muds are used in the fracturing experiment on cores having the same properties. This suggests that the differences observed are due to the varying mud properties.

Assuming that the variation in the fracture propagation pressures due to the different drilling muds is attributed to the sealing capacity of the mudcake formed. Thus, a mud that forms a cake with good sealing properties will have very low cake permeability. On the other hand, a mud that forms a cake with poor sealing properties will result in a cake of higher permeability.

An attempt to develop a model for fluid flow in fractures is made with a view to understanding the impact of the non-darcy flow assumption (perfectly sealing mudcake assumption) and also with a view to using it to predict the fracture propagation pressures.

The modeling will be made considering a fracture with rectangular geometry.
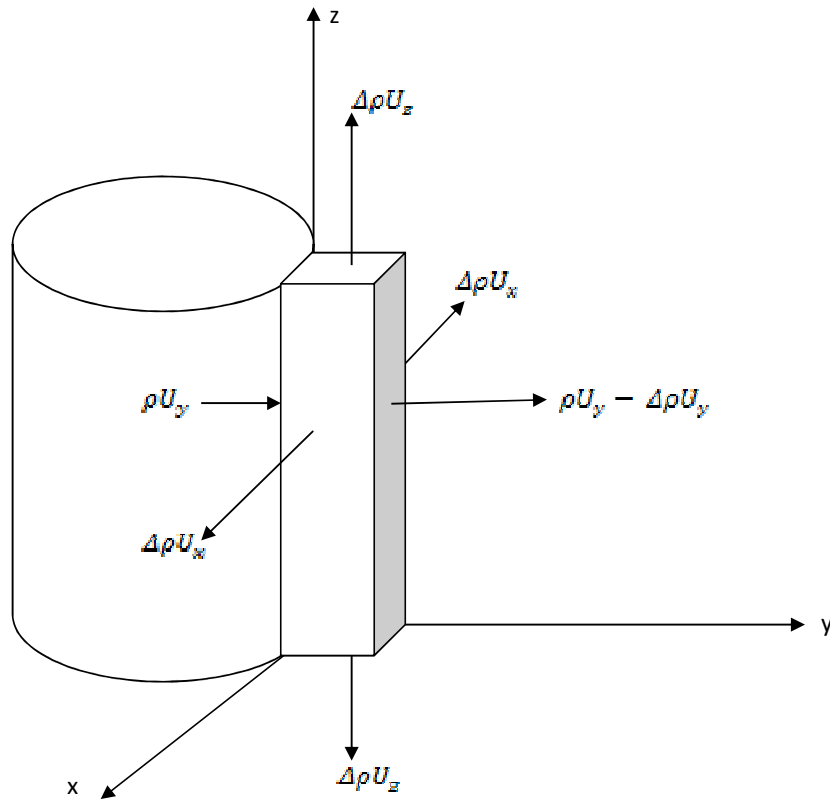
**Figure 53:** Flow from the wellbore into a fracture of rectangular geometry.

Fluid flows into the fracture from the well bore with a rate $\rho U_y$, and exits from the side parallel to the wellbore at a rate $\rho U_y - \Delta \rho U_y$. Fluid leaks off into the formation from all the other sides with rates $\Delta \rho U_i$ where subscript 'i' indicates direction of flow. $U_i$ is modeled using darcy's law

The sides of the fracture are of sizes $\Delta x, \Delta y, \Delta z$ in the x, y, z direction respectively. $\Delta x$ varies from 0 to the fracture width w, $\Delta y$ varies from 0 to the fracture length L, while $\Delta z$ varies from 0 to the fracture height h.

Mass balance:

The rate at which mass enters the element from the well bore

$$= \rho U_y \Delta x \Delta z$$

The rate at which mass leaves the element including leak off to the formation

$$= \left(\rho U_y - \Delta\rho U_y\right)\Delta x \Delta z + 2\Delta\rho U_x \Delta y \Delta z + 2\Delta\rho U_z \Delta y \Delta x \tag{5.45}$$

The rate of mass flows into the element – rate of mass flow out of the element

$$= \rho U_y \Delta x \Delta z - \left\{\left(\rho U_y - \Delta\rho U_y\right)\Delta x \Delta z + 2\Delta\rho U_x \Delta y \Delta z + 2\Delta\rho U_z \Delta y \Delta x\right\} \tag{5.46}$$

$$= \Delta\rho U_y \Delta x \Delta z - 2\Delta\rho U_x \Delta y \Delta z - 2\Delta\rho U_z \Delta y \Delta x \tag{5.47}$$

The rate at which mass changes over time interval $\Delta t$ is

$$= \frac{\left(\rho\emptyset_{t+\Delta t} - \rho\emptyset_t\right)}{\Delta t} \Delta x \Delta y \Delta z \tag{5.48}$$

Mass balance thus becomes:

$$\Delta\rho U_y \Delta x \Delta z - 2\Delta\rho U_x \Delta y \Delta z - 2\Delta\rho U_z \Delta y \Delta x = \frac{\left(\rho\emptyset_{t+\Delta t} - \rho\emptyset_t\right)}{\Delta t} \Delta x \Delta y \Delta z \tag{5.49}$$

Dividing through by $\Delta x \Delta y \Delta z$ and taking the limit as $\Delta x, \Delta y, and \ \Delta z$ tends to zero, we get

$$\frac{\partial\rho U_y}{\partial y} - 2\frac{\partial\rho U_x}{\partial x} - 2\frac{\partial\rho U_z}{\partial z} = -\frac{\partial(\rho\emptyset)}{\partial t} \ \ldots\ldots\ldots\ldots \text{Continuity equation} \tag{5.50}$$

Flow laws (Darcy's law) :

Assuming that gravity acts only in the z-direction, we can write Darcy's law as:

$$U_x = -0.001127\frac{k_x}{\mu}\frac{\partial P}{\partial x} \tag{5.51}$$

$$U_y = -0.001127\frac{k_y}{\mu}\frac{\partial P}{\partial y} \tag{5.52}$$

$$U_z = -0.001127\frac{k_z}{\mu}\left(\frac{\partial P}{\partial z} + 0.00694\rho\right) \tag{5.53}$$

If we ignore gravity effect, $U_z = -0.001127 \frac{k_z}{\mu}\left(\frac{\partial P}{\partial z}\right)$ (5.54)

After substituting the Darcy velocities into the continuity equation, we get:

$$\frac{\partial}{\partial y}\left(\frac{\rho k_y}{\mu}\frac{\partial P}{\partial y}\right) - 2\frac{\partial}{\partial x}\left(\frac{\rho k_x}{\mu}\frac{\partial P}{\partial x}\right) - 2\frac{\partial}{\partial z}\left(\frac{\rho k_z}{\mu}\frac{\partial P}{\partial z}\right) = \frac{1}{0.000264}\frac{\partial(\rho \emptyset)}{\partial t} \qquad (5.55)$$

Assuming single phase flow of slightly compressible fluids of constant compressibility c,

$$c = -\frac{1}{V}\frac{\partial V}{\partial P} = \frac{1}{\rho}\frac{\partial \rho}{\partial P}. \qquad (5.56)$$

We can rewrite it as $\rho = \rho_o e^{c(P-P_0)}$

We also assume constant porosity and isotropic property of the mud cake surrounding the fracture walls, such that $k_x = k_y = k_z = constant = k$

Substituting the expressions for density, the continuity equation then becomes:

$$\frac{\partial}{\partial y}\left(e^{c(P-P_0)}\frac{\partial P}{\partial y}\right) - 2\frac{\partial}{\partial x}\left(e^{c(P-P_0)}\frac{\partial P}{\partial x}\right) - 2\frac{\partial}{\partial z}\left(e^{c(P-P_0)}\frac{\partial P}{\partial z}\right) = \frac{\emptyset \mu c}{0.000264 k}\frac{\partial \left(e^{c(P-P_0)}\right)}{\partial t} \qquad (5.57)$$

This simplifies to:

$$\frac{\partial^2 P}{\partial y^2} - 2\left(\frac{\partial^2 P}{\partial x^2} + \frac{\partial^2 P}{\partial z^2}\right) + c\left[\frac{\partial^2 P}{\partial y^2} - 2\left(\frac{\partial^2 P}{\partial x^2} + \frac{\partial^2 P}{\partial z^2}\right)\right] = \frac{\emptyset \mu c}{0.000264 k}\frac{\partial P}{\partial t} \qquad (5.58)$$

Assuming that $c\left[\frac{\partial^2 P}{\partial y^2} - 2\left(\frac{\partial^2 P}{\partial x^2} + \frac{\partial^2 P}{\partial z^2}\right)\right]$ is negligible compared to the other terms because of the small compressibility c, then the diffusivity equation for fluid flow through a rectangular fracture is given as:

$$\frac{\partial^2 P}{\partial y^2} - 2\left(\frac{\partial^2 P}{\partial x^2} + \frac{\partial^2 P}{\partial z^2}\right) = \frac{\emptyset \mu c}{0.000264 k}\frac{\partial P}{\partial t} \qquad (5.59)$$

$$\frac{\partial^2 P}{\partial y^2} - 2\left(\frac{\partial^2 P}{\partial x^2} + \frac{\partial^2 P}{\partial z^2}\right) = \frac{1}{K}\frac{\partial P}{\partial t} \quad \ldots\ldots\ldots\ldots\text{Required continuity equation.} \quad (5.60)$$

where $\dfrac{1}{K} = \dfrac{\emptyset \mu C}{0.000264k}$

This equation will be solved numerically using explicit formulation.

The idea was to integrate fluid flow into and out of the fracture with both horizontal stresses and rock tensile strength so as to obtain a more complete model for fracture propagation. The objective was to develop a model for the fracture wall permeability K as a function of time. This permeability was to be used in the diffusivity equation above. The idea applies to a fracture that have been initiated and is no longer propagating due to the pressure decline. It was intended that as the permeability decreases with time and tends towards zero, with continued fluid flow into the fracture, the pressure in the fracture will build up towards the fracture propagation pressure and the fracture will start to propagate. If it was somehow possible to combine all the stresses and this diffusivity equation, then we can obtain a better prediction of the pressure at the wellbore required to propagate a fracture. Unfortunately the author cannot proceed from here due to the encountered challenges. I was at my former university two weeks ago and I discussed this idea with my professor at the Department of Petroleum Engineering. It turns out that he has pursued this same idea in conjunction with another lecturer and they have been able to solve the problem. However, their work is yet to be published. It would be interesting to know the nature of the solution.

## 5.5.2 Fracture propagation rate

One of the most important problems of fracture propagation is the determination of the fracture propagation velocity based on the main mechanical characteristics of the rock. A major limitation of the Griffith criterion and the Hillerborg Criterion therefore, is that they do not give any information about the fracture propagation rate.
Mott[14] worked with the fracture of metals and he found that there exist a limiting velocity for propagation cracks and that this velocity can be represented by

$$v_{max} = k \sqrt{\frac{E}{\rho}} \qquad\qquad (5.61)$$

However, the dimensionless coefficient k was not determined.

Roberts and Wells[15] worked on the velocity of brittle fracture and they found that for a poisson ratio ν of 0.25, the value of k was 0.38.

Dulaney and Brace[16] analyzed the velocity behavior of brittle solids based on conservation of energy. They modeled cracks as elliptical holes and arrived at the terminal velocity of crack propagation as

$$v_{terminal} = \left(\frac{2\pi E}{k\rho}\right)^{\frac{1}{2}} \left(1 - \frac{c_0}{c}\right) \qquad\qquad (5.62)$$

Where k = 0.38 assuming Poisson's ratio of 0.25 as determined by wells. The velocity of the propagating crack is then found by

$$v = v_{terminal} \left(1 - \frac{c_0}{c}\right) \qquad\qquad (5.63)$$

Chekunaev and Kaplan[17] modeled cracks as a continuous set of linear dislocations and thereafter determined the potential and kinetic energies of the crack environment. They obtained a complete analytical expression for the limiting crack propagation velocity in elastic materials as a function of the main mechanical characteristics of the material namely the elastic modulus E, the density ρ, and the poisons ratio ν.

The limiting velocity of crack propagation $v_{max}$ in solid materials can thus be calculated using:

$$v_{max} = \sqrt{\frac{1-\nu}{4(1+\nu)\left[\left(\nu^3 - \frac{3\nu}{2} + \frac{7}{8}\right) \ln 5.2 - \frac{3\nu}{8} + \frac{5}{32}\right]}} \sqrt{\frac{E}{\rho}} \qquad\qquad (5.64)$$

This quantity $v_{max}$ is the limiting velocity of crack propagation with infinite increase in crack size.

The crack propagating velocity at any point is a function of this limiting velocity $v_{max}$, the crack half-length a, the poisons ratio v, the elastic modulus E, the applied external stress Po, and the surface tension coefficient $\Gamma$ of the material.

Thus the crack propagating velocity

$$v = v_{max}\left(1 - \frac{a_{cr}}{a}\right) \qquad (5.65)$$

Where $a_{cr} = \frac{2\Gamma E}{\pi(1-v^2)P_0^2}$ is the critical crack size for positive acceleration of crack, and $a > a_{cr}$.

The schematics of the linear crack is shown Figure 52. In the diagram, h(x) is the variable crack width, the length of crack is 2a, p(x) is the external stress applied to the surface of the crack, and G(x) is the additional stress produced by the molecular adhesion forces.
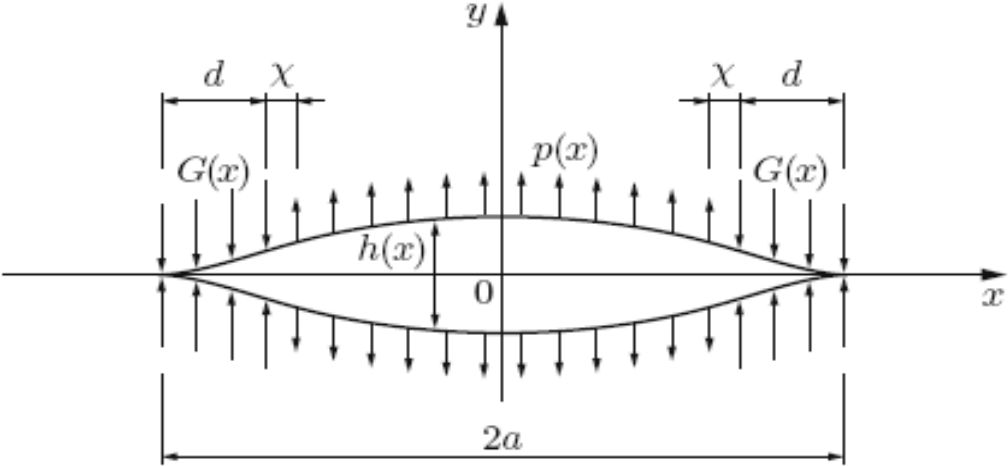


**Figure 54**: Diagram of a linear crack of length 2a[17].

It is therefore evident that fractures will travel with a similar velocity that is predicted by these models. To adapt this work for this analysis the following assumptions are made:

**Assumptions:**

In order to apply this velocity model to my work, the following assumptions were made:

- Rock is homogeneous and isotropic: since the model by Chekunaev and Kaplan was derived for solids which are homogeneous and isotropic, it is reasonable to assume that it would also apply for real rocks if they are assumed to be homogeneous and isotropic.

90

- Linear elasticity: If we assume linear elasticity, this analytical expression for the crack velocity may be applied to real rocks when the mechanical properties are known.

**Limitation:**

Whether the above assumptions are valid or not remains to be seen. More work may be needed to validate or adapt the crack propagating velocity model by Chekunaev and Kaplan for them to work satisfactorily for propagating fractures by introducing anisotropy and heterogeneity in the model. There is no doubt that the crack propagating velocities may hold the key to better understanding of the fracture propagating process. The proceeding work should therefore be used only quantitatively to understand the fracture propagation process better.

The mechanical characteristics of rocks necessary for the velocity calculations are easily obtained:

- The elastic modulus E and the poisons ratio $v$ may be obtained from laboratory tests
- while the density may be estimated from logs or seismic.

The solution procedure involves calculating the critical fracture length, and the crack propagating velocity $v$ at every corresponding fracture-half length. Then the fracture propagating pressure at the corresponding fracture-half length is also computed. Once we have the velocity and the fracture half length, we can determine the time from velocity relation used in physics.

The time needed to plot a fracture propagating pressure vs time curve, is obtained by using average values:

$$time = \frac{(a_{i+1} - a_i)}{(v_{i+1} - v_i)} \tag{5.66}$$

Assuming that the crack geometry used by Chekunaev and Kaplan can be approximated by an elliptical geometry as shown below:
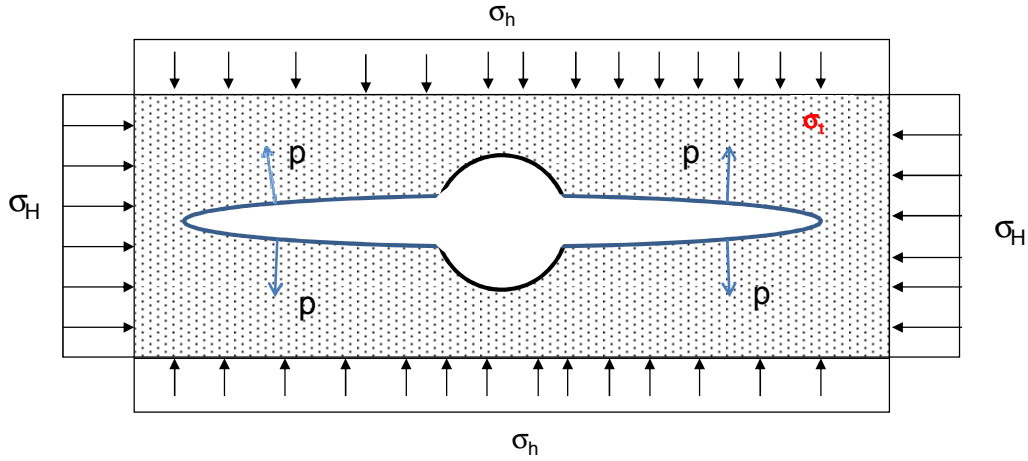
**Figure 55:** Elliptical fracture geometry

The arrow acting away from the wellbore in the block above just indicate the direction of the internal pressure acting inside the fracture.

An example will be done using the fracture propagation model developed for elliptical geometry:

$$P_f = \sigma_h + \frac{\sigma_t}{\left(1 + \frac{2L}{w}\right)} \qquad (5.67)$$

Numerical example:

The following data is used for the analysis:

**Table 11**: Data used for the analysis

| $\sigma_h$ | Po | $\sigma'_h$ | $\sigma_t$ |
|------|------|------|------|
| 1.6 | 0.2 | 1.4 | 0.6 |

Assuming also that a fracture with a width of unit thickness such that L/w ≡ L . Assuming also that a unit critical crack length such that acr/ a = 1/a. These assumptions are made simply to minimize computational work, while preserving the expected trend such that the result may still be interpreted correctly.

When the above model is applied, the plot of the fracture propagation pressure against fracture half-length is presented in Figure 54:
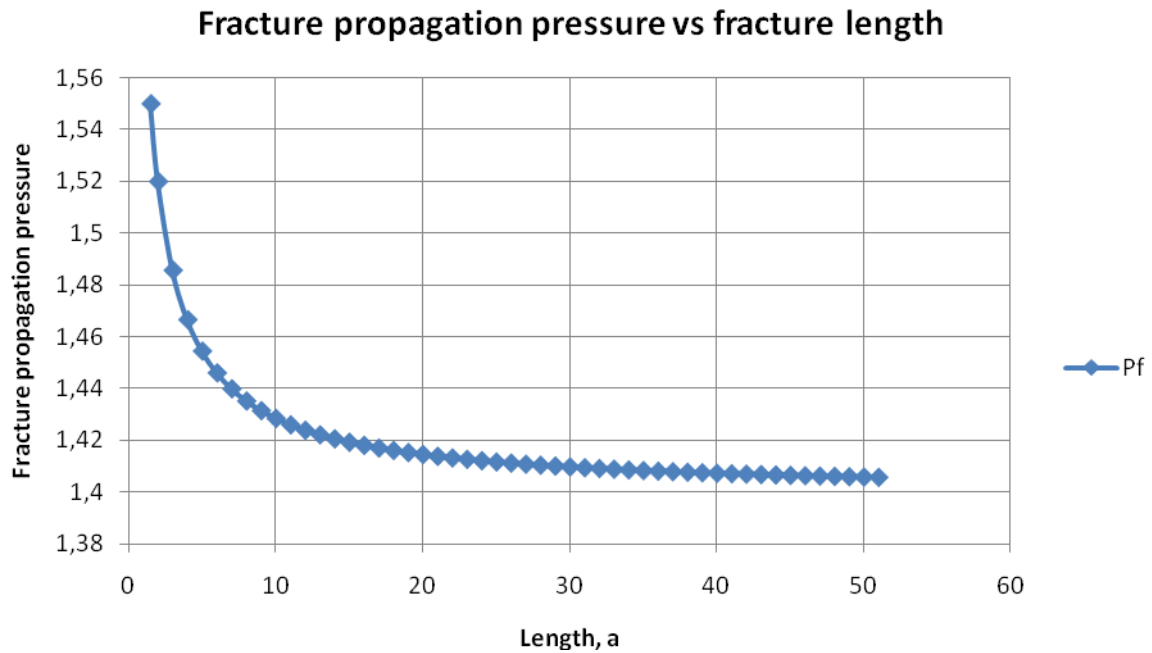
**Figure 56:** Fracture propagation pressure as a function of fracture length

This enables us to predict the fracture propagation pressure for any fracture length. However, it tells us nothing about the time it takes to create the fracture length.

When we introduce the velocity, we obtain;



**Figure 57:** Fracture propagation pressure as a function of time

We can thus see that the fracture pressure drops from 1.56 to 1.42 in just 0.01 seconds. Thereafter, the fracture propagation pressure tends towards a stable value which is the minimum horizontal stress. This gives us a better understanding of the duration of the fracture propagation and the entire process.
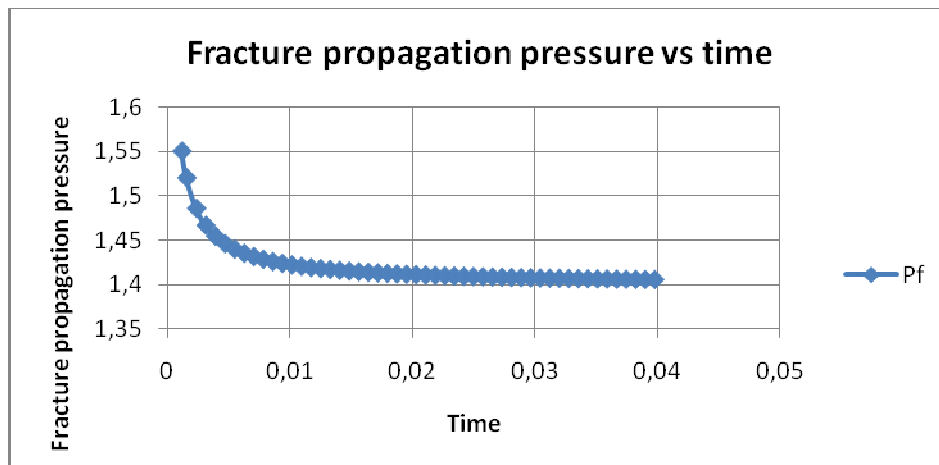
93

In summary, this chapter has been used to propose several fracture propagation models which were derived using varying criteria and concept.

Crack propagation velocities presented for solid mechanics were also analyzed with respect to fracture propagation using the appropriate assumptions.

If the fracture velocity model presented for crack propagation hold for fracture propagation, then it could hold the key to a better understanding of the fracture propagation process.

If it does not directly apply, then it opens the way for further modifications so that it can be confidently applied to fracture mechanics.

# CHAPTER 6 FRACTURE PROPAGATION EXPERIMENTS

The objective of the experiments

The aim of the experiments is to study the fracture propagation process closely so as to obtain a better knowledge of the process. Previous documented fracture propagation experiments assume an isotropic state of stress. In other words, the stresses acting on the cores used for the experiment are equal. This experimental setup however allows us to vary the horizontal stresses and observe the behavior of the fracture. These experiments will investigate the nature and direction of propagation of the fractures when the relative magnitudes of the horizontal stresses are varied. It is normally believed that the fracture propagate normal to the minimum horizontal stress. These experiments will validate that assumption and also seek to find out what happens when the relative magnitudes of the horizontal stresses are large or small:

will the fracture still propagate normal to the minimum horizontal stress or will it propagate in a different direction?

Is there a direct relationship between the relative magnitude of the horizontal stresses and the fracture orientation?

The experiment also seeks to take a closer look at the fracture process itself so as to understand it better. It seeks to know if the fracture propagates in steps or if it occurs instantaneously and continuously.

It also aims to study the geometry of the propagating fracture to see if any observable factor can be identified as being responsible for the fracture geometry.

**Experimental setup**

An experimental setup was designed that allows us to test with rectangular cores. The concept in the design involves two hydraulic hand-pumped jacks that will provide the external stresses on the faces of the core, and a manually controlled handle for applying the tensile stress to a hole in the core. The hydraulic jacks supply pressure to the faces of the core and it also consist of two pressure gauges to enable us know how much pressure the core is subjected to. This enables us to simulate the wellbore in a field with an anisotropic stress state. The plan of the basic structure of the apparatus without the hydraulic jacks is shown in figure …
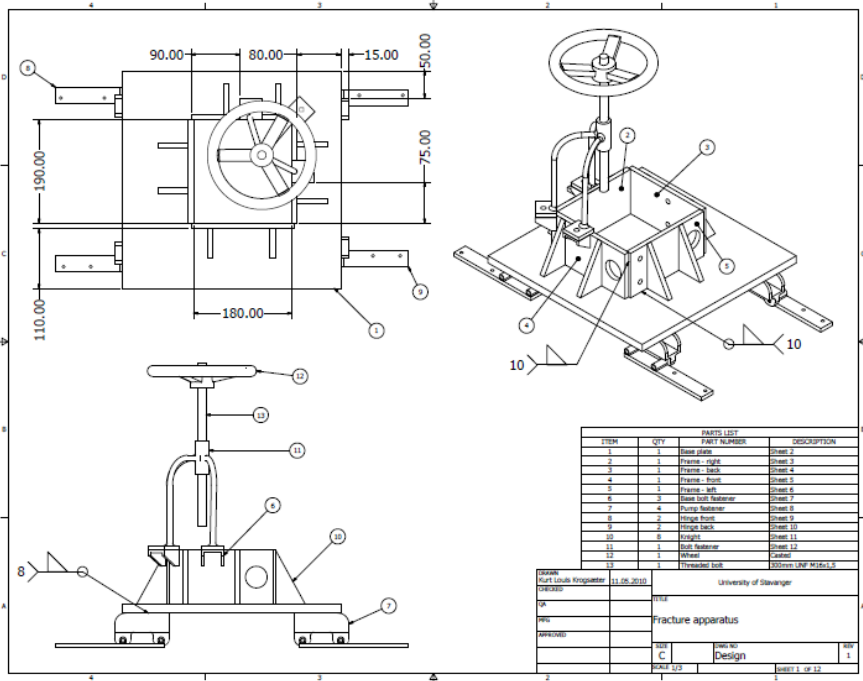


**Figure 58 :** Plan showing the structure of the apparatus

The fabricated apparatus with the core in place ready for testing is shown in figure…..
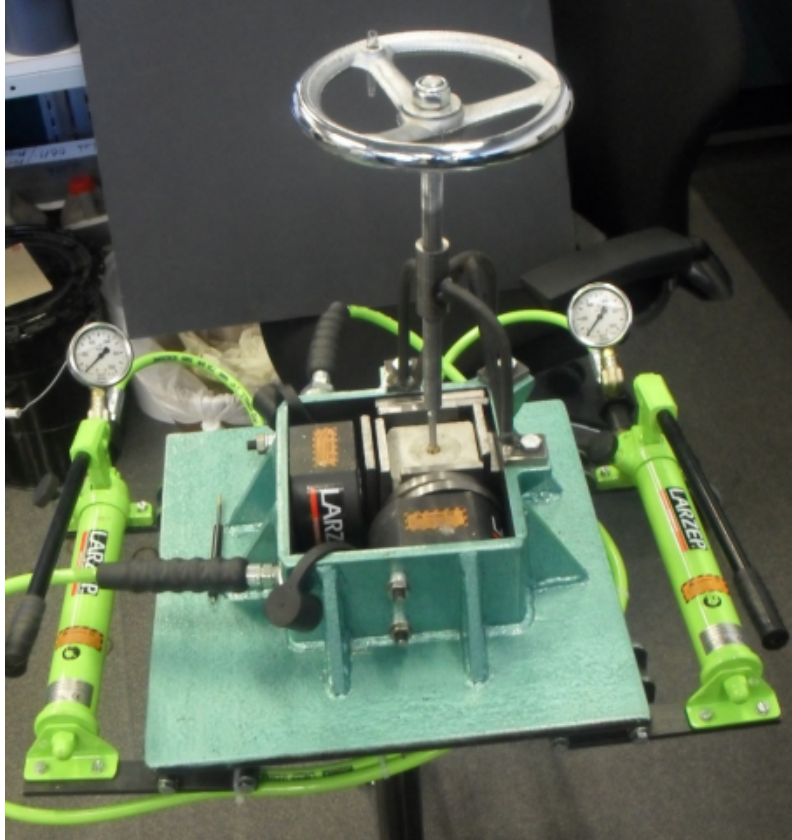
**Figure 59**: Experimental setup.

Rectangular core samples are used in this experiment. The advantage of using such a core is that unlike the conventional cylindrical cores, this core type allows us to apply different stresses to the different sides of the rectangular core thus better simulating field conditions. A sample of the core is shown in figure 60

**Figure 60:** Rectangular core sample

**Strengths of the apparatus**

- It has a simple design concept, with fewer parts that are likely to fail. A major advantage in the simplicity of the design is that it allows us to run tests easily and faster with fewer complications.

- It also allows us to directly observe the propagation process. We can even have a video camera to directly observe the process and then be able to study in more details at leisure.

- We can vary the magnitude of the external stresses on the core easily and observe the trends in propagation.

**Limitations of the apparatus**

- We are not able to measure the tensile stress acting in the hole in the core. Alternative means of calculating the stress value may be complicated

- The mechanism designed for applying the tensile strength on the core needs to be re-designed for better efficiency. It does not provide the necessary amount of tensile stress to fracture the core.

Procedure

1. Place the core in the core compartment in the apparatus and surround it with the appropriate metal supports.
2. Use the handles of the hydraulic jack to apply external stresses on the core. Increase the value of the stresses to a pre-determined value.
3. Increase the tensile stress on the hole in the core by turning the wheel until the core fractures. This should be done gradually so as to obtain gradual fracture propagation.

Results

A test was conducted to see the direction of fracture propagation relative to the applied stresses. A pressure of 400 kg/cm$^2$ was applied on two opposite faces of the core to represent the maximum horizontal stress, while another pressure of 200 kg/cm$^2$ was applied to the other faces to represent the minimum horizontal stress. The core fractured and propagated in a direction normal to the ninmum horizontal stress as shown in figure 61.



**Figure 61:** Fracture propagates normal to minimum stress

When the direction of the maximum stress was reversed, another fracture was seen propagating in the direction of the new maximum horizontal stress as shown in figure 62.



**Figure 62:** Core showing two fracture directions due to reversed maximum stress

It was decided to apply a fixed tensile stress to the hole in a new core and then increase the external stress one by one to the same value. For instance, both applied external pressures were initially at 0 kg/cm$^2$. One of the hydraulic jacks was then pumped gradually to 100 kg/cm$^2$ while the other was kept at zero. Then the other jack was pumped to 100 kg/cm$^2$. Then the previous jack was pumped to 150 kg/cm$^2$ while the other was kept constant at 100 kg/cm$^2$ and then later increased to have both jacks at 150 kg/cm$^2$. The objective was to observe the nature of the fractures after the cyclic loading. When the core finally fractured, multiple fractures was observed travelling in different directions as shown in figure 63.

**Figure 63:** Core showing multiple fractures traveling in different directions

Close observation of the propagating fractures revealed that the fractures were propagating in steps. This is supported by the series of breakage sounds heard during the process that indicates that bonds were being broken. Perhaps this could be due to the uneven strength of the sand particles that constitute the frame-work of the core.

Due to time constraints, extensive experiments could not be conducted. The was also a delay due to broken down concrete cutting machinery as well as challenges presented due to the design of the means of applying tensile force in the hole in the core. All these factors have put some serious limitations on the number of experiments that I can conduct within the time frame. It is recommended that more experiments be conducted in the future after revisiting the design to make some changes.

# CHAPTER 7 DISCUSSION AND CONCLUSION

## Discussion

This thesis focused on the development of fracture propagation models. Rectangular, triangular and elliptical fracture propagation models are developed and presented. The results of the model development show that the fracture propagation pressures increases with increasing wellbore inclination. The reverse is the case for fracture initiation whereby the fracture initiation pressures decreases with increasing inclination.

Comparison of the fracture propagation models with experimental results show that each model has its unique properties. Some models give good prediction when compared to experimental results obtained using some mud types but the result appears to be either too high or too low when compared to experimental results obtained using other mud types. This clearly shows the effect of the drilling fluid on the fracture propagation pressures.

The models developed are limited by their assumptions to just specific geometries. It will be nice to have just one model that can be applicable to different geometries, yet considering all the necessary stresses and fluid properties. Such a model will have to be formulated from the first principle of fuild flow in media. It is recommended that futher work on the diffusivity equation concept should be pursued as it promises to generate a more complete fracture propagation model.

A new concept on the fracture propagation process (section 5.11) is introduced that combined the stress bride concept[7] and a new concept involving fluid loss through fracture walls.

Experimental results show that fractures propagate normal to the minimum horizontal stress however the fracture pattern differs from this when the core is subjected to cyclic stress patterns.

# Conclusion

Based on the work done in this thesis, the following conclusions can be made:

- Different drilling muds have different properties and they therefore give different effects on the fracture propagation pressures. Thus, the fracture propagation pressures vary when different mud systems are used even on similar cores.

- Fracture propagation models for the triangular, elliptical and rectangular geometries have been developed and presented.

- Comparison with experimental data show that the models give good results for some mud types but either over-predicts or under-predicts for other mud types. Thus this calls attention to developing a model that incorporates fluid properties.

- An attempt to incorporate the  fluid effect was made by developing a diffusivity equation for fluid flow into and out of fractures which takes the varying fracture wall permeability as a function of time into account. It was assumed that the different fluids formed mud cakes of different permeabilities and this was responsible for the observed disparity in results when different muds were used on the same core samples. The plan was to use this fluid model to compute the pressure at the fracture tip, and then combine this pressure, the rock tensile strength, and the horizontal stresses to develop a single fracture propagation equation. Unfortunately this line of thought was not pursued to the end due to encountered challenges.

- Results show that the triangular model 1 predicts the highest fracture propagation pressures. The Triangular model 2 and the rectangular model presented in section 5.3.2 predict the next highest pressures and they both predict approximately the same pressures. The elliptical models give the lowest predictions while the other rectangular models gives values that are in-between.

- A new concept of fracture propagation was presented (section 5.1) that considers the fluid effect and the stress bridge concept[7].

- Experiments were conducted that confirm that fracture propagate normal to the minimum horizontal stress. Fracture patterns under cyclic stressing do not follow this principle though. Experiment show that a core subjected to cyclic loading produces multiple fractures in different directions. More test need to be performed to be sure that this observation is not a one-off occurrence.

- Experiments also show that fracture propagates in steps. More tests and even more sophisticated video cameras with better resolution will be required for proper documentation.

## Recommendations for future work

- More work is required in the design of the apparatus, particularly the mechanism for the application of tensile stress to the core. The pin designed to convert axial pressure to tensile stress clearly fails in performing this function (see the figure 64)
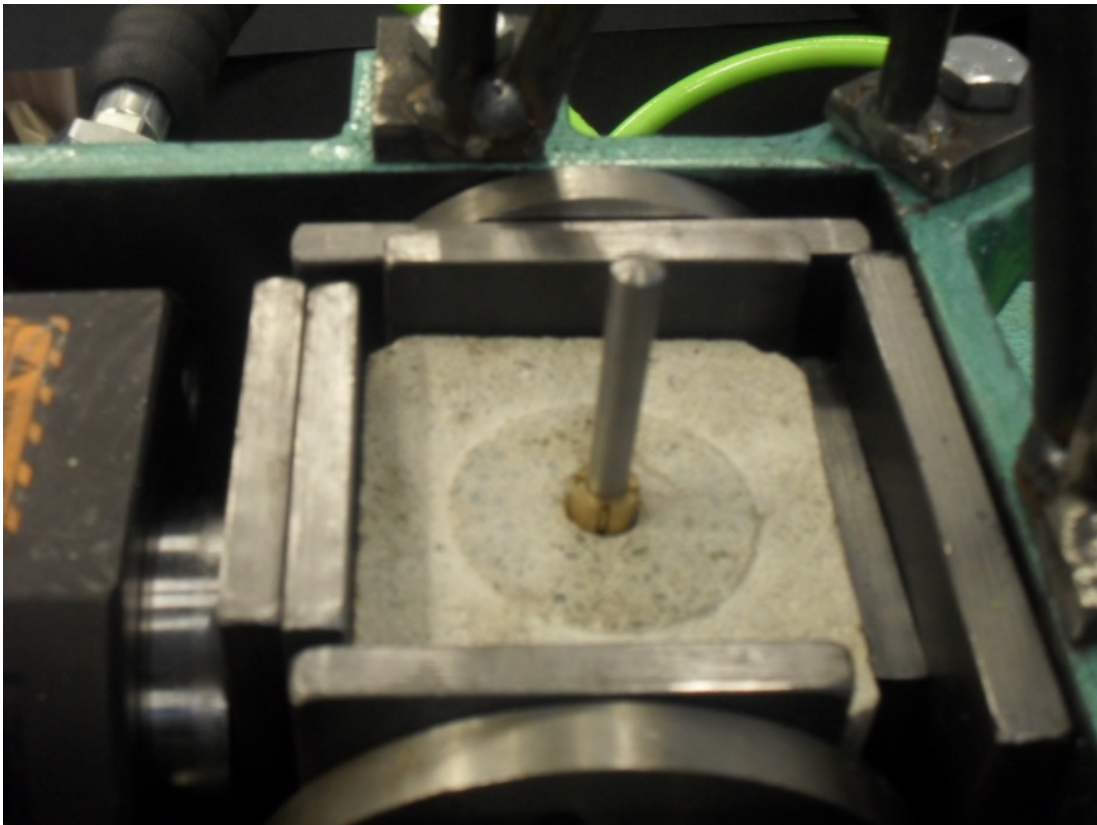


**Figure 64:** Inserted in the hole in the core is the pin required to provide tensile stress

- More experiments will also be required for better understanding of the fracture process. The number of experiments performed is grossly unsatisfactory and this is due to uncontrollable challenges, both technical and otherwise.

- A hydraulic system is recommended for applying tensile stress to the core unlike the manual system used here. That will make things a lot easier and also allow for easy measurement of the fracture propagation pressures.

- The idea of combining a fluid flow eequation with stresses and rock strength should be explored to obtain a better fracture propagation equation.

# References

1. Daneshy A. A, 'Principles of Hydraulic Fracturing', Chapter 2 - Rock Fracturing and Fluid Flow I Solution Mining Symposium 1974, Society of Mining Engineers AIME, ISBN 73-94005, 1974

2. Mavko B. B. et al, 'Hydraulic Fracture Model For Application To Coal Seams', The 27th U.S. Symposium on Rock Mechanics (USRMS), Tuscaloosa, AL, A. A. Society of Mining Engineers, June 23 - 25, 1986

3. Fjær et al, 'Petroleum Related Rock Mechanics', 2nd ed., Development in Petroleum Science, 53, Elsevier, 2008.

4. 'Fracture Mechanics', http://en.wikipedia.org/wiki/Fracture_mechanics, and 'Solid mechanics', http://en.wikipedia.org/wiki/Solid_mechanics.

5. Aadnøy B. S. and M. Belayneh, (2004), 'Elasto-plastic fracturing model for well bore stability using non-penetrating fluids', Journal of Petroleum Science and Engineering, 45(3-4): 179-192.

6. 'Griffith Criterion', http://en.wikipedia.org/wiki/Fracture_mechanics#Griffith.27s_criterion

7. Aadnøy B. S. et al, (2008), 'Design of well barriers to combat circulation losses', Society of Petroleum Engineers, 23 (3): 295-300.

8. Ong S. H. and J. Roegiers, (1996) 'Fracture initiation from inclined wellbores in anisotropic formations', Journal of Petroleum Technology, 48 (7): 612-619.

9. Kårstad E. and B.S. Aadnoy, (2005) 'Optimisation of Borehole Stability using 3-D stress optimisation', Society of Petroleum Engineers, SPE 97149-MS.

10. Zhang et al, 'Fracturing mechanism in soils with 3-dimensional stress state', 2008

11. Addis M. A. Et al, (1990), 'Laboratory studies on the stability of vertical and deviated boreholes', Society of Petroleum Engineers, SPE 20406.

12. Guenot A. and F.J. Santarelli, (1988), 'Bore hole stability: a new challenge for an old problem', American Rock Mechanics Association, 88-0453, pp. 453-459.

13. Aadnøy B. S. and M. Belayneh, (2008), 'A new fracture model that includes load history and poisson's effect', IADC/SPE Asia Pacific Drilling Technology Conference and Exhibition, SPE 114829-MS.

14. Mott, NF, Fracture of metals: some theoretical considerations. Engineering, 165 (1948) pp. 16-18

15. Roberts and Wells, (1954 ), 'The velocity of brittle fracture', Engineering 178, no. 4639, 820,

16. Dulaney and Brace, (1960), 'Velocity behaviour of a growing crack', Journal of Applied Physics, volume 31, number 12, Department of geology and geophysics, MIT.

17. Chekunaev and Kaplan, (2009), 'Limiting velocity of crack propagation in elastic materials', Journal of Applied mechanics and technical physics', Vol. 50, No. 4, pp.667-683.

18. Aadnoy B. S. et al, (2009) 'Fracture Mechanics Interpretation of Leak-Off Tests', Society of Petroleum Engineers, SPE 126452.

19. Outmans, (1963) 'Mechanics of Static and Dynamic Filtration in the Borehole', Society of Petroleum Engineers, SPE 491.

20. Dewan J. T. and Chenevert M. E., (2001) 'A Model for Filtration of Water-base Mud During Drilling: Determination of Mudcake Parameters', Society of Professional Well Log Analysts, Vol. 42.

21. Fossen and Gabrielsen, StrukturGeologi .

22. Belayneh M., Unpublished works, 2010.

23. Kurt Louis Krogsæter, (2010), Designing and building an apparatus for fracture propagation testing, Bachelor thesis for the University of Stavanger.